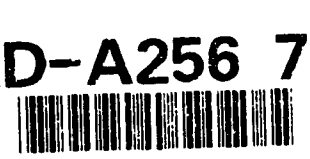

(2)

NAVAL POSTGRADUATE SCHOOL

Monterey, California

THESIS

SIMULATION OF ACOUSTIC MULTIPATH ARRIVAL STRUCTURE IN THE BARENTS SEA

by

John M. Elliott

June, 1992

Thesis Advisor: C-S Chiu
Co-Advisor: J.H. Miller

REPORT DOCUMENTATION PAGE

1a. REPORT SECURITY CLASSIFICATION Unclassified	1b. RESTRICTIVE MARKINGS
2a. SECURITY CLASSIFICATION AUTHORITY	3. DISTRIBUTION/AVAILABILITY OF REPORT Approved for public release; distribution is unlimited.
2b. DECLASSIFICATION/DOWNGRADING SCHEDULE	
4. PERFORMING ORGANIZATION REPORT NUMBER(S)	5. MONITORING ORGANIZATION REPORT NUMBER(S)
6a. NAME OF PERFORMING ORGANIZATION Naval Postgraduate School 6b. OFFICE SYMBOL (*If applicable*) 35	7a. NAME OF MONITORING ORGANIZATION Naval Postgraduate School
6c. ADDRESS (*City, State, and ZIP Code*) Monterey, CA 93943-5000	7b. ADDRESS (*City, State, and ZIP Code*) Monterey, CA 93943-5000
8a. NAME OF FUNDING/SPONSORING ORGANIZATION 8b. OFFICE SYMBOL (*If applicable*)	9. PROCUREMENT INSTRUMENT IDENTIFICATION NUMBER
8c. ADDRESS (*City, State, and ZIP Code*)	10. SOURCE OF FUNDING NUMBERS Program Element No. / Project No. / Task No. / Work Unit Accession Number

11. TITLE (*Include Security Classification*)
SIMULATION OF ACOUSTIC MULTIPATH ARRIVAL STRUCTURE IN THE BARENTS SEA

12. PERSONAL AUTHOR(S) **Elliott, John M.**

13a. TYPE OF REPORT	13b. TIME COVERED	14. DATE OF REPORT (*year, month, day*)	15. PAGE COUNT
Master's Thesis	From To	1992, June	110

16. SUPPLEMENTARY NOTATION
The views expressed in this thesis are those of the author and do not reflect the official policy or position of the Department of Defense or the U.S. Government.

17. COSATI CODES			18. SUBJECT TERMS (*continue on reverse if necessary and identify by block number*)
FIELD	GROUP	SUBGROUP	Acoustic Tomography, Ocean Acoustics, Oceanography, Barents Sea

19. ABSTRACT (*continue on reverse if necessary and identify by block number*)

In support of the Barents Sea Polar Front Experiment (BSPFEX) in September 1992 (Barents Sea Polar Front Group, 1992), the planned 224 Hz tomography signal transmissions from a near bottom sound source to a vertical receiver array consisting of 16 hydrophones were simulated. Acoustic rays were traced to the receiver array at a range of 50 km using the NOAA Hamiltonian Raytracing Program for the Ocean (HARPO). Input to HARPO was a mathematical ocean environment based on historical bathymetric and sound speed data. Acoustic multipath arrival structure was constructed through eigenray searches and estimation of raytube spreading and surface and bottom losses. A resolvability analysis of the simulated arrival structure reveals that there are a total of 49 unique resolvable ray arrivals. Among them, 42 are from individual omnidirectional hydrophones and 7 from plane wave beamforming.

20. DISTRIBUTION/AVAILABILITY OF ABSTRACT	21. ABSTRACT SECURITY CLASSIFICATION	
☒ UNCLASSIFIED/UNLIMITED ☐ SAME AS REPORT ☐ DTIC USERS	Unclassified	
22a. NAME OF RESPONSIBLE INDIVIDUAL Dr. Ching-Sang Chiu	22b. TELEPHONE (*Include Area code*) 408-646-3239	22c. OFFICE SYMBOL OC/Ci

DD FORM 1473, 84 MAR — 83 APR edition may be used until exhausted. All other editions are obsolete.

Approved for public release; distribution is unlimited.

SIMULATION OF ACOUSTIC MULTIPATH ARRIVAL STRUCTURE IN THE BARENTS SEA

by

John M. Elliott
Lieutenant Commander, United States Navy
B.S., University of Florida, 1977
M.E., University of Florida, 1978

Submitted in partial fulfillment
of the requirements for the degrees of

MASTER OF SCIENCE IN PHYSICAL OCEANOGRAPHY
MASTER OF SCIENCE IN ENGINEERING ACOUSTICS

from the

NAVAL POSTGRADUATE SCHOOL
June 1992

Author: John M. Elliott
John M. Elliott

Approved by:
Ching-Sang Chiu, Thesis Advisor

James H. Miller, Thesis Co-advisor

Curtis A. Collins, Chairman
Department of Oceanography

Anthony A. Atchley, Chairman
Engineering Acoustics Academic Committee

ABSTRACT

In support of the Barents Sea Polar Front Experiment (BSPFEX) in September 1992 (Barents Sea Polar Front Group, 1992), the planned 224 Hz tomography signal transmissions from a near bottom sound source to a vertical receiver array consisting of 16 hydrophones were simulated. Acoustic rays were traced to the receiver array at a range of 50 km using the NOAA Hamiltonian Raytracing Program for the Ocean (HARPO). Input to HARPO was a mathematical ocean environment based on historical bathymetric and sound speed data. Acoustic multipath arrival structure was constructed through eigenray searches and estimation of raytube spreading and surface and bottom losses. A resolvability analysis of the simulated arrival structure reveals that there are a total of 49 unique resolvable ray arrivals. Among them, 42 are from individual omnidirectional hydrophones and 7 from plane wave beamforming.

TABLE OF CONTENTS

I. INTRODUCTION 1

A. OCEAN ACOUSTIC TOMOGRAPHY 1

B. BARENTS SEA POLAR FRONT EXPERIMENT 2

C. THESIS OBJECTIVES AND APPROACHES 6

D. THESIS OUTLINE 7

II. PHYSICAL OCEANOGRAPHY 9

A. INTRODUCTION 9

B. WATER MASSES AND SURFACE WAVES 9

C. BARENTS SEA POLAR FRONT 12

III. ACOUSTIC EFFECTS 15

A. INTRODUCTION 15

B. ABSORPTION 15

C. SPREADING AND REFRACTIVE EFFECTS 15

D. SURFACE LOSS 16

E. BOTTOM LOSS 18

IV. RAY THEORY ACOUSTICS 20

A. INTRODUCTION 20

B. HAMILTONIAN RAY TRACING 20

C. HARPO OVERVIEW 21

D. MODELING THE BARENTS SEA ACOUSTIC ENVIRONMENT . 22
1. General 22
2. Sound Speed Field, Bathymetry, and Sea Surface 23
3. Summary 27

V. ARRIVAL STRUCTURE SIMULATION & ANALYSIS 29
A. INTRODUCTION 29
B. RAY PATH STRUCTURE 29
C. ARRIVAL STRUCTURE 30
D. ARRIVAL TIME STRUCTURE 32
E. RELATIVE AMPLITUDE 34
F. RESOLVABILITY ANALYSIS 39
1. Introduction 39
2. Method I - Individual Hydrophones 40
a. Time Analysis 40
b. σ_t Analysis 41
c. Resolvable Rays 43
3. Method II - Plane Wave Beamformer 46

VI. CONCLUSIONS 51

LIST OF REFERENCES 53

APPENDIX A: LIST OF EXTERNAL PROGRAMS 55

APPENDIX B: INDIVIDUAL HYDROPHONE RESOLVABILITY ANALYSIS TABLE 81

APPENDIX C: LINE ARRAY RESOLVABILITY ANALYSIS TABLE . . 92

INITIAL DISTRIBUTION LIST 98

LIST OF FIGURES

Figure 1 Barents Sea bathymetry (after Eldhom and Talwami, 1977). Box centered at 74.6N 24.0E indicates the specific area of study. 3

Figure 2 Barents Sea Polar Front experiment configuration and the details of the bathymetry (20 m contour interval). ((A)-224 Hz Source, (B)-16 element vertical hydrophone array, (C,D)-400 Hz transceivers.) . . 5

Figure 3 A three dimensional view of the study area. ((A)-224 Hz source; (B)-Vertical hydrophone array; (C,D)-400 Hz transceivers.) 6

Figure 4 Geographical distribution of water masses in the Barents Sea (Loeng, 1991). The Barents Sea Polar Front is defined by the shaded line. Water masses are described in the text. Box centered at 74.6N 24.0E indicates the BSPFEX area. 11

Figure 5 Mean wave heights (ft) for the Barents Sea, July - September (NAVOCEANO, 1990). 12

Figure 6 Temperature structure in °C (1°C contour interval) of the Polar Front in an area 100 km SW of the BSPFEX area. The shaded area is defined by the 3-4°C contour. (Johannessen and Foster, 1978). . . . 13

Figure 7 Topographically controlled section of the Barents Sea Polar Front (broad line) around Bear Island (Johannessen and Foster, 1978) 14

Figure 8 Surface loss at a sea state of 3 (Emblidge, 1991) 17

Figure 9 Bottom loss along the 50 km path from the source location (A) to vertical hydrophone array location (B) (Kerr, 1990 and Blodgett, et al., 1987). 19

Figure 10 Historical sound speed profiles. SSP1-North Atlantic Water, SSP2-Polar Front, SSP3-Arctic Water.(NAVOCEANO MOODS, 1991). 24

Figure 11 Linear interpolation of historical sound speed profiles. A1-A5 are defined in the text. (Emblidge,1991). 24

Figure 12 Grid overlay for bathymetry model. 25

Figure 13 Orientation of modeled sound speed profile. (P3 - Arctic Water, P2 - Polar Front, P1 - North Atlantic Water, A1 - A5 represent the linear interpolated averages.) 26

Figure 14 Modeled sound speed field along the track from source A to hydrophone array B. 27

Figure 15 Ray path along a vertical slice from source (A) to receiver array (B) for a launch angle of 5.00°. 30

Figure 16 Ray path along the track from source (A) to hydrophone array (B) for a launch angle of 8.89°. . 31

Figure 17 Ray path along the track from source (A) to hydrophone array (B) for a launch angle of 10.40°. 31

Figure 18 Arrival depth versus launch angle for the near bottom sound source (A). 32

Figure 19 Arrival depth versus arrival angle for the near bottom sound source (A). 33

Figure 20 Arrival depth versus arrival time for the near bottom sound source (A). 34

Figure 21 Arrival angle versus arrival time for the near bottom sound source (A). 35

Figure 22 Launch angle versus arrival time for the near bottom sound source (A). 35

Figure 23 Individual ray transmission loss versus launch angle for a near bottom sound source (A) at a sea state of 3. 37

Figure 24 Individual ray transmission loss versus launch angle for a near bottom sound source (A) at a sea state of 5. 37

Figure 25 Individual ray transmission loss versus arrival angle for a near bottom sound source (A) at a sea state of 3. 38

Figure 26 Relative amplitude of all rays from source (A) arriving at a vertical surface 50 km away at location (B) for a sea state of 3. 39

Figure 27 SNR versus σ_t for two pulse widths. The 224 Hz source has a d of 62.5 ms whereas the 400 Hz source has a d of 10 ms. 43

Figure 28 Simulated arrival structure at hydrophone #8 (depth 220 m) at a sea state of 3. 46

Figure 29 Beam pattern for modeled linear array with beam steered to 20 degrees off broadside. 47

Figure 30 Simulated beamformed arrival structure in sector 13 (+13.5° grazing angle). R9 and R10 are resolvable and have $\sigma_t \leq 6.3$ ms. 50

LIST OF TABLES

Table I LOCATIONS AND CHARACTERISTICS OF ACOUSTIC ELEMENTS 4

Table II BARENTS SEA WATER MASSES 10

Table III INDIVIDUAL HYDROPHONE RESOLVABLE RAY ARRIVALS WITH $\sigma_t \leq 6.3$ ms 45

Table IV PLANE WAVE BEAMFORMED RESOLVABLE ARRIVALS WITH $\sigma_t \leq 6.3$ ms 49

I. INTRODUCTION

A. OCEAN ACOUSTIC TOMOGRAPHY

Ocean tomography is an acoustical method to monitor the ocean interior (Munk and Wunsch, 1979). Like the computer assisted tomography (CAT) scans used in medicine and seismic tomography used in geology, ocean tomography employs beams of energy to create a three-dimensional image of the volume traversed. In CAT scans, these energy beams consist of X-rays; in seismic tomography, shock waves from earthquakes or explosions; and in ocean tomography, low frequency sound waves. As sound waves travel through the ocean they gather information on the changes in ocean temperature and currents. The data are in the form of changes in sound pulse travel times. Using inverse techniques the best estimate of the ocean structure is constructed.

An ocean acoustic tomography problem can be divided into two parts. The first is known as the "forward" and the second as the "inverse" (Munk and Wunsch, 1979). The forward problem establishes the physical relationship between data and the unknown ocean structure. Simulation studies using this relationship can be used to investigate signal and array design issues. The inverse problem deals with the

reconstruction of the unknown ocean structure based on the gathered data and the established forward relationship.

The feasibility of using tomography for ocean monitoring depends on four factors (Munk and Wunsch, 1979):

1. Stability
2. Resolvability
3. Identifiability
4. Signal to Noise Ratio (SNR)

Useful time series of acoustic travel time can only be derived from stable and resolvable multipath arrivals over successive transmissions. Identification (i.e. association) of the observed arrivals with modeled arrivals is required to determine the geometry of the acoustic paths. SNR determines the accuracy of the travel time measurement.

B. BARENTS SEA POLAR FRONT EXPERIMENT

The Barents Sea Polar Front Experiment (BSPFEX) is planned for August 1992 (Barents Sea Polar Front Group, 1992). The experiment will be conducted jointly by the Naval Postgraduate School (NPS), Woods Hole Oceanographic Institution (WHOI), and Science Applications International Corporation (SAIC). The experiment will take place within an approximately 70 x 80 km polygon centered at about 100 km east of Bear Island and situated over the steep northwestern slope of Bear Island Trough as shown in Figure 1.

This field study will emphasize small-scale to mesoscale processes, and will utilize both traditional oceanographic measurements and acoustic tomographic techniques.

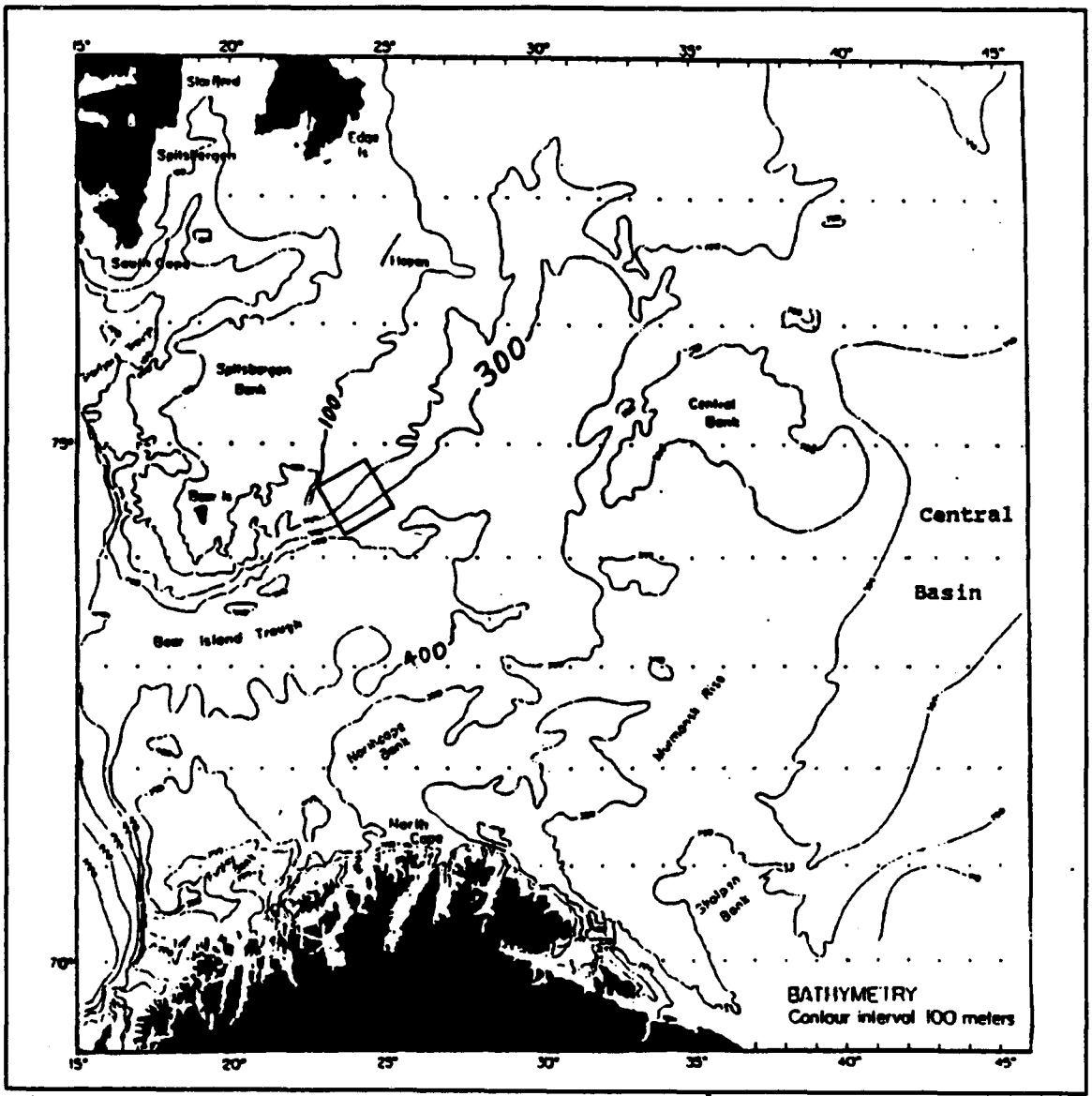

Figure 1 Barents Sea bathymetry (after Eldhom and Talwami, 1977). Box centered at 74.6N 24.0E indicates the specific area of study.

Figure 2 shows the experimental configuration and details of the bathymetry. The tomography system will consist of a 224 Hz source (A), a vertical array composed of 16 hydrophones (B), and two 400 Hz transceivers (C,D). Figure 3 shows a three dimensional view of the test area. Some of the characteristics of the sources and receivers are summarized in Table I. This study will focus on the 224 Hz source and the hydrophone array. The 224 Hz source is mounted 3 m off the bottom on an oceanographic mooring. The hydrophone array consists of 16 hydrophones mounted at a 10 m interelement spacing on a vertical oceanographic mooring with the top hydrophone at 150 m.

Table I LOCATIONS AND CHARACTERISTICS OF ACOUSTIC ELEMENTS

MOORING	TYPE	LAT (deg N)	LON (deg E)	FREQ (Hz)	BAND WIDTH(Hz)
A	Source	74.91	24.39	224	16
B	Hyd Array	74.51	25.28	N/A	N/A
C	Trans-ceiver	74.28	23.85	400	100
D	Trans-ceiver	74.67	22.95	400	100

The scientific objectives of the tomography experiment can be summarized as follows (Barents Sea Polar Front Group, 1992):

1. Provide a detailed physical description of the front.

2. Enhance the understanding of dynamics of the front, including frontogenesis and its influence on regional

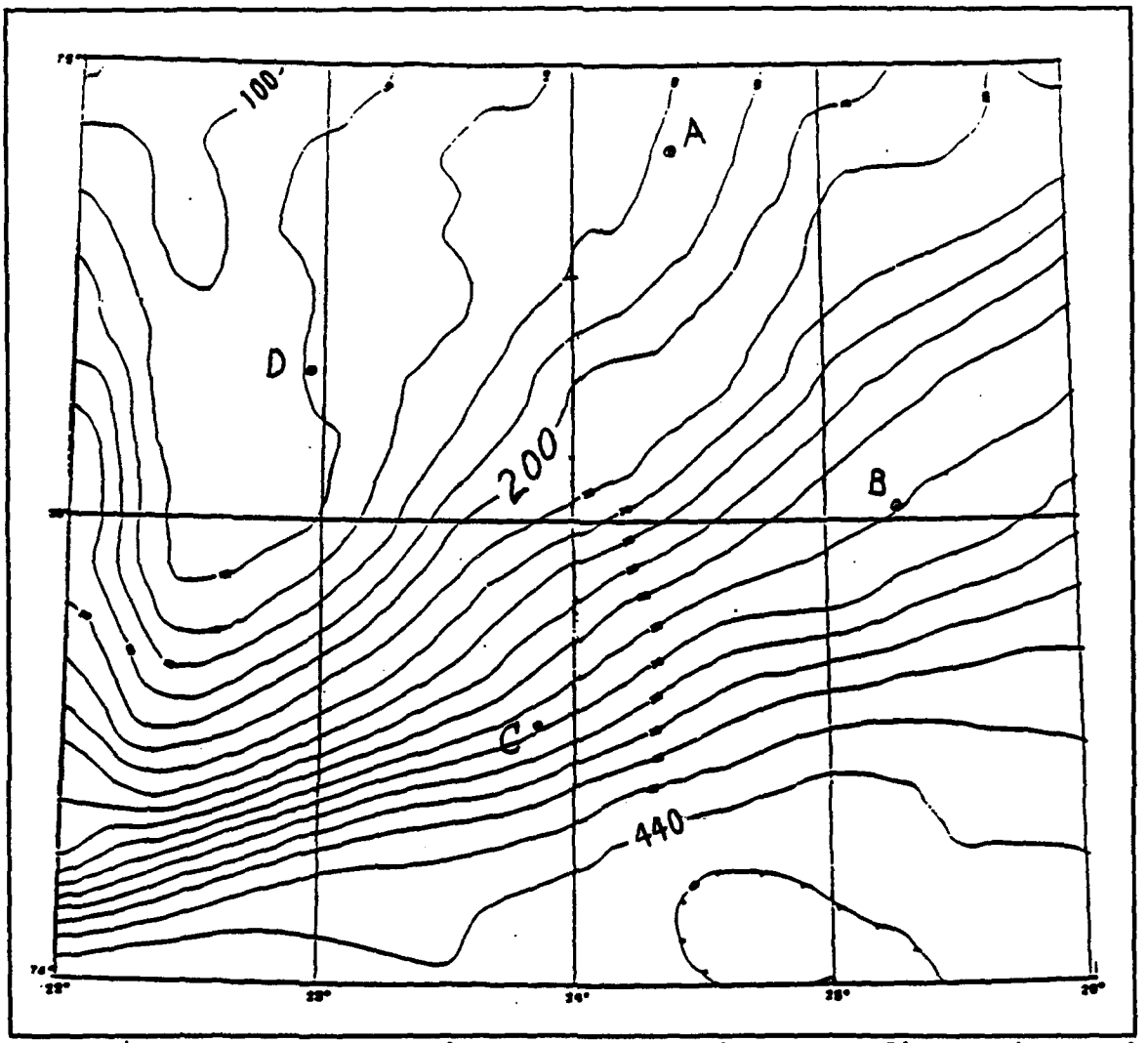

Figure 2 Barents Sea Polar Front experiment configuration and the details of the bathymetry (20 m contour interval). ((A)-224 Hz Source, (B)-16 element vertical hydrophone array, (C,D)-400 Hz transceivers.)

oceanographic processes.

3. Assess the ability of acoustic tomography to define frontal and associated mesoscale features.

4. Provide improved documentation of shallow water acoustic propagation in this region and the effect of the environment on acoustic ASW operations.

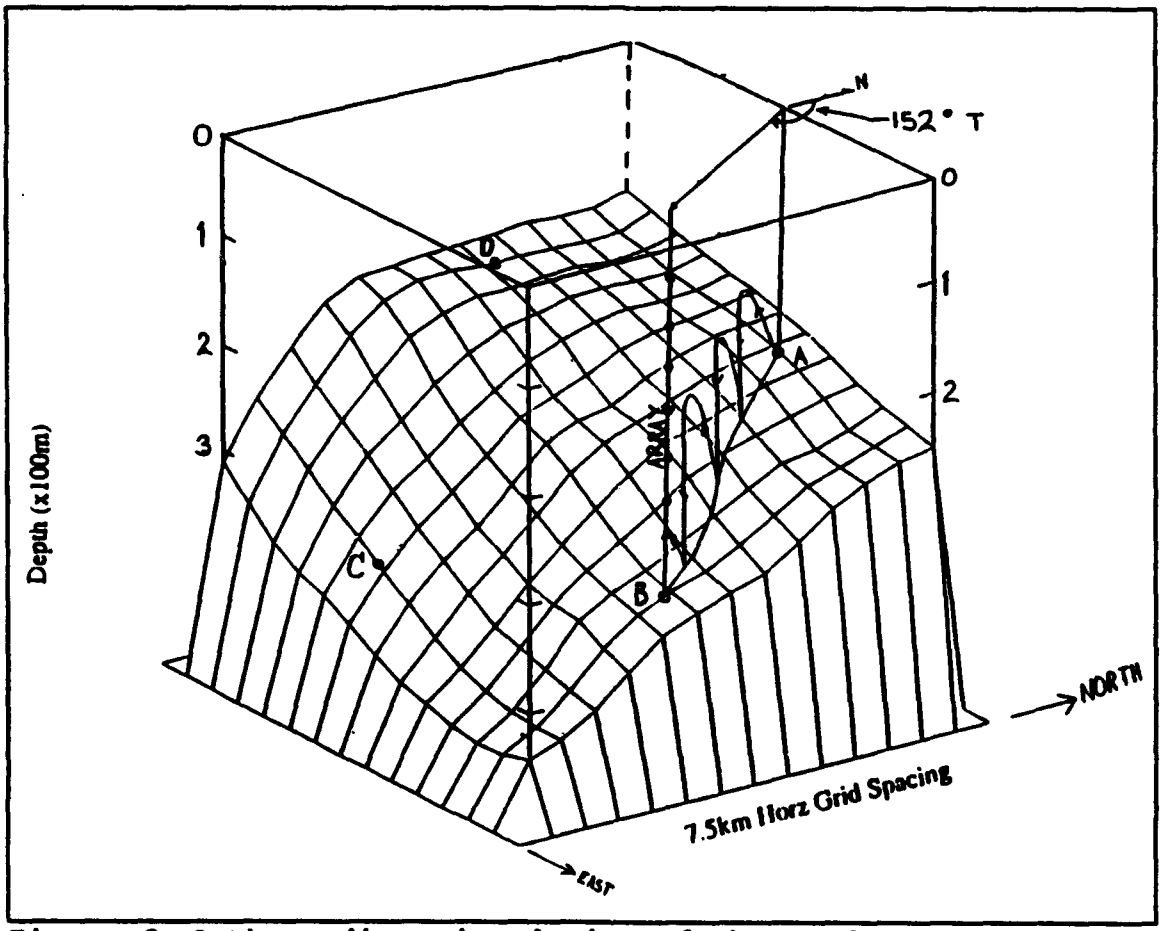

Figure 3 A three dimensional view of the study area. ((A)-224 Hz source; (B)-Vertical hydrophone array; (C,D)-400 Hz transceivers.)

C. THESIS OBJECTIVES AND APPROACHES

The objective of this thesis was to address the tomographic forward problem in the Barents Sea. The study simulated and examined the expected multipath arrival structure of the 224 Hz signal at the hydrophone array. The simulation used a three-dimensional ray theory acoustics

model. The major focus was to investigate resolvability and its relation to SNR.

In simulating the multipath arrival structure, the computer program HARPO (Hamiltonian Acoustic Raytracing Program for the Ocean) was used to trace a fan of rays to the hydrophone array location. Input to HARPO was a mathematical ocean based on a high resolution bathymetry chart (Norsk, 1986) and historical sound speed profiles. Transmission loss for each ray was then computed using computer programs external to HARPO. Eigenrays and hence arrival structure were then determined for each hydrophone of the vertical array by analysis of the rays' arrival depths and times.

Resolvability of the eigenray arrivals at the hydrophone array were examined for two cases. The first case considered each hydrophone of the vertical array as an independent omnidirectional receiver. The second case considered the hydrophones of the vertical array together as a plane wave beamformer.

D. THESIS OUTLINE

The remainder of this thesis consists of five chapters. Chapter II describes the physical oceanography of the Barents Sea including water masses, surface waves, and Polar Front features. Much of this chapter is taken from Emblidge (1991).

Chapter III describes the acoustic properties of the Barents Seas. Here the method of calculating transmission loss of individual acoustic arrivals is discussed.

In Chapter IV a review of ray theory, the ray tracing program HARPO, and the environmental models used are presented. Chapter V provides the simulated arrival structure results, transmission loss calculations, and resolvability analysis.

Chapter VI discusses the conclusion of this study.

II. PHYSICAL OCEANOGRAPHY

A. INTRODUCTION

The Barents Sea is bordered to the south by the coasts of Scandinavia and Russian Republic, to the north by the Svalbard Archipelago and Franz Joseph Land in the southern edge of the Arctic Ocean. It is bounded on the eastern side by Novaya Zemlya. Its western boundary is nearly open and can be approximated by the 15 degree east meridian (Figure 1). With an average depth of 230 m and a maximum depth of 500 m, the Barents Sea is among the shallowest seas of the world ocean (Klenova, 1966).

The Barents Sea contains a complex oceanographic structure. The meeting of Polar and Atlantic water masses to the east of Bear Island forms the Barents Sea Polar Front.

The oceanographic conditions described in this chapter are those that are expected to exist at the time of the BSPFEX (August and September).

B. WATER MASSES AND SURFACE WAVES

Currents in the region transport water of both Arctic and Atlantic origin. These water masses have vastly different temperature and salinity characteristics (Table II).

Table II BARENTS SEA WATER MASSES (after Loeng, 1991)

TYPE	T (deg C)	S (psu)
Arctic Water (AW)	<0.0	34.2 - 34.8
Polar Front Water (PW)	-0.5 to 2.0	34.8 - 35.0
North Atlantic Water (NAW)	>3.0	>35.0

Figure 4 shows Loeng's model of the geographic regions occupied by the major water masses. The abbreviations are AW for Arctic Water, SBW for Svalbard Bank Water, NAW for North Atlantic Water, BW for Bottom Water, BSW for Barents Sea Water, and CW for Coastal Water. The BSPFEX region is indicated by a small square in Figure 4.

As shown in Table II the NAW flowing north introduces warm saline water while AW flowing south introduces cold, relatively fresh water into the Barents Sea. The confluence of these flows creates the Barents Sea Polar Front. As in many frontal situations in the ocean, the front has a complex horizontal and vertical structure.

An important effect on sound transmission is the roughness of the sea surface. Many acoustic paths are expected to be surface interacting because of the shallowness of the sea. Figure 5 shows the mean wave height in feet, in the summer months of July - September (NAVOCEANO, 1990). Note that the BSPFEX area has mean summer wave heights of about 3 feet (1

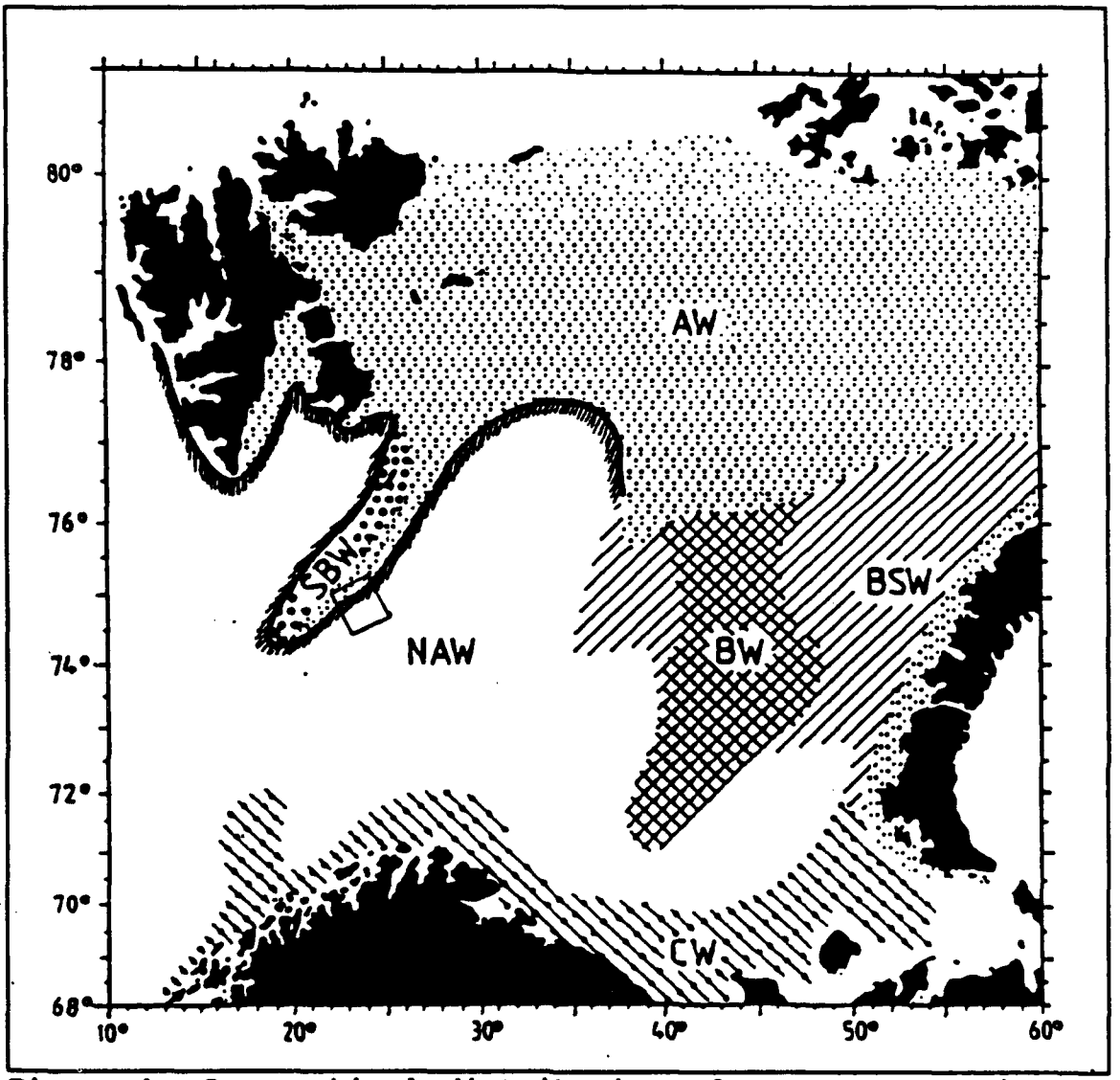

Figure 4 Geographical distribution of water masses in the Barents Sea (Loeng, 1991). The Barents Sea Polar Front is defined by the shaded line. Water masses are described in the text. Box centered at 74.6N 24.0E indicates the BSPFEX area.

meter). The effects of sea surface roughness on the scattering of sound will be discussed in Chapter III.

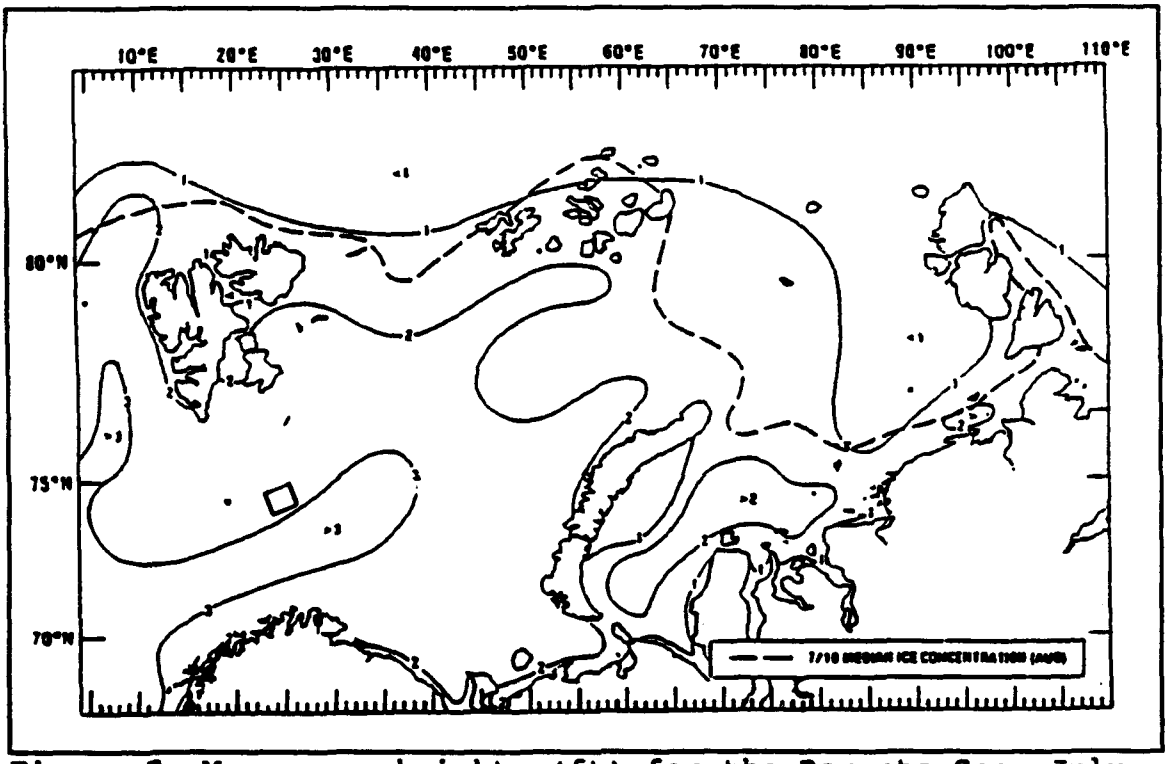

Figure 5 Mean wave heights (ft) for the Barents Sea, July - September (NAVOCEANO, 1990).

C. BARENTS SEA POLAR FRONT

Across the western interior of the Barents Sea a front exists due to the adjacent position of the NAW to the south and AW to the north (Figure 4). The front near Bear Island has been studied in some detail by Johannessen and Foster (1978). Figure 6 shows the structure of the front, annotated by the shaded area, with a complex vertical and horizontal structure.

Johannessen and Foster (1978) suggested that the mean position of the front was approximately locked to the outer part of the Svalbard Shelf by the 100-m isobath (Figure 7).

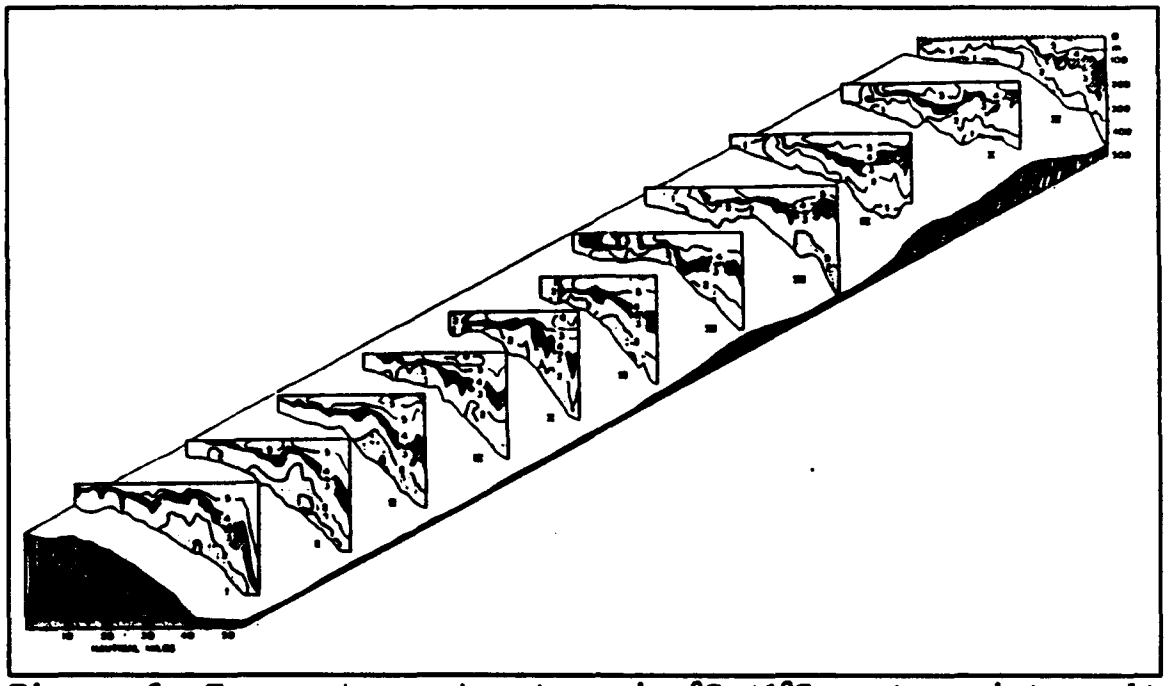

Figure 6 Temperature structure in °C (1°C contour interval) of the Polar Front in an area 100 km SW of the BSPFEX area. The shaded area is defined by the 3-4°C contour. (Johannessen and Foster, 1978).

Figure 6 shows a baroclinic subsurface structure of the front and that the surface signature is nearly absent.

The frontal core oscillates with the tides and seasons. The tidal oscillation is on the order of 10 km/cycle around Bear Island (Johannessen and Foster, 1978). The seasonal and yearly positions vary on the order of 50 km/year (NAVOCEANO, 1991).

The Barents Sea Polar Front is characterized by a change in temperature of about 5°C and salinity of 1 psu over the 100 km of its horizontal extent near Bear Island (Dickson et al., 1970).

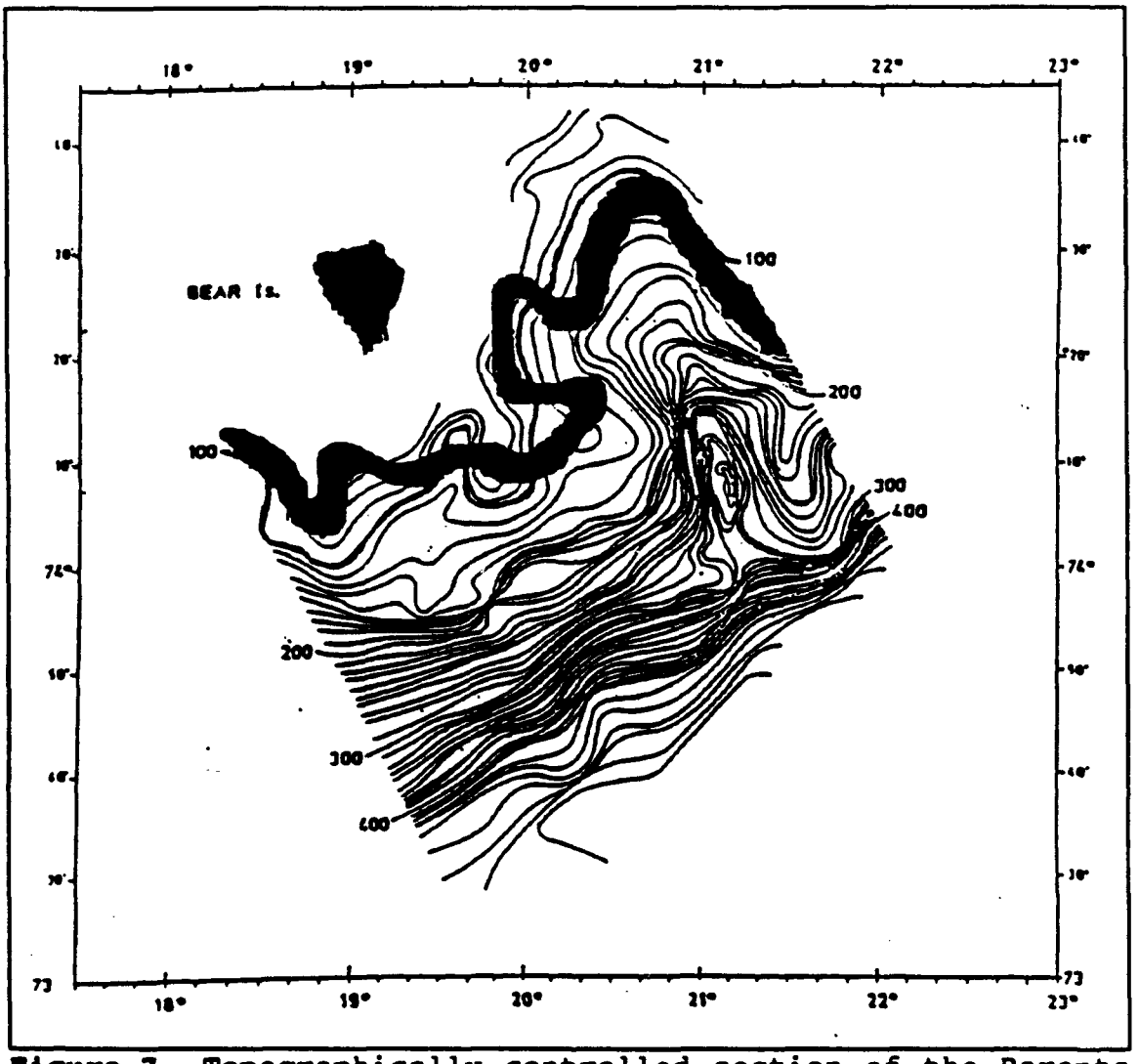

Figure 7 Topographically controlled section of the Barents Sea Polar Front (broad line) around Bear Island (Johannessen and Foster, 1978)

The BSPFEX location is about 100 km NE of the area studied by Johannessen and Foster. Frontal conditions in the BSPFEX area are expected to be similar to those found by Johannessen and Foster.

III. ACOUSTIC EFFECTS

A. INTRODUCTION

Understanding the propagation of sound in the ocean requires a knowledge of the properties of the ocean medium, its boundaries and their influence on sound propagation. Among the many environmental factors the principal ones include: absorption, spreading and refraction, and surface/bottom interactions.

B. ABSORPTION

Absorption is the loss of acoustic energy along its path due to the conversion of acoustic energy into thermal energy. This absorption loss (TL_{abs}) can be approximated by the following equation:

$$TL_{abs} = r\gamma \qquad (1)$$

where r is the ray path distance in meters and γ is the absorption coefficient. For 224 Hz, γ is approximately 0.000006 dB/m (Kinsler, et al., 1982). So for a distance of 50 km TL_{abs} is 0.3 dB.

C. SPREADING AND REFRACTIVE EFFECTS

Spreading and refractive loss (TL_{rl}) is the loss or apparent gain of acoustic energy over the traveled path due to

the defocusing or focusing of adjacent rays as they travel away from a small spherical source. TL_{rl} was calculated using a FORTRAN computer algorithm 'cordat.f' (Appendix A) for each ray by comparing the separation between adjacently launched rays. Assuming cylindrical symmetry, the equation for TL_{rl} from C.S. Chiu (1992) is

$$TL_{rl} = 10\log\frac{rh}{(\Delta\theta)\cos(\theta)} \qquad (2)$$

where r is the range between source and receiver, h is the ray tube cross sectional distance at the receiver (the cross section is orthogonal to the eigen-ray path), θ is the launch angle of the ray and $\Delta\theta$ is the difference in launch angle between adjacently launched rays.

D. SURFACE LOSS

Due to the high potential for acoustic ray interaction with the surface in a shallow ocean, the losses at the surface can be important. Acoustic energy is lost at each ray reflection with the surface due to the scatter of energy out of the ray path. This loss in energy can be described by the reflection coefficient at the sea surface which is the ratio of ray energy reflected to incident ray energy.

Using an equation in Clay and Medwin (1977), for scattering loss by a rough surface having a gaussian distribution, Emblidge (1991) calculated the surface loss per

bounce corresponding to a rms waveheight of 1 m or a sea state of 3. Figure 8 is a plot of the calculation.

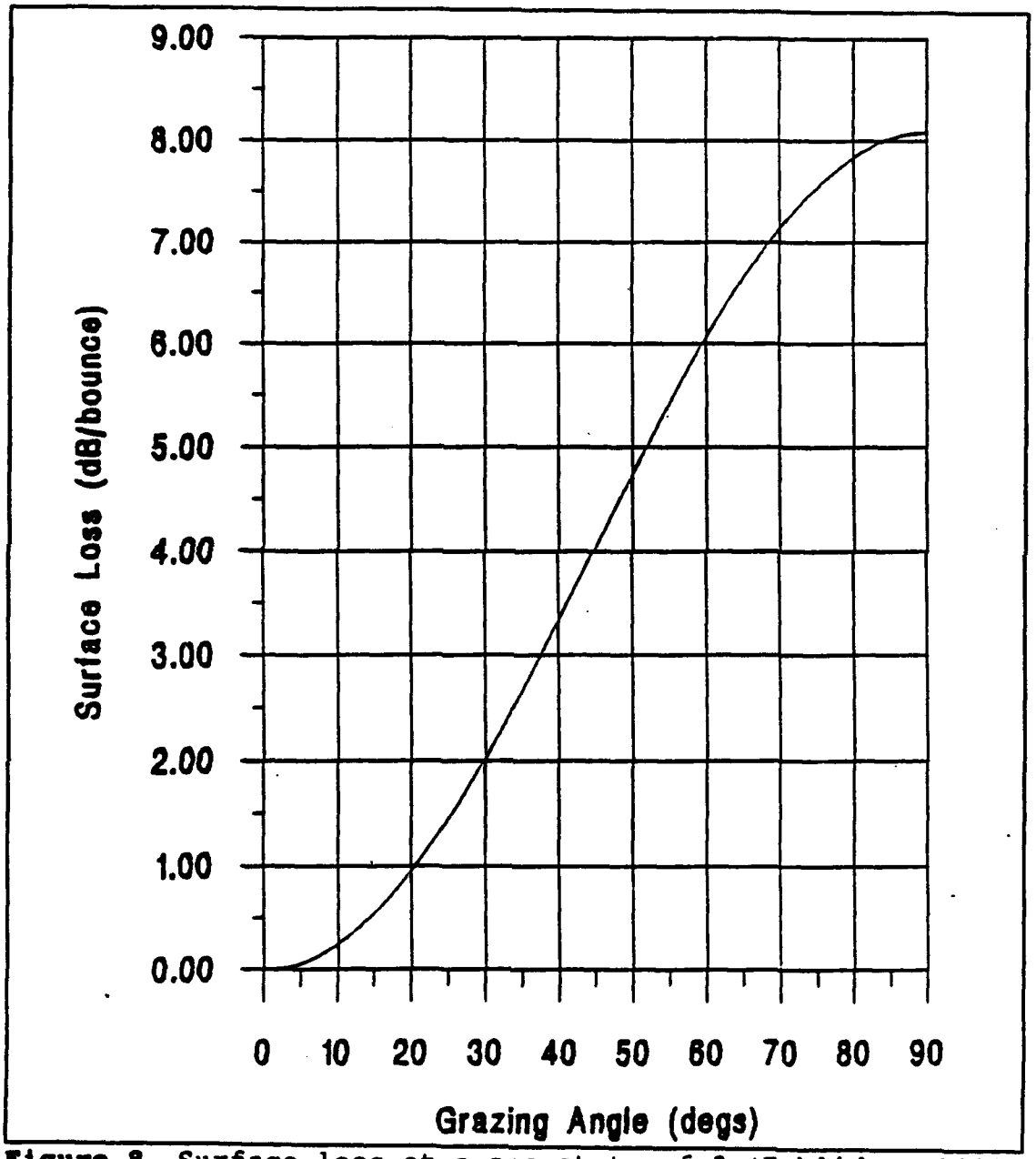

Figure 8 Surface loss at a sea state of 3 (Emblidge, 1991)

The total loss due to surface interactions, TL_{sfc}, can be computed by summing the losses of each surface interaction, $sloss_i$, that the ray encounters over its path:

$$TL_{sfc} = \sum_{i=1}^{N} sloss_i \qquad (3)$$

E. BOTTOM LOSS

The acoustic energy lost by the ray interacting with the bottom is due to the transmission of some of the acoustic energy into the bottom and the scattering of acoustic energy out of the ray tube. The loss of energy can be described by the reflection coefficient at the bottom which is the ratio of acoustic energy reflected to that incident at the bottom.

To get an estimate of the bottom loss, the U.S. Navy standard Bottom Loss Upgrade (BLUG) is used (Kerr, 1990). BLUG is an interactive routine to compute a bottom loss curve from user-defined geoacoustic inputs. Using the standard Navy BLUG computer algorithm and geoacoustic parameters from an arctic acoustic model called ICECAP (Blodgett, et. al., 1987) a bottom loss profile for the BSPFEX area was computed (Keenan, 1992). The results for 224 Hz are shown in Figure 9.

As can be seen in Figure 9 bottom loss per bounce for grazing angles less than 25 degrees are less than 7 dB for ranges less than 18 km. The bottom loss per bounce is about 0.01 dB for ranges greater than 18 km.

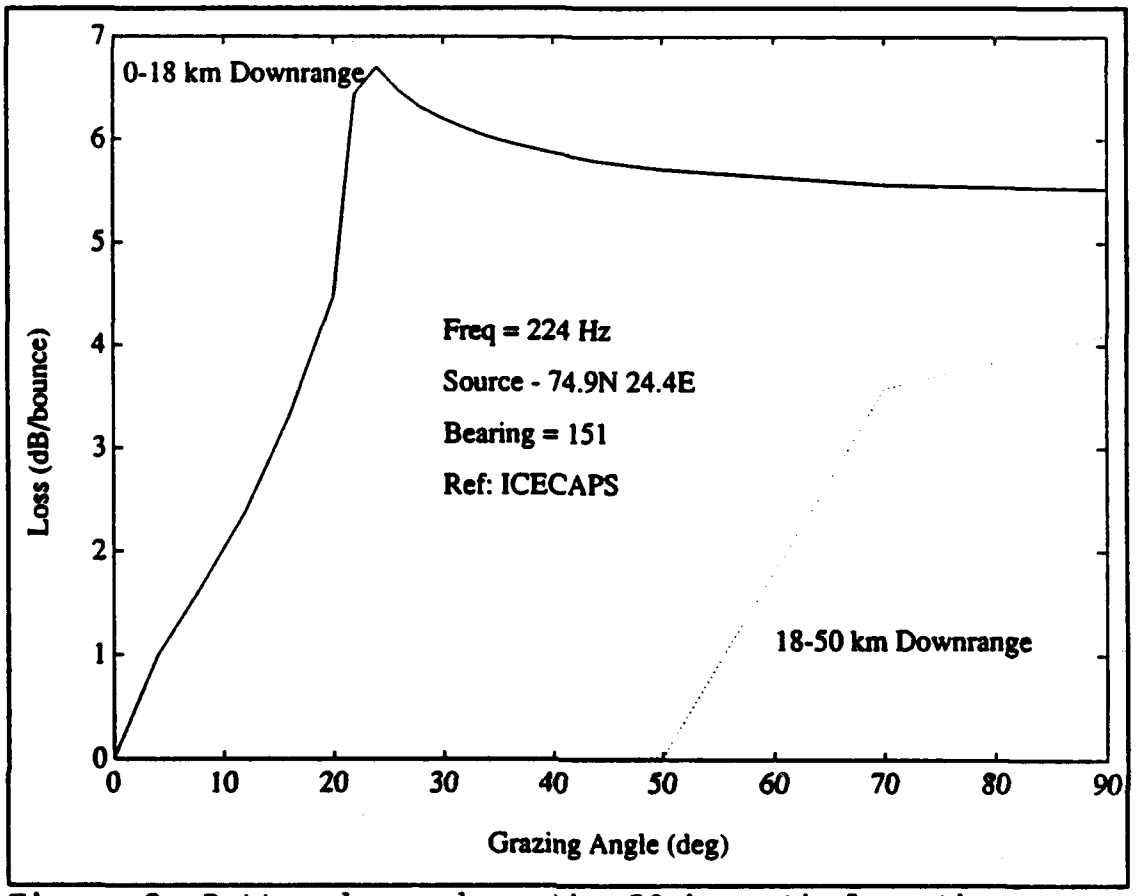

Figure 9 Bottom loss along the 50 km path from the source location (A) to vertical hydrophone array location (B) (Kerr, 1990 and Blodgett, et al., 1987).

If a constant loss per bottom bounce is assumed then the loss due to the bottom for the entire ray path, TL_{bot}, can be expressed as:

$$TL_{bot} = N(bloss) \qquad (4)$$

where N is the number of bottom bounces the ray encounters and bloss is the transmission loss in Db per bounce.

IV. RAY THEORY ACOUSTICS

A. INTRODUCTION

The propagation of sound in an ocean medium can be represented as rays. Ray theory provides a visual representation of the paths taken by sound energy and graphically illustrates how various ocean parameters affect the path of each ray. The ocean acoustic model used in this thesis is the Hamiltonian Acoustic Raytracing Program for the Ocean (HARPO).

HARPO is a three-dimensional acoustic ray theory computer model. A significant advantage of HARPO is that it deals with continuous sound speed and bathymetric structure. This continuous treatment overcomes the problems of false caustics. (Jones et al., 1986)

B. HAMILTONIAN RAY TRACING

Acoustic energy travels in the form of compressional waves. In the high frequency approximation waves behave like particles. The path of these "acoustic particles" can then be determined by integrating a differential form of the wave equation. Hamilton's equation, which governs changes of position and momentum in mechanical systems, are applicable to sound propagation at high frequency (Lighthill, 1978).

Hamilton's equation has the general form:

$$\frac{dp_i}{dt} = \frac{\partial H}{\partial q_i} \qquad i=1,2,3$$
$$\frac{dq_i}{dt} = \frac{\partial H}{\partial p_i} \qquad i=1,2,3 \tag{5}$$

where $H(p_1,p_2,p_3;q_1,q_2,q_3)$ is a Hamiltonian function describing the total energy of a system in terms of generalized coordinate system p and momenta q. For acoustic application q is the wave number vector and p is a coordinate system. In HARPO the coordinate system is spherical polar. Solutions to equation (5) are obtained by choosing initial values for the six values of q_i and p_i and integrating this system of six differential equations. For sound propagation in the ocean the Hamiltonian takes on the form:

$$H(p_i,q_i) = \omega^2 - c(p_i)\,q^2 \tag{6}$$

where ω is the angular wave frequency, $c(p_i)$ is the sound speed field and q^2 is the magnitude squared of the wave number vector (Jones, et al., 1986). Along the raypath, the Hamiltonian is defined to be zero.

C. HARPO OVERVIEW

HARPO is a computer ray tracing algorithm that numerically integrates Hamilton's equations. It requires, for input, a continuous three-dimensional representation of the sound speed field, and a continuous two-dimensional representation of the

upper and lower reflecting surfaces. The upper and lower surfaces are the ocean surface and bottom respectively.

Gridded sound speed and bathymetry fields can be made continuous by the use of empirical orthogonal functions (EOF's) and splines using computer subroutines external to HARPO. These routines originated from Newhall et al. (1987).

HARPO does not compute signal amplitude or eigenrays. Amplitude and eigenray determinations are made by external programs applied to the HARPO output files called DOUTP and RAYSET. The documentation of HARPO by Jones et al. (1986) provides a complete description of the mathematics and computer coding of HARPO.

D. MODELING THE BARENTS SEA ACOUSTIC ENVIRONMENT

1. General

The accuracy with which HARPO calculates ray paths is primarily dependent on the accuracy with which the ocean is described by the input models. Chapter II described the environment of the BSPFEX area. Modeling the environment for the simulation of acoustic ray arrival structure was accomplished by selecting environmental data that provided adequate mathematical description for the sound speed field and bathymetry.

2. Sound Speed Field, Bathymetry, and Sea Surface

The bathymetry input to HARPO is shown in Figure 12. The square box was manually gridded into 13 subdivisions along each side with a 7.5 km spacing. The bottom depths were then visually read off the chart (Norsk, 1986) at the gridded intersections. This gridded bathymetry input was splined to provide a continuous topography using FORTRAN computer subroutines 'tgridin.f' (Emblidge, 1991), 'tgridder.f' (Newhall, et al., 1987), and 'bottom.f' (Newhall, et al., 1987). Appendix A contains a copy of 'tgridin.f' which has been extensively modified for this research. Programs 'tgridder.f' and 'bottom.f' only required a one line modification to change the size of the horizontal and vertical grid spacing.

Figure 10 shows the three sound speed profiles (SSPs), extracted from the NAVOCEANO MOODS data base, chosen to represent conditions on the North Atlantic side of the Polar Front (SSP1), front interior (SSP2), and on the Arctic side (SSP3), respectively. See Figure 4 for the water mass orientation. From the three SSPs described above, five others were created by Emblidge (1991) by linear interpolation, as shown in Figure 11 (A1,A2,A3,A4,and A5), to provide a gradual change in sound speed on each side of the front.

The three-dimensional sound speed field was generated by tying a specific SVP or linear interpolated SVP to a diagonal of the bathymetry field (Figure 12). Figure 13 shows the

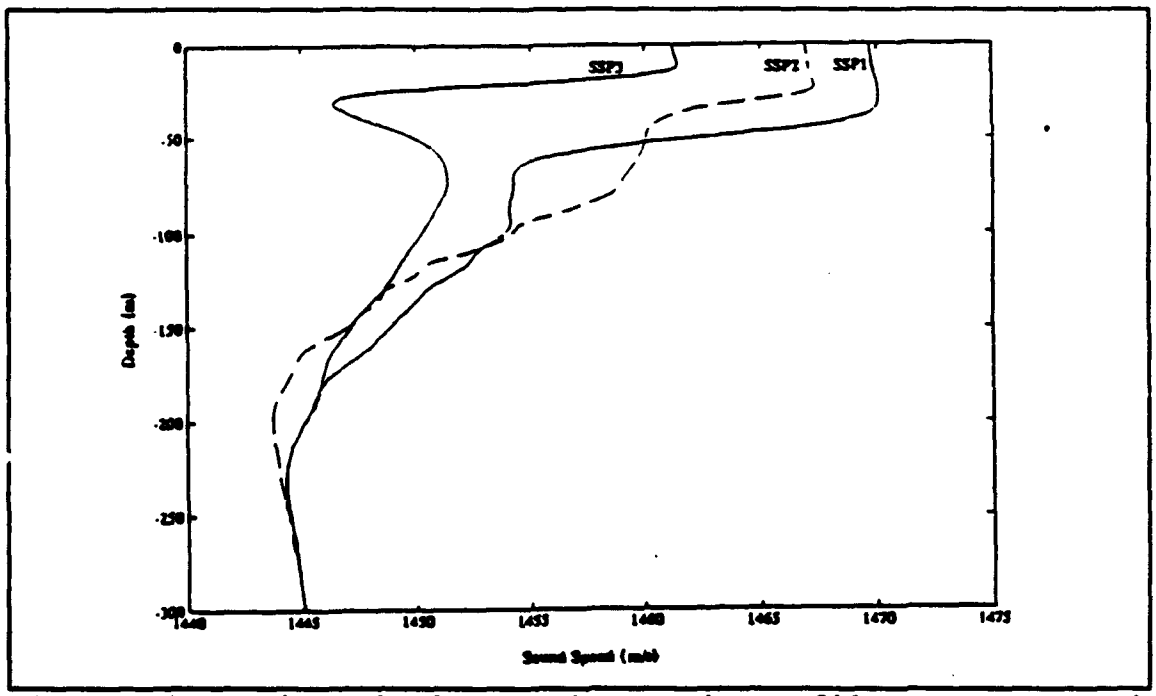

Figure 10 Historical sound speed profiles. SSP1-North Atlantic Water, SSP2-Polar Front, SSP3-Arctic Water. (NAVOCEANO MOODS, 1991).

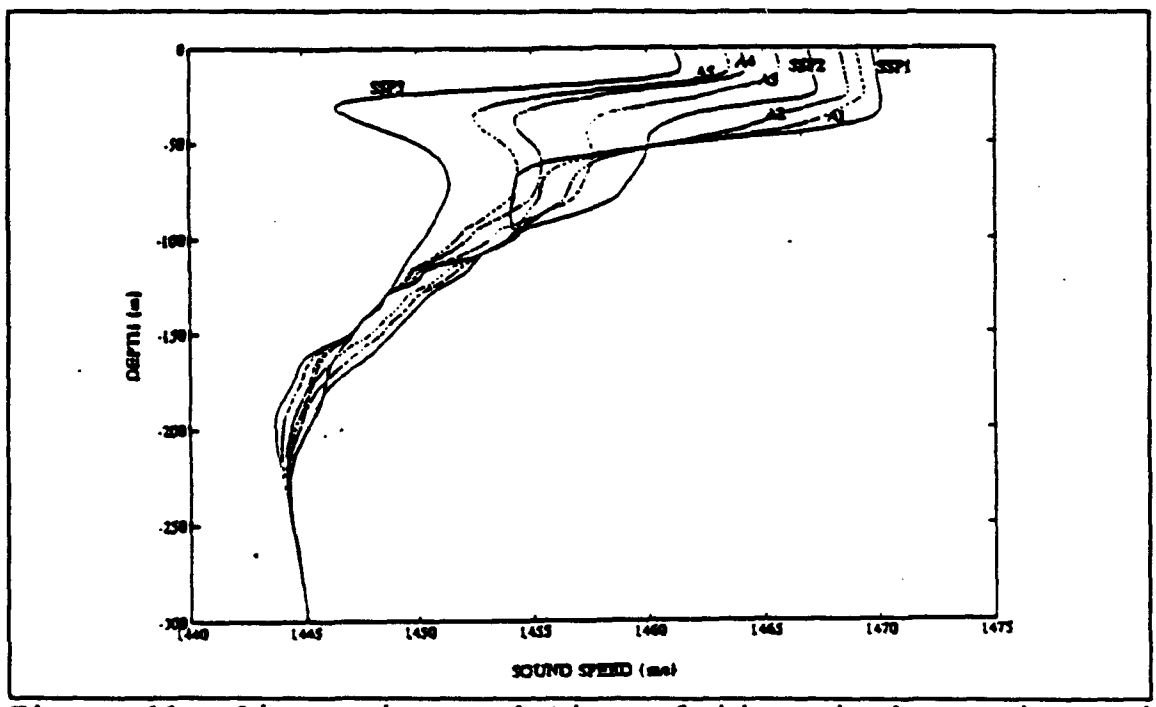

Figure 11 Linear interpolation of historical sound speed profiles. A1-A5 are defined in the text. (Emblidge, 1991).

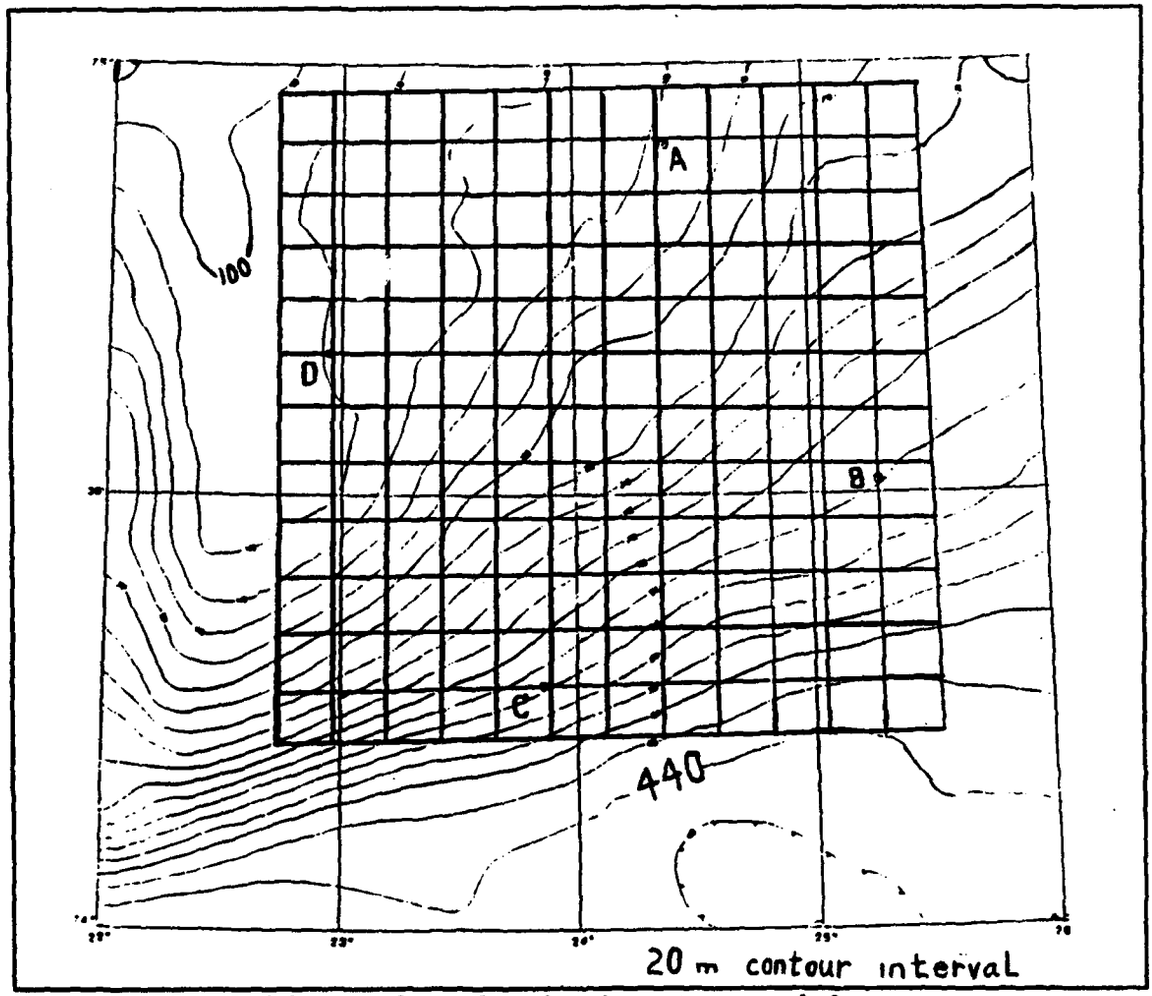

Figure 12 Grid overlay for bathymetry model.

orientation of the SVP's in the modeled BSPFEX area. This sound velocity input was then used to generate a continuous sound velocity field by EOF's and splines using FORTRAN computer subroutines 'gridin.f' (Emblidge, 1991), 'gridder.f' (Newhall, et al., 1987), and 'cgrid.f' (Newhall, et al., 1987). Appendix A contains a copy of 'gridin.f' which has been extensively modified for this work. Programs 'gridder.f' and 'cgrid.f' only required a one line modification to change the size of the horizontal and vertical grid spacing. This

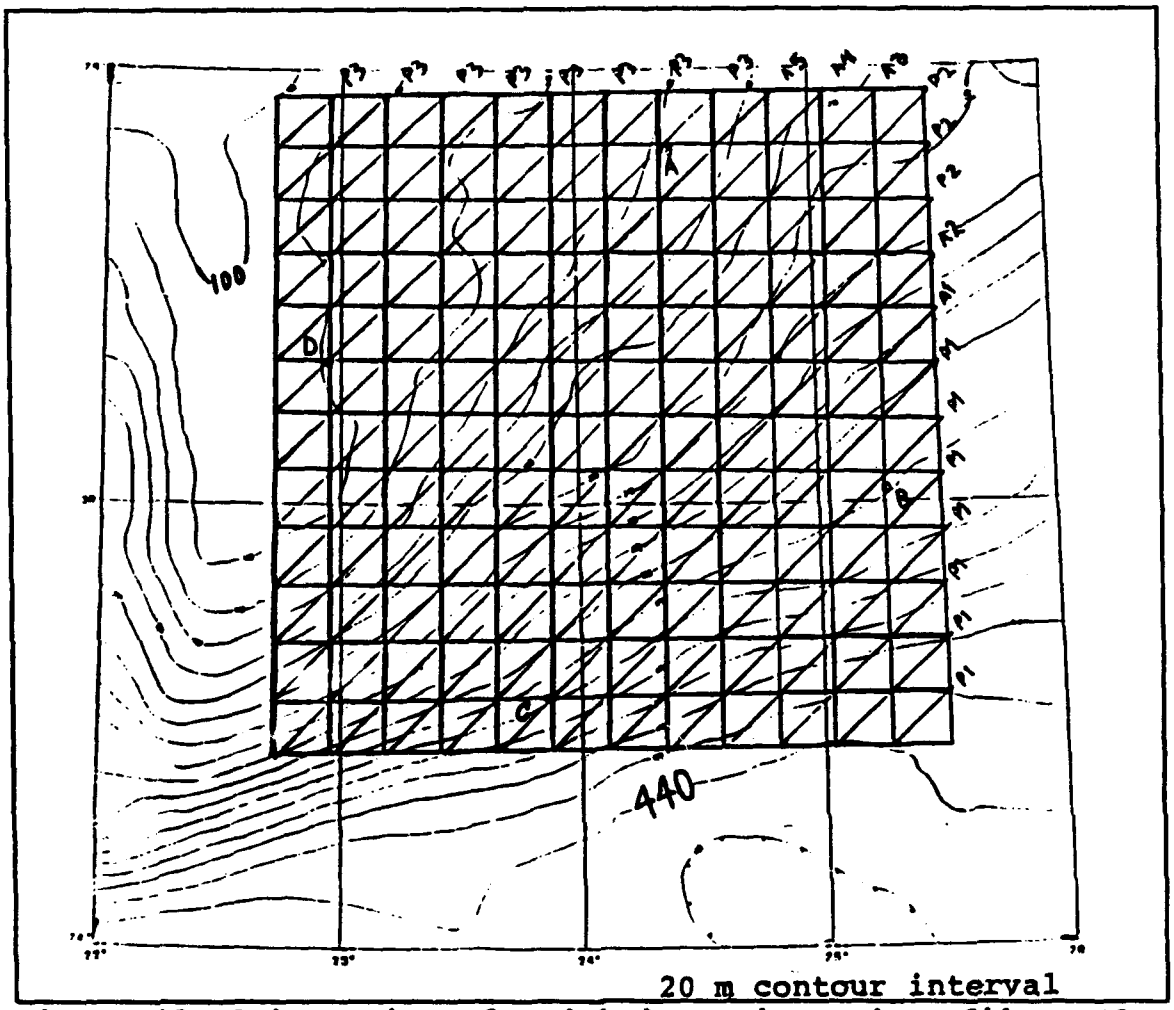

Figure 13 Orientation of modeled sound speed profile. (P3 - Arctic Water, P2 - Polar Front, P1 - North Atlantic Water, A1 - A5 represent the linear interpolated averages.)

generated a modeled Polar Front about 40 km wide, oriented along the bathymetry contours, centered approximately between the source and receiver. A contour plot of the modeled SSP field along the track between the 224 Hz source (A) and the vertical array (B) is shown in Figure 14. This modeled cross front vertical slice compares favorably to actual data as shown in Figure 6.

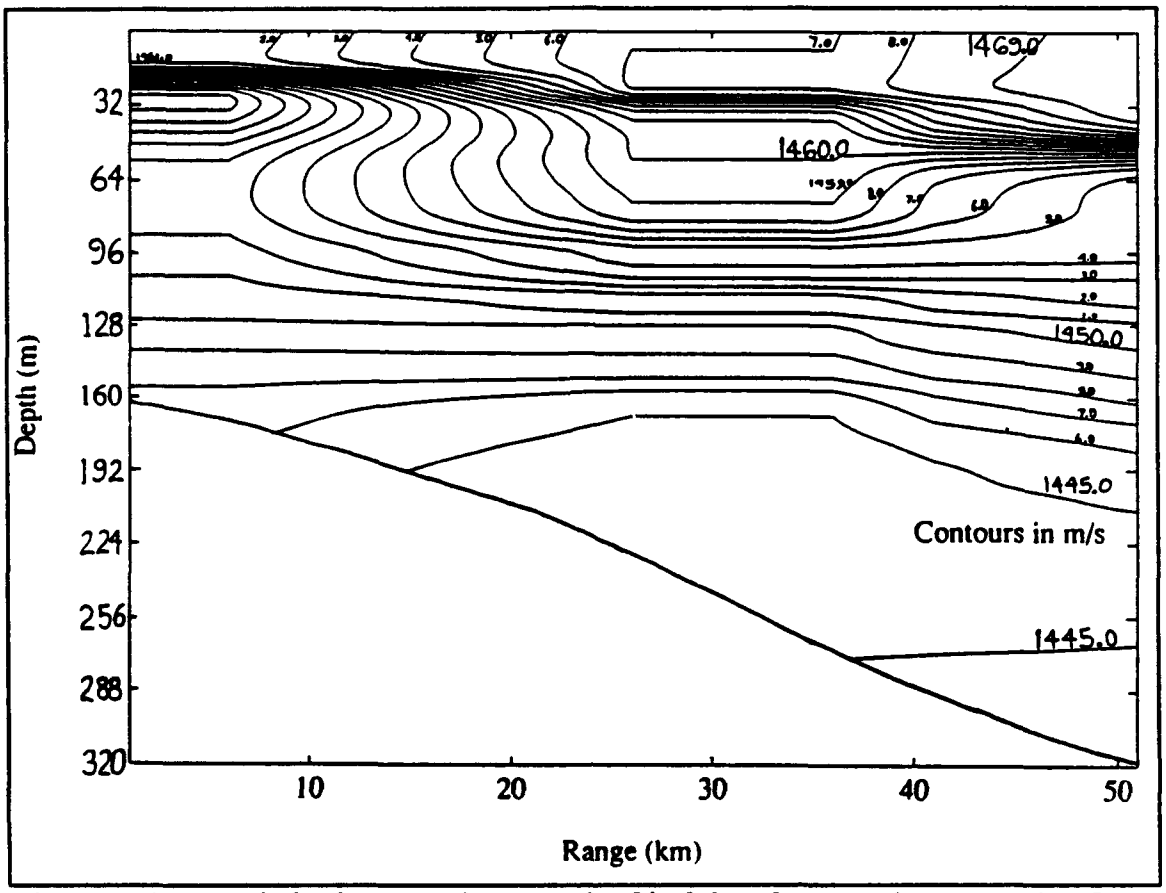

Figure 14 Modeled sound speed field along the track from source A to hydrophone array B.

The sea surface was modeled as a flat sphere concentric with the earth with a radius of 6370 km.

3. Summary

The environmental model designed provided for a 40 km wide front between the source (A) and the receiver array (B), with the source in the cold Arctic water, and the receiver array in the warm North Atlantic Water. Table I provides a description of the source/receiver positions.

In the simulation, the source was placed about 3 m off the bottom in about 163 m of water. The receiver was placed 50 km

away in about 318 m of water (Figure 3). The track from the source to the receiver array has a bearing of 151.8° true.

V. ARRIVAL STRUCTURE SIMULATION & ANALYSIS

A. INTRODUCTION

To simulate the propagation of the 224 Hz pulse signal from a near-bottom sound source, through the front to the vertical receiver array, ray traces were performed for launch angles between 0.00 to 25.00° at 0.01° increments. The rays were terminated after passing 50 km in horizontal distance. Since HARPO does not stop the rays exactly at 50 km, a correction was made via the FORTRAN program 'cordat.f' to "back-up" the rays and compute arrival depth and time at the 50 km receiver surface.

B. RAY PATH STRUCTURE

Rays with launch angles less than 8.89° are refracted bottom-reflected (RBR) as expected due to the downward refracting sound profile (Figure 10). Figure 15 shows a ray launched at 5.00°. The first ray to interact with the sea surface is the ray launched at 8.89°. Figure 16 shows the ray launched at 8.89 degrees. The first ray to become completely surface-reflected and bottom-reflected (SRBR) is the ray launched at 10.40 degrees. Figure 17 shows the ray launched at this angle.

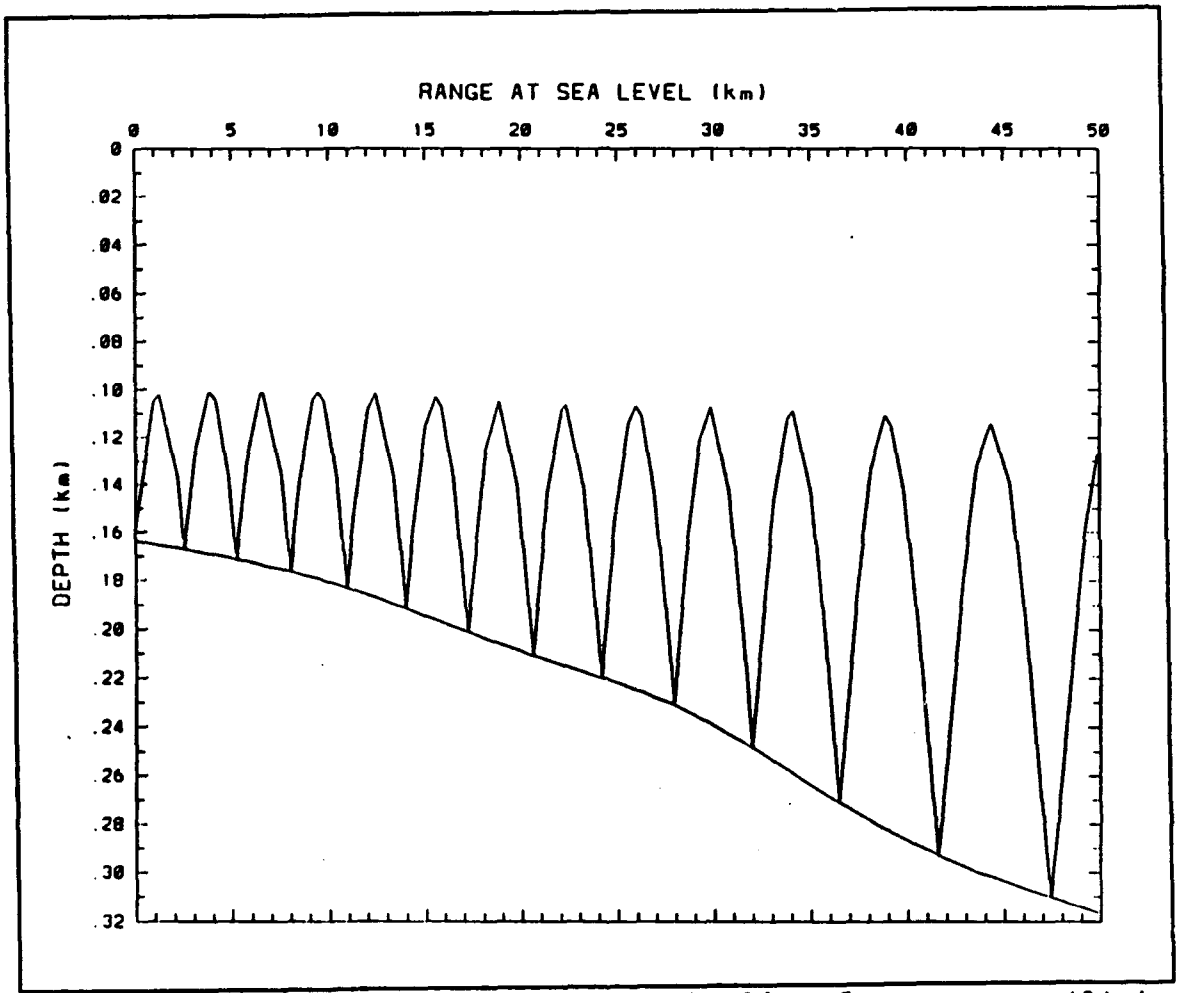

Figure 15 Ray path along a vertical slice from source (A) to receiver array (B) for a launch angle of 5.00°.

C. ARRIVAL STRUCTURE

For the 2500 rays traced between 0.00 and 25.00° various plots were made to study the arrival structure. The launch angle versus arrival depth plot is shown in Figure 18. The number of ray arrivals at any one receiver in the vertical array can be found by drawing a horizontal line across Figure 18 at the corresponding receiver depth. Eigenrays are given by the intersection of the horizontal line with the curve.

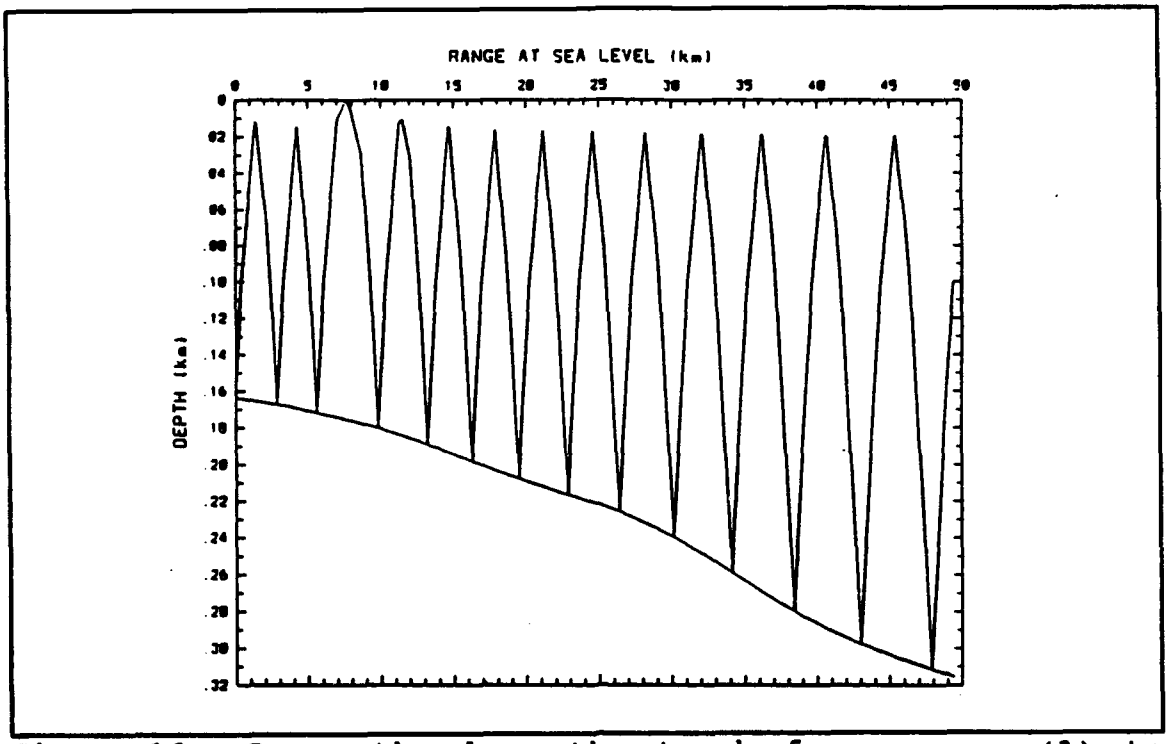

Figure 16 Ray path along the track from source (A) to hydrophone array (B) for a launch angle of 8.89°.

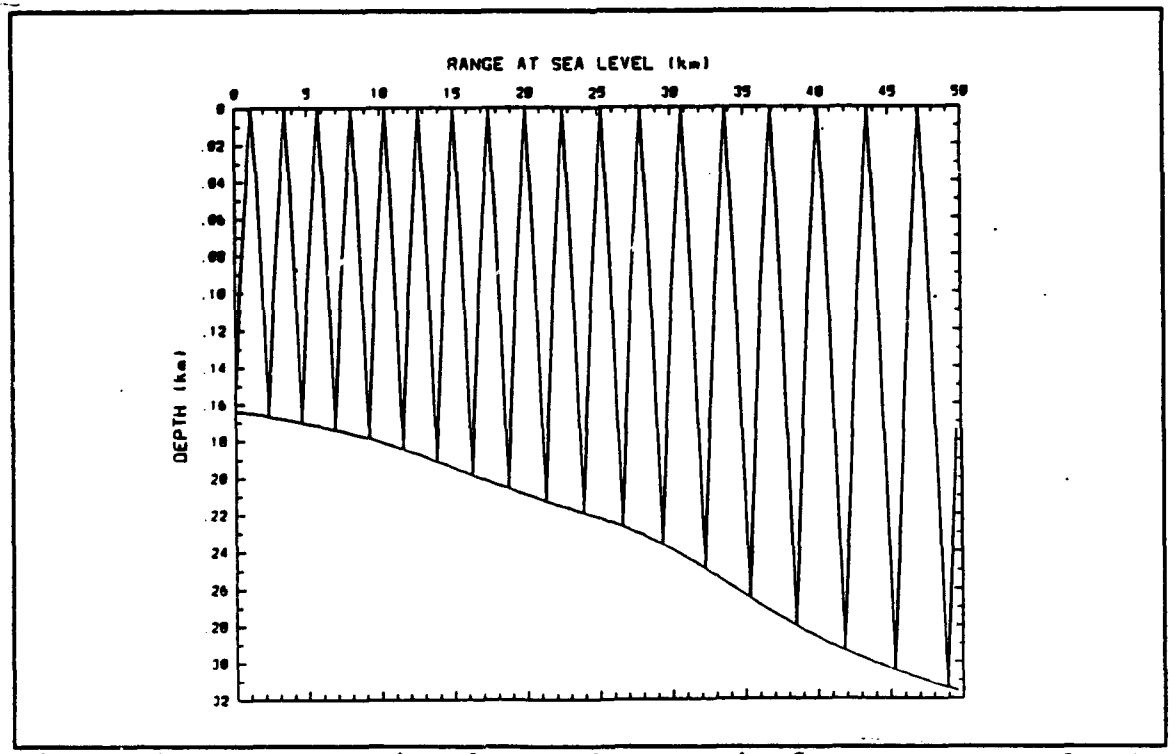

Figure 17 Ray path along the track from source (A) to hydrophone array (B) for a launch angle of 10.40°.

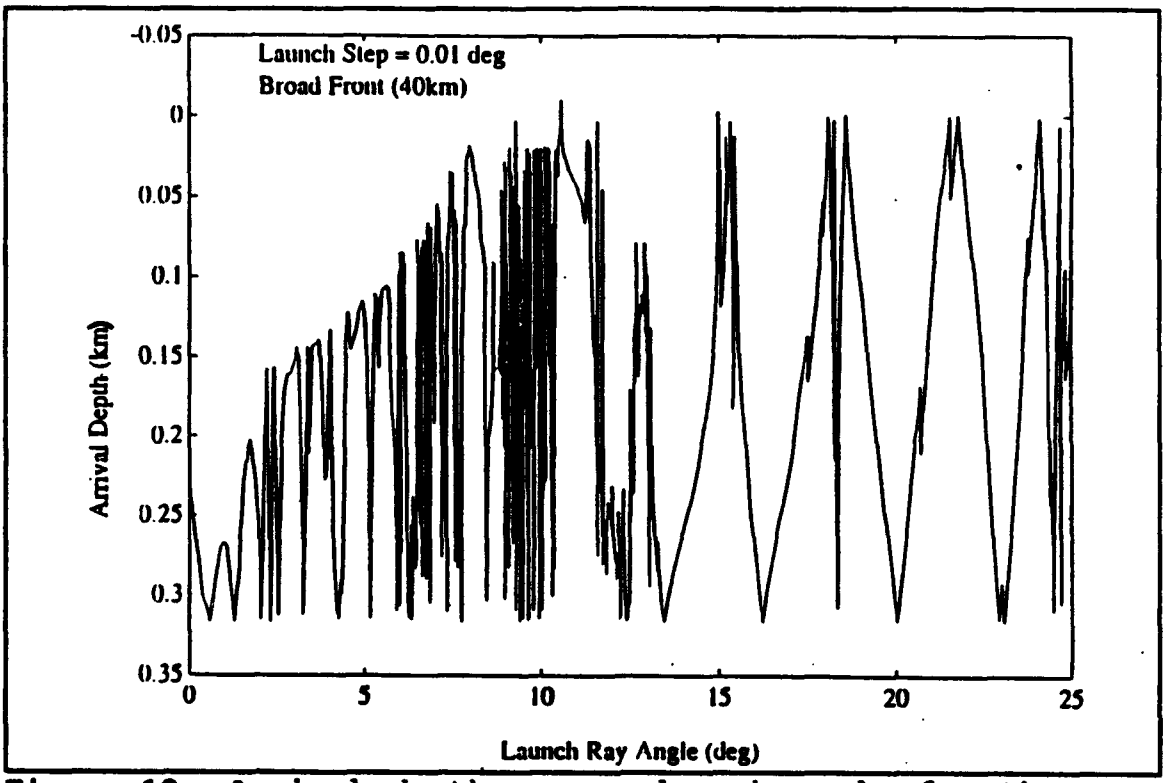

Figure 18 Arrival depth versus launch angle for the near bottom sound source (A).

Figure 18 shows more arrivals for receivers deeper than 150 m. The hydrophone array occupies the water column between 150 m and 300 m.

The arrival angle versus arrival depth plot is shown in Figure 19. It is interesting to note that the rays tend to arrive at some preferred directions independent of arrival depth, especially for arrival angles larger than 10°.

D. ARRIVAL TIME STRUCTURE

Examination of the arrival times of the acoustic rays reveals information about temporal resolvability of acoustic signals for tomographic inversion. To accomplish this

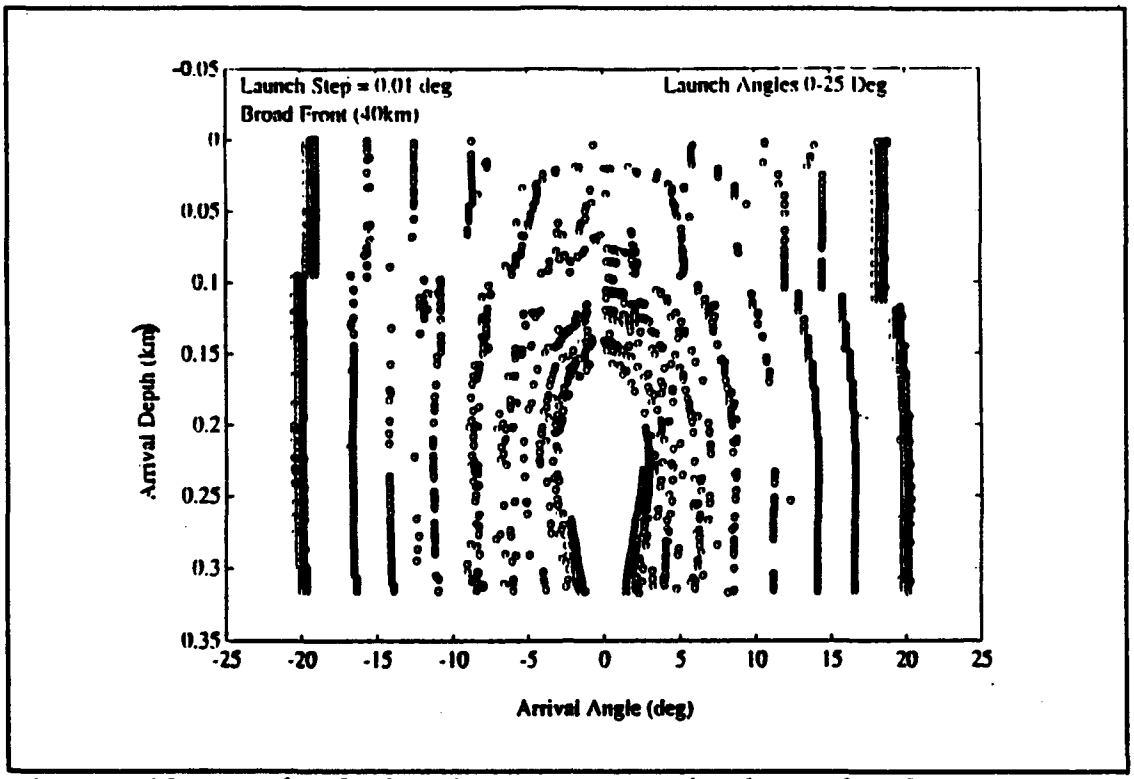

Figure 19 Arrival depth versus arrival angle for the near bottom sound source (A).

examination various plots were made of the 2500 rays launched between 0.00 and 25.00°.

The arrival time versus arrival depth plot is shown in Figure 20 for all rays launched. This plot indicates that the later acoustic arrivals are associated with a more tilted wave front. The figure also indicates that the duration of the multipath arrival structure is about 4 s.

The arrival time versus arrival angle plot is shown in Figure 21. In this plot one can see that the earliest arrivals come in at small grazing angles.

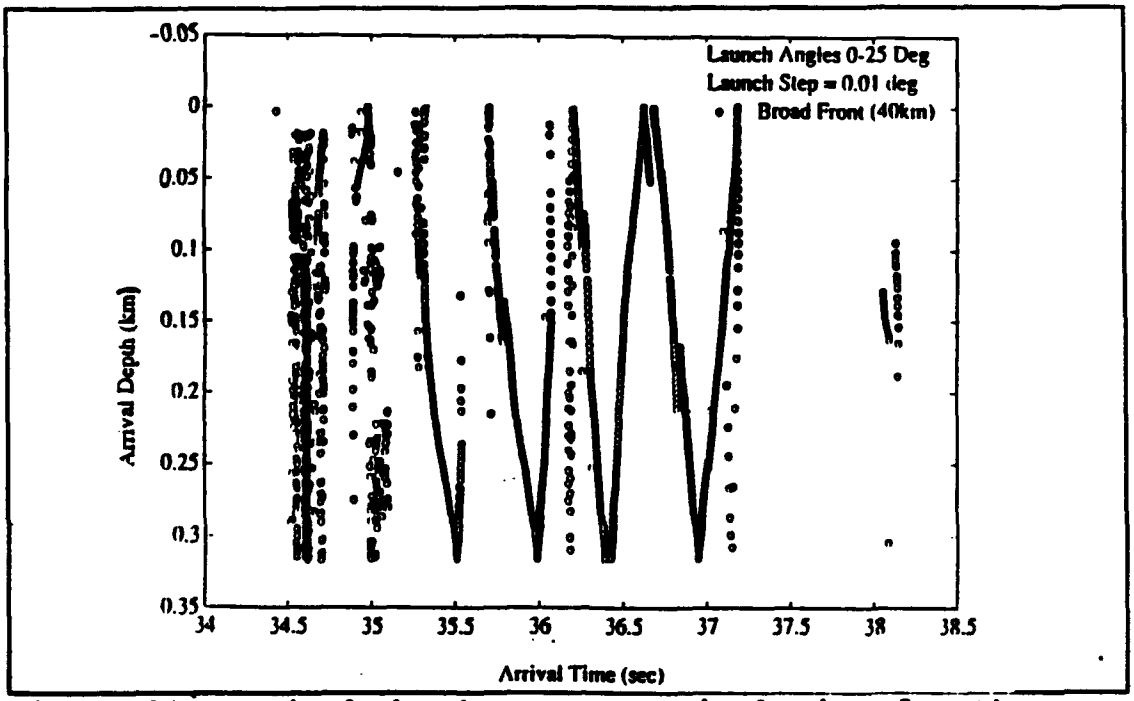

Figure 20 Arrival depth versus arrival time for the near bottom sound source (A).

The arrival time versus launch angle plot is shown in Figure 22. Consistent with Figure 21, this plot shows generally that rays with smallest launch angles arrive first.

E. RELATIVE AMPLITUDE

The ray amlitude of each ray that arrives at the vertical receiver surface 50 km away from the source can be computed using the transmission loss analysis discussed in Chapter III. The source level for the 224 Hz source (A) is 183 dB so the ray amplitude of the i'th ray, $RAMP_i$, may be computed as follows:

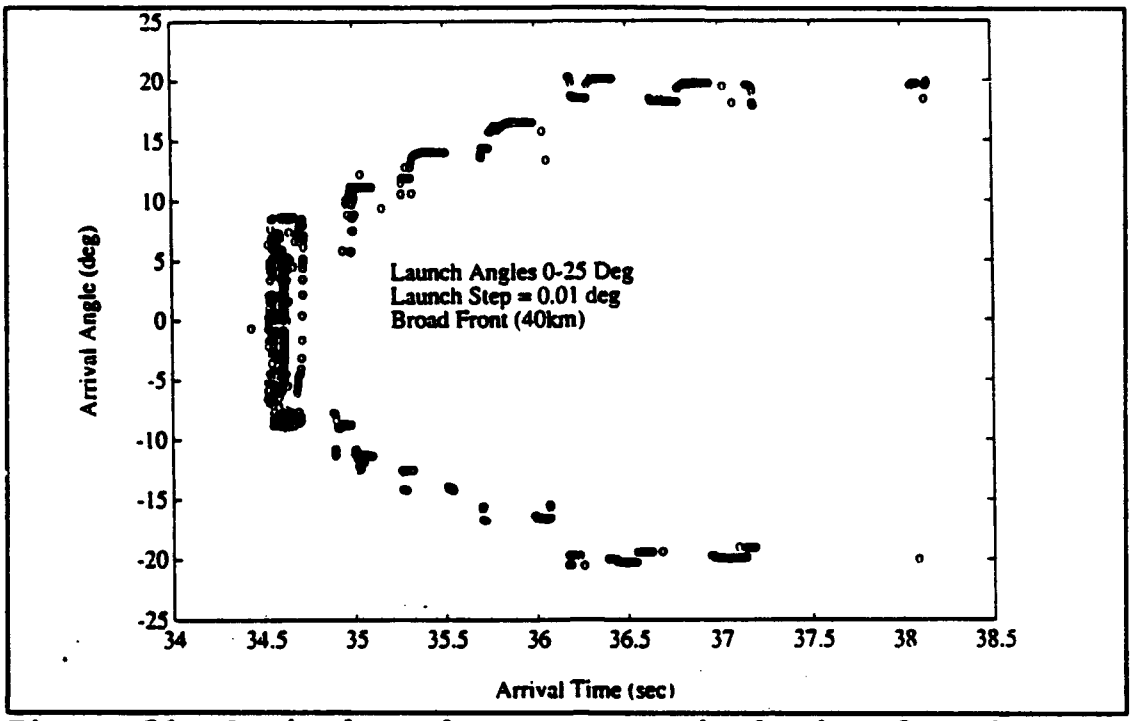

Figure 21 Arrival angle versus arrival time for the near bottom sound source (A).

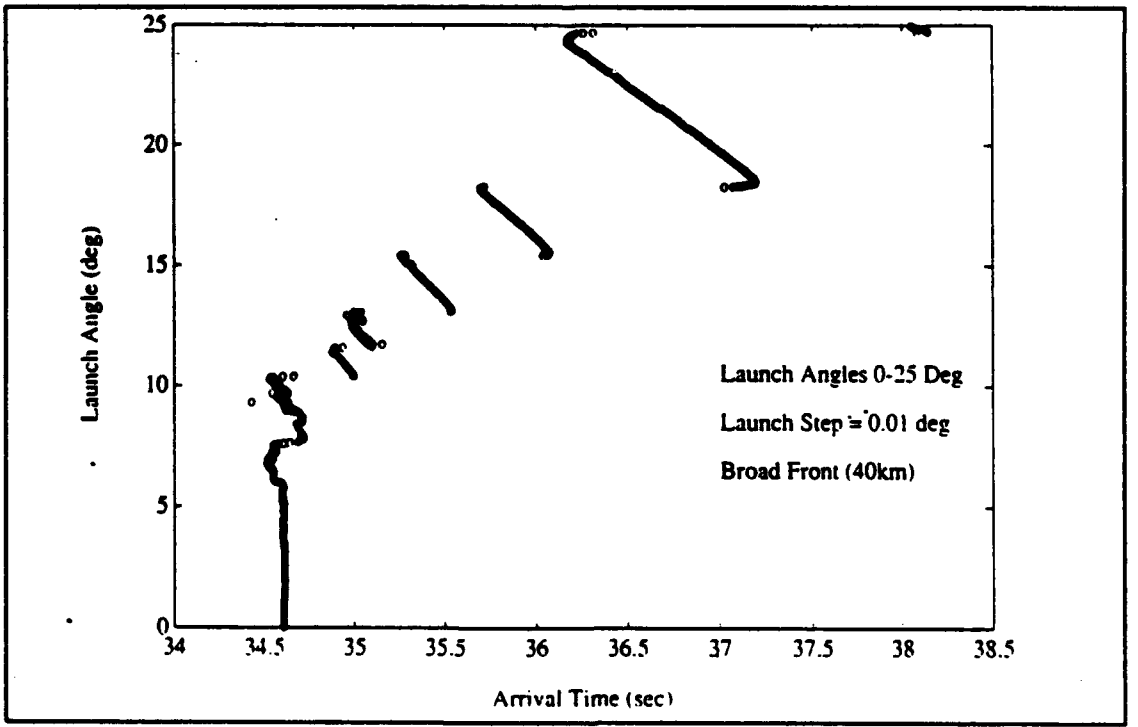

Figure 22 Launch angle versus arrival time for the near bottom sound source (A).

$$RAMP_i = 183 - TL_{tot_i} \quad (7)$$

where TL_{tot} is the total transmission loss of the i'th ray. The total transmission loss for each ray is a sum of the energy losses due to absorption, spreading and refraction, and surface/bottom interactions as discussed in Chapter III. Neglecting absorption (which is insignificantly small) then the total transmission loss TL_{tot} is

$$TL_{tot} = TL_{rl} + TL_{sfc} + TL_{bot} \quad (8)$$

Using Equations (2), (3), (4), and (8) the total transmission loss was calculated for each ray using 'cordat.f'. For simplification the bottom loss was taken to be a constant of 0.5 dB per bounce (i.e., an average over the 50 km track). Figures 23 and 24 are plots of the results of the transmission loss calculation for launch angles from 0 to 25° at 0.01° steps over the 50 km horizontal distance for sea states 3 and 5 respectively. These figures show a strong dependence of acoustic energy loss due to interactions with the sea surface. Clearly, ray angle and sea state acoustic energy losses are quite significant for launch angles ≥13° at a sea state of 5. The corresponding mean wave heights is 4 m. Due to the large surface losses, the horizontal axis of Figure 24 was intentionally terminated at 15°.

Figure 25 is a plot of transmission loss versus arrival angle of all rays arriving at the vertical receiver surface 50

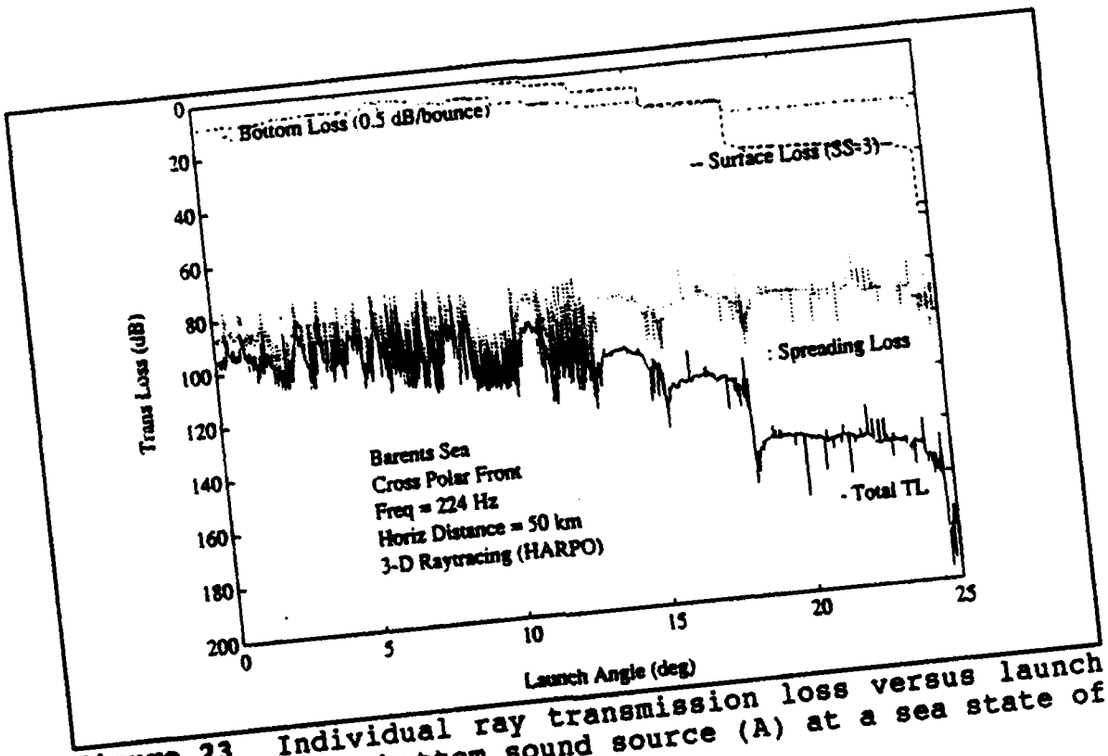

Figure 23 Individual ray transmission loss versus launch angle for a near bottom sound source (A) at a sea state of 3.

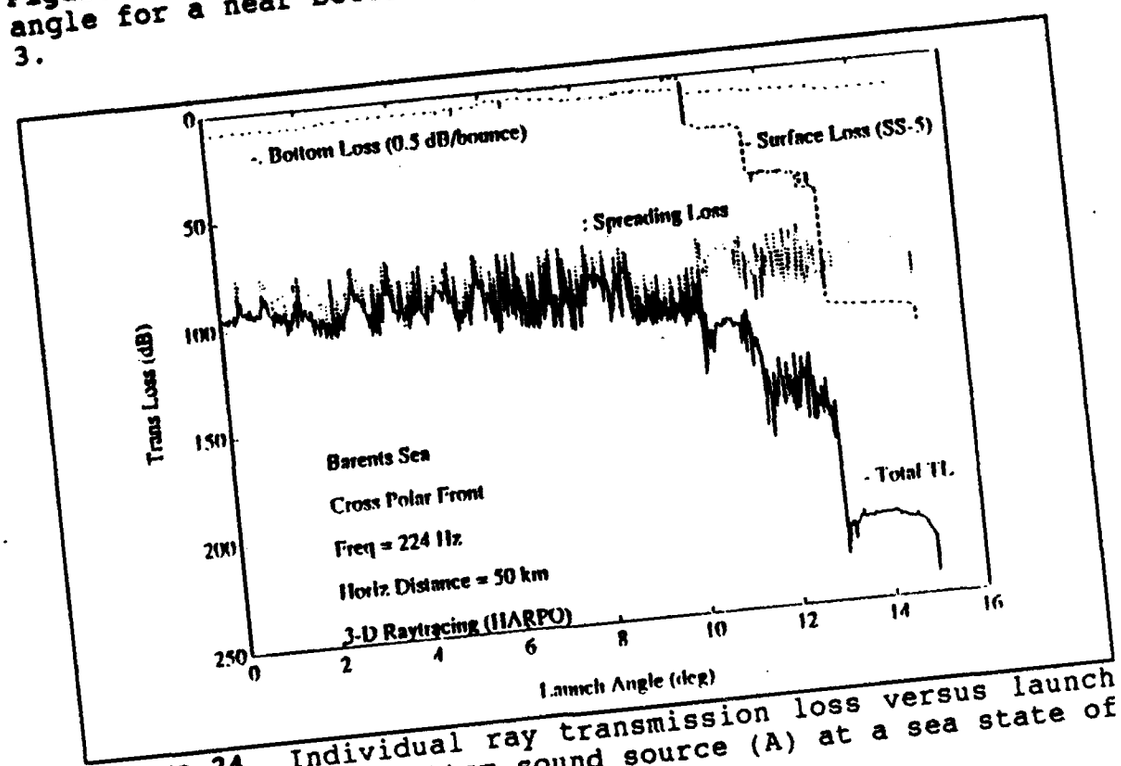

Figure 24 Individual ray transmission loss versus launch angle for a near bottom sound source (A) at a sea state of 5.

km away. It shows consistently that rays arriving at narrow angles will encounter the least transmission loss.

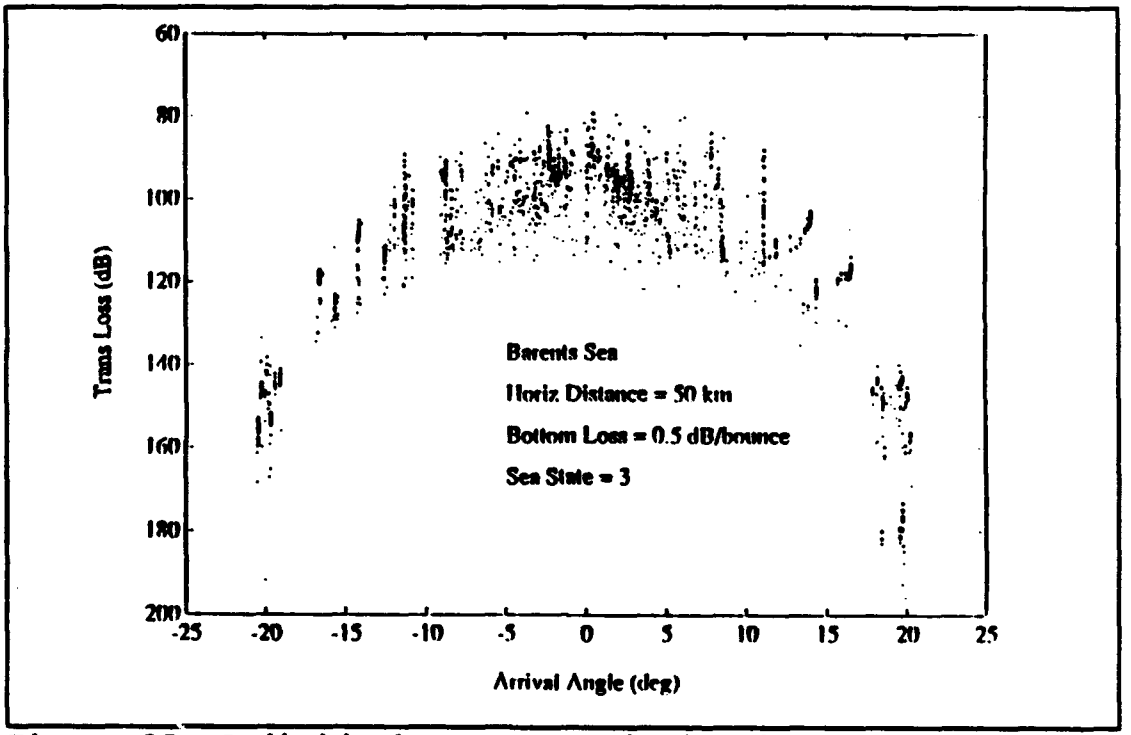

Figure 25 Individual ray transmission loss versus arrival angle for a near bottom sound source (A) at a sea state of 3.

A plot of ray amplitude versus arrival time of all rays arriving at the vertical receiver surface at a sea state of 3 is shown in Figure 26. This figure shows that the trend of the amplitude decreases with increasing ray arrival time. The later arrivals are associated with rays having larger launch and arrival angles and thus are subject to interaction with the sea surface.

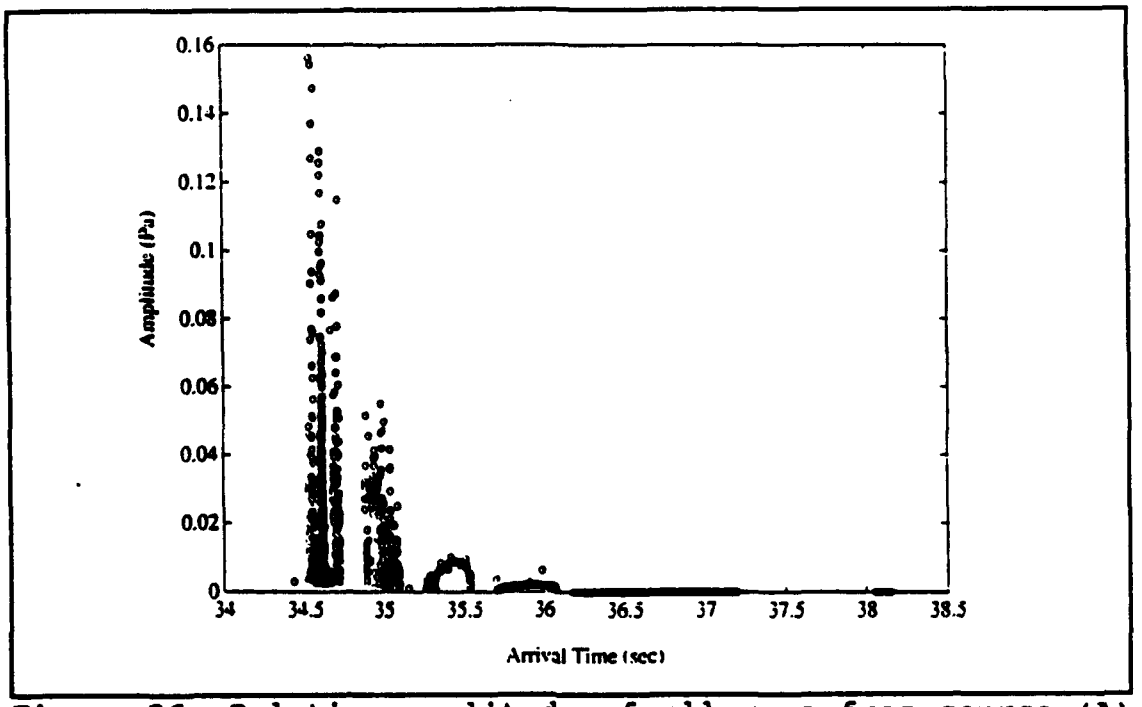

Figure 26 Relative amplitude of all rays from source (A) arriving at a vertical surface 50 km away at location (B) for a sea state of 3.

F. RESOLVABILITY ANALYSIS

1. Introduction

Two methods for resolving ray arrivals using a vertical array of 16 hydrophones with a 10 m interelement spacing were considered. The first method used the hydrophones as independent omnidirectional receivers with resolvability in time. The second method used all the hydrophones together as a plane wave beamformer with resolvability not only in time but also in arrival angle. Thus, in order to estimate the total number of resolvable ray arrivals analyses of time and angle separations of the

eigenrays were required. For the time analysis the eigenrays for each individual phone were compared to each other for a minimum time separation requirement. For the angle analysis the plane wave beam pattern of the line array was used to construct the beamformed arrival structure. The beamformed arrivals within each beam were then compared to each other for the same minimum time separation requirement as used for individual phones.

In addition to addressing resolvability it was also important to consider the accuracy of the travel time measurements. A resolved arrival may not be a useful datum for tomographic inversion if its travel time uncertainty σ_t is large. This uncertainty depends on the signal-to-noise ratio (SNR) associated with the individual arrival and can be estimated by considering the source level, ambient noise, and array gains from directivity and signal processing. Estimates of σ_t for both methods are included in this section. (Chiu, 1992)

2. Method I - Individual Hydrophones

a. Time Analysis

The investigation of resolvability in time was accomplished by comparing each ray arrival in time with its neighbor. If the separation in time was more than the width of the transmitted pulse then the ray was resolved from all other arrivals. The 224 Hz source signal has a bandwidth of

16 Hz. Therefore, the theoretical width of the received pulses is 1/16 Hz or 62.5 msec.

b. σ_t Analysis

To determine the σ_t's of the resolvable arrivals an SNR estimate was needed for each arrival. Using an approach similar to Spindel (1979) and from Miller (1992) the SNR estimate at the receiver for a single pulse used was:

$$SNR = RAMP - DNL + PCG + CAG \quad (9)$$

where RAMP is the ray amplitude (source level (SL) minus the total transmission loss (TL_{tot})), DNL is the detected ambient noise level, PCG is the pulse compression gain, and CAG is the coherent average gain. The SL for the 224 Hz source is 183 dB. TL_{tot} was computed for each ray as described in section E. DNL was computed from the following equation (Kinsler et al., 1982):

$$DNL = NSL + 10\log(BW) - DI \quad (10)$$

where NSL is the ambient noise level, BW is the band width of the transmitted signal and DI the array directivity index. NSL has many contributions including shipping, agitation of sea surface, bioacoustics, sea ice and seismic sources. Ambient noise due to shipping and the sea surface was only considered here. For medium shipping density and a sea state of 3, a NSL of 67 dB was found in Kinsler et al. (1982). The ambient noise information from Kinsler et al. (1982) is for

deep water and was used here as an approximation. Using a 16 Hz BW the DNL increased by 12 dB. For individual omnidirectional hydrophones DI = 0 so DNL = 67 + 12 = 79 dB.

The PCG and CAG are signal processing gains. Using equations from Spindel (1979) and the planned signal parameters for the 224 Hz source, the following values were calculated. With a kernel sequence of 63 digits the PCG is 10log(63) or 18 dB. With 30 repetitions of the sequences, a CAG of 10log(30) or 15 dB was obtained.

According to Spindel (1979) a reception with a SNR of about 20 dB is desired in order to clearly distinguish multipath arrivals from noise and to reduce the error in travel time estimation to a figure adequate for tomographic inversion. Since the error is approximately given by (Spindel, 1979)

$$\sigma_t = \frac{d}{\sqrt{SNR_{raw}}} \qquad (11)$$

a 20 dB SNR and a pulse width of d = 62.5 ms yields a σ_t of 6.3 ms. Figure 27 provides a plot of SNR verses σ_t for two values of d.

Solving Equation (9) for RAMP with SNR ≥ 20 dB, DNL = 79 dB, PCG = 18 dB and CAG = 15 dB yielded a RAMP ≥ 66 dB. The implication was that resolvable arrivals with RAMP ≥ 66 dB have travel time uncertainty ≤ 6.3 ms. These strong arrivals

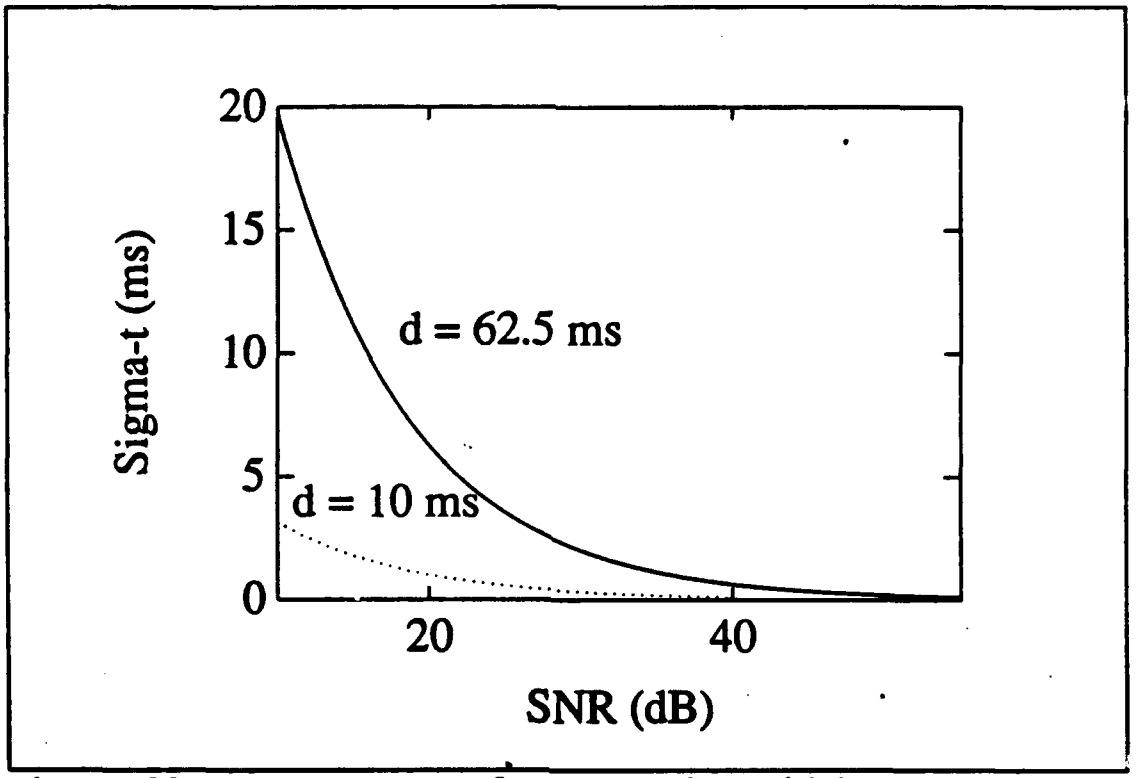

Figure 27 SNR versus σ_t for two pulse widths. The 224 Hz source has a d of 62.5 ms whereas the 400 Hz source has a d of 10 ms.

would give high quality travel time data for tomographic inversion.

c. Resolvable Rays

To assist in identifying the resolvable ray arrivals a table summarizing all of the eigenrays for each of the sixteen hydrophones was compiled using a MATLAB (The Mathworks, Inc, 1989) computer program 'resanl.m' (Appendix A). The table is given in Appendix B and the list is in order of increasing travel time. For all the rays traced to a range of 50 km, the rays that arrived within 1/2 wavelength of each hydrophone were picked as eigenrays.

Each arrival was then compared to its adjacent arrival in time. Arrivals with greater than 62.5 ms separation to the arrivals before and after were considered resolvable in time and are annotated with a 'R' next to the arrival time in the table in Appendix B.

The arrivals resolvable in time were then inspected for adequate σ_t. Arrivals with a $\sigma_t \leq 6.3$ ms corresponding to a RAMP $\geq$ 66 dB were considered as having adequate travel time accuracy (see Sec. F.2.b). Inspection of the table in Appendix B yielded 42 resolvable arrivals that met this criterion. Table III provides a summary of these 42 arrivals.

Figure 28 shows the simulated arrival structure at the eighth hydrophone from the top of the vertical hydrophone array. This phone is located at a depth of 220 m. The plot was created using the MATLAB program 'hyd8beam.m' (Appendix A). The figure shows a total of 27 ray arrivals at this hydrophone. The arrivals resolvable in time and have a $\sigma_t \leq$ 6.3 ms are annotated by R17, R18, R19, and R20. The numbers correspond to the numbering in Table III.

Table III INDIVIDUAL HYDROPHONE RESOLVABLE RAY ARRIVALS WITH $\sigma_t \leq 6.3$ ms

No.	Launch Angle (deg)	Arrival Angle (deg)	Hyd No.	RAMP (dB)	σ_t (ms)	Arrival Time (s)
1	11.49	-10.7803	1	82.0474	1.0	34.8858
2	12.74	+10.6750	1	74.9298	2.2	34.9759
3	14.83	+13.4689	1	72.2280	3.1	35.3221
4	11.51	-11.0427	2	80.6225	1.2	34.8846
5	12.65	+10.8853	2	82.0131	1.0	34.9881
6	7.78	+8.0024	3	70.2431	3.9	34.7172
7	11.52	-11.1197	3	76.0964	2.0	34.8853
8	14.74	+13.7346	3	76.0389	2.0	35.3332
9	8.62	+ 8.2148	4	85.9763	0.6	34.7075
10	11.53	-11.2162	4	78.5257	1.5	34.8852
11	14.60	+13.9993	5	77.0836	1.8	35.3518
12	11.54	-11.3108	6	75.0689	2.2	34.8864
13	14.53	+13.9967	6	76.7759	1.8	35.3615
14	11.55	-11.3583	7	76.8271	1.8	34.8868
15	14.45	+14.0910	7	76.9178	1.8	35.3719
16	13.10	-14.2447	7	66.9958	5.6	35.5378
17	8.50	+8.4845	8	79.5235	1.3	34.7140
18	11.63	-11.3509	8	75.6184	2.1	35.0917
19	14.38	+14.0919	8	77.3569	1.7	35.3814
20	17.01	+16.5614	8	66.5519	5.9	35.8676
21	7.68	-8.3897	9	78.1157	1.6	34.6960
22	11.56	-11.3548	9	75.7405	2.0	34.8880
23	11.61	-11.3504	9	73.5302	2.6	35.0963
24	14.29	+14.1118	9	78.1330	1.6	35.3934
25	16.92	+16.5555	9	67.5459	5.2	35.8819
26	14.18	+14.1081	10	79.2232	1.4	35.4087
27	13.13	-14.2383	10	73.2166	2.7	35.5376
28	16.83	+16.5507	10	66.6980	5.8	35.8963
29	14.06	+14.0723	11	78.8534	1.4	35.4251
30	13.15	-14.1958	11	72.7723	2.9	35.5364
31	16.72	+16.6531	11	66.8359	5.7	35.9145
32	7.71	-8.3325	12	79.3256	1.4	34.6980
33	13.94	+14.0684	12	78.8688	1.4	35.4415
34	13.18	-14.1533	12	72.5735	2.9	35.5344
35	16.65	+16.5382	12	66.1088	6.2	35.9256
36	7.72	-8.3059	13	83.3586	0.9	34.6982
37	13.83	+14.0650	13	78.6391	1.5	35.4564
38	13.19	-14.1535	13	70.6539	3.7	35.5337
39	16.57	+16.5326	13	66.5419	5.9	35.9380
40	7.74	-8.2335	15	80.9442	1.1	34.6987
41	12.10	-11.2190	15	72.4460	3.0	35.0256
42	8.45	-8.3734	16	74.1797	2.4	34.7021

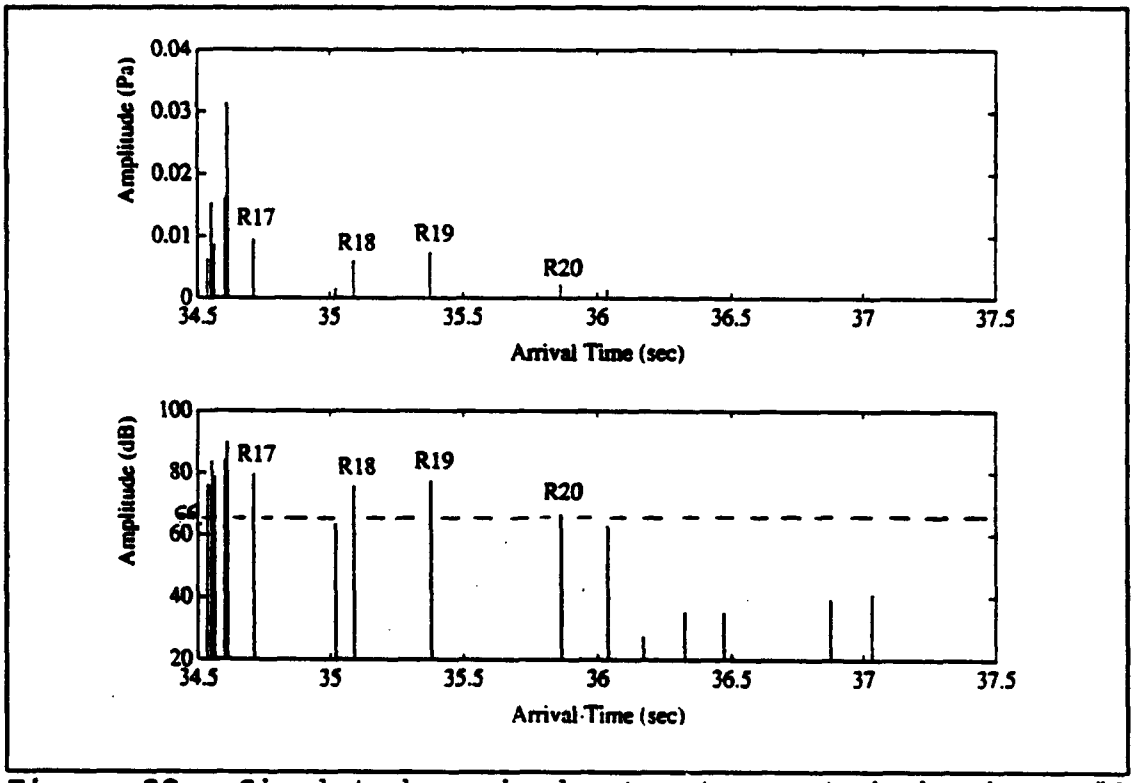

Figure 28 Simulated arrival structure at hydrophone #8 (depth 220 m) at a sea state of 3.

3. Method II - Plane Wave Beamformer

If the vertical array of 16 hydrophones is used as a plane wave beamformer then angle, in addition to time, becomes another parameter available for resolving arrivals. To determine the resolution in angle, the plane wave beamforming method of Ziomek (1985) for a linear array of equally spaced point hydrophones was used. The far-field directivity function or beam pattern of the linear array can be computed using a Fast Fourier Transform (FFT) computer algorithm.

Using a MATLAB computer program 'beampat.m' (Appendix A) incorporating such FFT algorithms, the theoretical beam pattern of the hydrophone array was computed.

Figure 29 shows the beam pattern of the vertical receiver array with the beam steered to 20° off broadside. The corresponding beam width defined by the 3 dB down point (0.7071 normalized directivity) is about 3.0°. The beam pattern steered to broadside was found to be about 2.5° wide. The grating lobe for this array appears 48° away from the steered beam so should not cause a problem for arrivals within 20° of broadside.

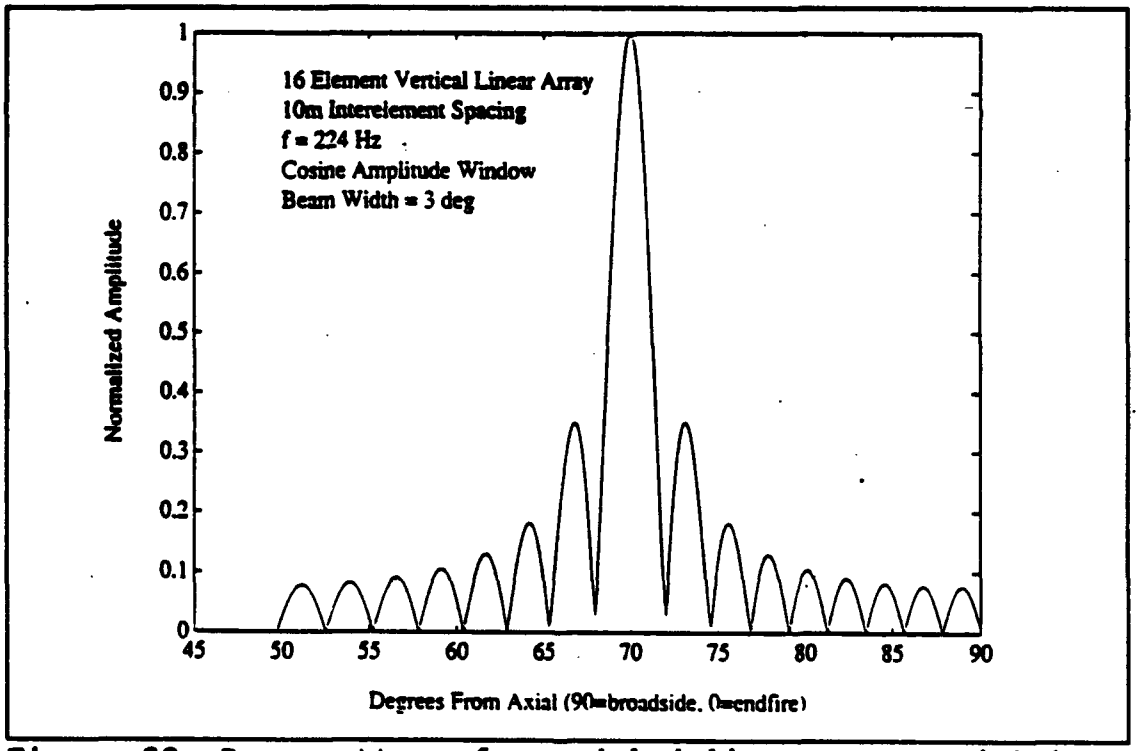

Figure 29 Beam pattern for modeled linear array with beam steered to 20 degrees off broadside.

To assist in identifying the resolvable beam formed arrivals, a table was compiled using 'resanl.m'. This table is

presented in Appendix C. The method used here was similar Method I for individual hydrophones with the following exceptions. Following extraction of all eigenrays arriving within 1/2 wavelength of each hydrophone, the eigenrays were separated into fifteen groups associated with their arrival angles. The 15 groups are associated with 15 nonoverlapping angular sectors. Each angular sector is three degrees wide. The three degree width was based on the beam pattern analysis discussed above. The limiting arrival angles defining these sectors are given at the end of the table in Appendix C.

Similarly, the beamformed ray arrivals were compared in time for a 62.5 ms separation. The rays meeting this time separation criterion within each angular sector are annotated with an 'R' next to the arrival time in the table in Appendix C.

For the σ_t analysis, the same parameter values for PCG, CAG and BW as before are used here. The only difference is that a directivity gain was added. The directivity index (DI), according to Ziomek (1985), may be approximated by 10Log(number of hydrophones). For 16 phones it is 12 dB. Thus from Equation (10), DNL is now 67 + 12 - 12 = 67 dB. Using Equation (9), this results in a minimum RAMP requirement of 54 dB for resolvable arrivals to attain a σ_t smaller than 6.3 ms.

By inspection of the table in Appendix C, 11 resolvable beamformed arrivals that also have an adequate σ_t of 6.3 ms or

less (i.e., with RAMP ≥ 54 dB) were obtained. Table IV provides a summary of these 11 arrivals. Seven of these arrivals are unique to the 42 arrivals determined using Method I.

Table IV PLANE WAVE BEAMFORMED RESOLVABLE ARRIVALS WITH σ_t ≤ 6.3 ms

No.	Launch Angle (deg)	Arrival Angle (deg)	Sector	RAMP (dB)	σ_t (msec)	Arrival Time (sec)
1	15.59	-16.5311	2	62.4927	2.4	36.0685
2	15.41	-14.2058	3	55.6390	5.2	35.2809
3	13.10	-14.2447	3	64.9958	1.8	35.5378
4	11.56	-11.3548	4	74.7405	0.6	34.8880
5	13.02	-12.2672	4	73.3231	0.7	35.0269
6	11.61	-11.3504	4	73.5302	0.7	35.0963
7	11.71	+11.1330	12	67.3867	1.3	35.1003
8	14.83	+13.4689	12	72.2280	0.8	35.3221
9	13.55	+14.0571	13	77.6399	0.4	35.4936
10	17.21	+16.3884	13	64.2685	1.9	35.8375
11	16.35	+16.5172	14	65.0820	1.8	35.9726

Figure 30 shows a total of three arrivals in angular sector 13. Arrivals resolvable in time within this sector which have a σ_t ≤ 6.3 ms are annotated with 'R9' and 'R10'. The numbers correspond to the numbers in Table IV.

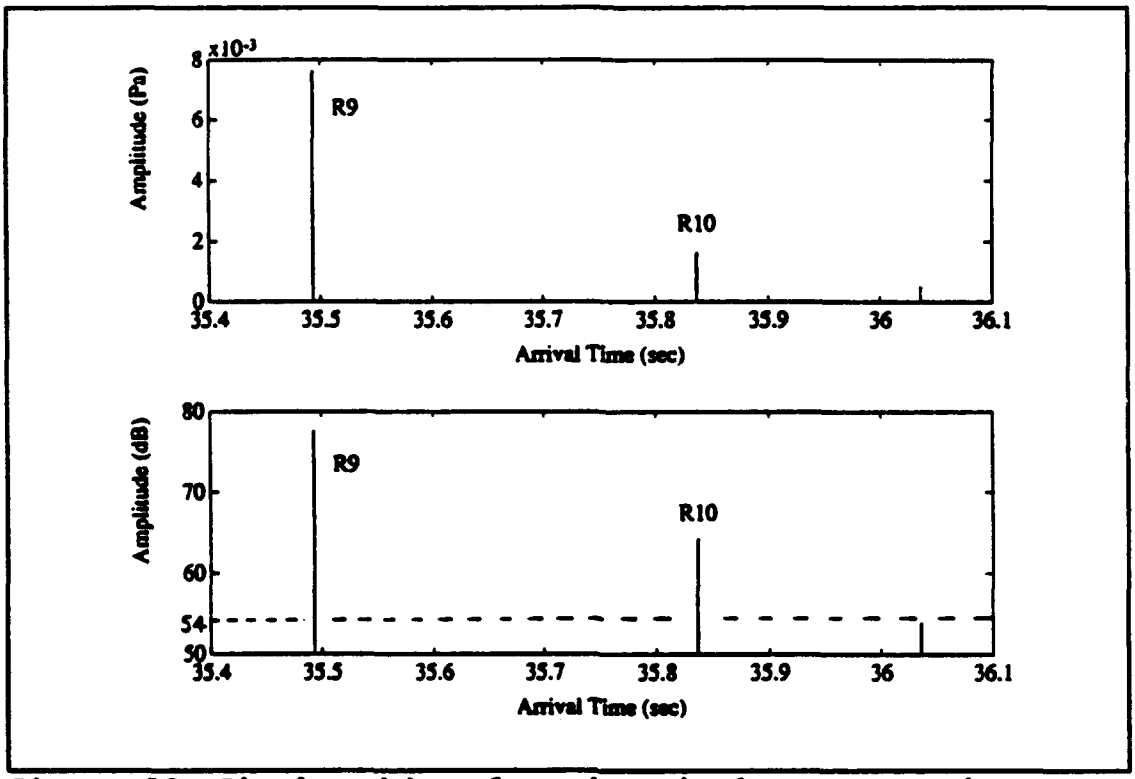

Figure 30 Simulated beamformed arrival structure in sector 13 (+13.5° grazing angle). R9 and R10 are resolvable and have $\sigma_t \leq 6.3$ ms.

VI. CONCLUSIONS

The objective of this thesis was to examine the arrival structure of the planned tomographic transmissions in the upcoming BSPFEX using computer simulation. This study examined the resolvability of those rays that intersected a vertical hydrophone array 50 km from a near bottom source. Conclusions are:

1. The duration of the multipath arrival structure is about 4 s.

2. The arrival structure can be grouped into the following two distinctive regimes:

a. Early Arrivals (0-600 ms)

(i) These arrivals have angles less than 10°. They exhibit the least transmission loss due to minimum interactions with the sea surface.

(ii) They exhibit mode-like properties. Large number of simultaneous ray arrivals are found. The investigation of the resolvability of modes will require a simulation using full-wave acoustic models based on parabolic equation or coupled mode methods.

(iii) Fewer ray arrivals are resolved in this regime.

b. Late Arrivals (600-4000 ms)

(i) These arrivals have angles greater than 10°. They exhibit higher transmission loss due to greater interactions with the surface. For sea states ≥5 (i.e., mean wave heights ≥ 4 m) little signal amplitude is expected of rays launched at ≥ 13°.

(ii) Individual ray arrivals are separated more in time.

(iii) More ray arrivals are resolved in this regime.

3. One to four accurate ray arrivals are resolvable per single hydrophone. Accuracy is measured by σ_t and a requirement of $\sigma_t \leq 6.3$ ms is used for extraction of the accurate arrivals.

4. A total of 42 ray arrivals with the required amplitude are resolvable from the sixteen individual hydrophones. All of these arrivals come within the first 1500 ms in the multipath arrival structure.

5. Seven additional, non-redundant, ray arrivals with the required amplitude are resolvable through plane wave beamforming using the 16 hydrophones. All of these arrive within two 6 degree bands of +11 to +17° and -11 to -17°.

LIST OF REFERENCES

Clay, C.S. and H. Medwin, Acoustical Oceanography, John Wiley & Sons, New York, 1977.

Chiu, C.S., Department of Oceanography, Naval Postgraduate School, Monterey, CA., Personal communication, 1992.

Blodgett, M.L., M. Bradley, J. Hanna, R. Keenan, D. Rubenstein, ICECAP: Arctic models and data bases for the Navy standard tactical desktop computer, SAIC-86/1906, 1987.

Barents Sea Polar Front Group, A.J. Plueddemann, Experimental Plan Barents Sea Polar Front Experiment August 1992, May 1992. (Bourke, R.H., C.S. Chiu, J.F. Lynch, J.H. Miller R.D. Muench)

Devore, J.L., Probability and Statistics for Engineering and the Sciences, Brooks/Cole Pub. Co., Monterey, CA., 1987.

Dickson, R.R., L.S. Midttun, and A.I. Mukhin, The hydrographic conditions in the Barents Sea in August-September 1965-1968, in International 0-Group Fish Survew in the Barents Sea Cooperative Research Report ser. A, no. 18, edited by O. Dragesund International Council for the Exploration of the Sea, Charlottenlund Slot, Denmark, 3-24, 1970.

Eldholm, O. and M. Talwani, Sediment distribution and structural framework of the Barents Sea. Geological Society of America Bulletin, 88, 1015-1029, 1977.

Emblidge, J.M., A Feasability Study of Ocean Acoustic Tomography in the Barents Sea, Naval Postgraduate School Thesis, 1991.

Johannessen, O.M. and L.A. Foster, A note on the topographically controlled oceanic polar front in the Barents Sea, J. Geophysical Reasearch, 83, 4567-4571, 1978.

Jones, R.M., J.P. Riley and T.M. Georges, HARPO a versatile three-dimensional hamiltonian ray-tracing program for acoustic waves in an ocean with irregular bottom., Wave Propagation Laboratory, NOAA, Boulder, Colorado, 457 pp.

Keenan, R. E., Science Applications International Corporation, Mashpee, MA., Personal communication, 1992.

Kerr, G., Data base description for low frequency bottom loss (LFBL), OAML-DBD-12B, 1990.

Kinsler, L., A. Frey, A. Coppens, and J. Sanders, Fundamentals of Acoustics, fourth edition, John Wiley & Sons, N.Y., 1982.

Klenova, M.V., Barents Sea and White Sea, in The Encyclopedia of Oceanography, edited by Faibridge, R.W., Reinhold Publishing Corp., N.Y., 95-101, 1966.

Lighthill, M.J., Waves in Fluids, Cambridge Univ. Press, sec 4.5. 1978.

Loeng, H., Features of the physical oceanographic conditions of the Barents Sea, (In press), 1991.

Miller, J.H., Department of Electrical and Computer Engineering, Naval Postgraduate School, Monterey, CA, personal communication, 1992.

Munk, W. and C. Wunsch, Ocean acoustic tomography: a scheme for large scale monitoring, Deep Sea Res., Part A, 26, 123- 161, 1979.

NAVOCEANO Publication SP-279-2, U.S. Naval Oceanographic Office, NSTL Mississippi, 1989.

Newhall, A.E., J.F. Lynch, C.S. Chiu, and J.R. Daugherty, Improvements in three-dimensional raytracing codes for underwater acoustics, Computational Acoustics, Vol 1, 1987.

Norsk Polarinstitutt, Bathymetry Barents Sea, Chart No. 7421, Oslo, Norway, 1986.

Spindel, R.C., An Underwater Acoustic Pulse Compression System, IEEE Transactions on Acoustics, Speech, and Signal Processing, Vol. ASSP-27, No. 6, 1979.

The Mathworks, Inc., MATLAB for SUN Workstations User's Guide, South Natick, MA, 1989.

Tolstoy I. and C.S. Clay, Ocean Acoustics, McGraw-Hill, New York, 1966.

Ziomek, L.J., Underwater Acoustics A Linear Systems Theory Approach, Academic Press, inc., San Diego, 1985.

APPENDIX A: LIST OF EXTERNAL PROGRAMS

The following programs were developed or extensively modified during the course of this research. They include:

1. cordat.f - Path and time correction for a vertical receiver and TL calculation.
2. tgridin.f - HARPO topography input generator.
3. gridin.f - HARPO sound speed profile input generator.
4. beampat.m - vertical hydrophone array beam pattern generator.
5. resanl.m - Ray resolvability analysis table generator.
6. hyd8beam.m - Arrival structure plotting program including pulse shape generation.

```
c                                   cordat.f
c
ccccccccccccccccccccccccccccccccccccccccccccccccccccccccccccccccccccccccccccc
c
c   Written by: J. Mark Elliott, LCDR/USN, NPS, Dec  1991
c
ccccccccccccccccccccccccccccccccccccccccccccccccccccccccccccccccccccccccccccc
c   Modified 23 Jan 92 by J.M. Elliott to correct for total ray travel time
c to the vertical receiver surface.
c
c   Modified 27 Jan 92 by J.M. Elliott to calculate Transmission Loss due to
c spreading.
c
c   Modified 21 Feb 92 by J.M. Elliott account for trans loss due to bot and
c surface reflections.
c
c   Modified 20 Apr 92 by J.M. Elliott to count the no of surface, bottom,
c and turning point interactions.
ccccccccccccccccccccccccccccccccccccccccccccccccccccccccccccccccccccccccccccc
c
c   Purpose:
c   This program extacts from  RAYSET (HARPO output file) the last line of
c data for a particular launch ray corresponding to the first event (ray point)
c after passing max range (W28 of DINP). Then this is backed up the ray path
c geometrically to compute the height above msl and arrival time for a ray
c crossing a vertical recvr surface at max r.
c   This program also computes the fol: Transmission Loss due to spreading,
c surface interactions, bottom interactions; and counts the number of surface
c interactions, bottom interactions, and turning points.
c   This program will skip rays that are trapped above the surface.  This
c problem was later found to be mitigatied but not eliminated by reducing W44
c (initial integration step size) from .1km to .05km or less.
c
ccccccccccccccccccccccccccccccccccccccccccccccccccccccccccccccccccccccccccccc
c
c   Define the 10 Columns of RAYSET data output, max range specified in
c DINP W28 (rmax), and initial launch elevation angle specified in DINP
c W15 (ths), and the step in launch ele angle W17 as dths.
c    Also six indexes are used i, tlbot, sloss, botcnt, srfcnt, and tpcnt.
c The index i is to be used in the spreading trans loss calc.  The indexs
c tlbot and sloss are used to measure the TL due to bottom and surface
c reflections respectively that the ray makes along its total path.
c The number of bottom, surface and turning points are counted by 'botcnt',
c 'srfcnt',and 'tpcnt' respectively.

      real*4  f(10),ths,thr,r,zp,dum1,t,tlbot,sloss,tlt,z,rp,ds,dt,tp,
     a        cave1,cave2,z2,rmax,rmax2,thr2,h,a11,a12,a21,a22,b1,b2,
     a        w,zi,ri,tlspn,tlspo,theta,sigma,k,botcnt,srfcnt,tpcnt
      rmax = 50.
      ths = 0.00
      dths = 0.01
      i = 1
      tlbot = 0
      sloss = 0
      botcnt = 0
      srfcnt = 0
```

```
      tpcnt = 0

c   Define output files:
c      raysetX_Y = rayset data from harpo output, launch angles from X to Y
c      f3.dat    = launch angle vs arrival depth output
c      f3time.dat= arrival time vs arrival depth output
c      f3tl.dat  = launch angle vs transmission loss due to spreading
c      f3ttl.dat = arrival time, total trans loss (dB)
c      f3res.dat = ths, thr, z, tpcnt, srfcnt, botcnt, ramp, t

      open(unit=10,file='rayset0_10',status='old',form
     A    ='formatted')
c       open(unit=20,file='f3.dat',status='new',form='formatted')
c      open(unit=30,file='f3time.dat',status='new',form='formatted')
c     open(unit=40,file='f3tl.dat',status='new',form='formatted')
      open(unit=50,file='f3ttl.dat',status='new',form='formatted')
      open(unit=60,file='f3res.dat',status='new',form='formatted')

c
c skip the first 7 lines of RAYSET
c
      DO 15  i = 1,7
         read(10,*)
  15  continue
c
c
c  Read in the 10 columns of RAYSET  data and call the data n for new
c     Define RAYSET columns:
c        f(1) = earth radius to mean sea level (msl) in km
c        f(2) = earth radius to ocean floor in km
c        f(3) = horiz range to ray point along msl in km
c        f(4) = earth radius to ray point in km
c        f(5) = ray phase angle ?
c        f(6) = ?
c        f(7) = phase arrival time in sec
c        f(8) = local sound speed in m/s
c        f(9) = ?
c        f(10)= local ray elevation angle in deg

   1  read(10,*)f(1),f(2),f(3), f(4),f(5),f(6), f(7),f(8),f(9),f(10)
      f1n = f(1)
      f2n = f(2)
      f3n  = f(3)
      f4n  = f(4)
      f5n  = f(5)
      f6n  = f(6)
      f7n  = f(7)
      f8n  = f(8)
      f9n  = f(9)
      f10n  = f(10)
c
c
c   Look for the last line -999 flag of each launch ray data set, otherwise
c (else) call the new data line the old (fxo) data, compute surface
c and bottom trans loss, and then look at the next data line in RAYSET:
      if(f1n.lt.-900.)then
```

```
         go to 2
        end if
c
c    Compute bottom/surface interaction trans loss.  Let each bottom ref
c equal 0.5 dB of loss.  For surface loss compute the trans loss
c (sloss) using  gaussian scattering theory (Clay & Medwin, 1985):
c       Define:
c         zp = arrival ht above msl in km
c         dum1 = arrival ht above bottom in km
c         sloss = -20*log10(abs(exp(-2*(k**2)*(sigma**2)*(sin(f(10)))**2)))
c         k = wavenumber at surface using avg surf sound speed of c(m/s) and
c              frequency f (Hz)
c           = 2*pi*f/c = 2*pi*224/1465 = 0.9607
c         sigma = rms wave ht in meters( 0.7071 used for sea state 3)
c               = 0.0707 for sea state 1
c               = 0.7071 for sea state 3
c               = 2.8284 for sea state 5
c         f(10) = graze angle assumed to be appx = local ele angle f10
c          botcnt = no of bottom interactions
c          srfcnt = no of surface interactions
c          tpcnt = no of turning points

c First test to see if the RAYSET data line was a repeat by checking range f3,
c and if so skip the computation and repeat (cause of this problem is unk):
        if(f3n.eq.f3o)then
         go to 1
        end if
        zp = f4n - f1n
        dum1 = f4n - f2n
        if(abs(dum1).le.0.00009)then
         tlbot = tlbot + 0.5
         botcnt = botcnt + 1
        end if
c       k = 0.9607
c        sigma = 2.8284
        if(abs(zp).le.0.00009)then
          theta = sin(f10n*3.14159/180)**2
c          sloss = -20*log10(abs(exp(-2*(k**2)*(sigma**2)*theta))) +  sloss
c Can't get program to compute sloss in this form, cuse unk, must use fol:
          sloss = -20*log10(abs(exp(-0.9229*theta))) + sloss
          srfcnt = srfcnt + 1
        end if
c  Now count the no of turning points.  Since the method I use just counts the
c no of times grazing angle changes sign I subtract out the sign changes due to
c surface and bot bounces at the end of this program just before the write
c statement:
        if(abs(f10o-f10n).ge.abs(f10o))then
           tpcnt = tpcnt + 1
        end if
c
         f1o = f1n
         f2o = f2n
         f3o = f3n
         f4o = f4n
         f5o = f5n
         f6o = f6n
```

```
          f7o = f7n
          f8o = f8n
          f9o = f9n
          f10o = f10n
          go to 1
c
c
c
c  Look  when f(3)(range) > max range specified(W28) otherwise (else) the ray
c is trapped above the surface and must be skipped
c
   2    if(f3o.GT.rmax)then
         go to 3
        else
         ths = ths + dths
         go to 1
        end if


c
c   Correct the ray arrival depth back up the raypath from the last event
c to where it crossed an imaginary vertical surface at r max (W28 of DINP).
c (C-S Chiu, NPS, 1991).
c    Define
c             zp   = arrival  ht above msl (km)
c             dum1 = arrival  ht above bot(km)
c             thr  = local arrival  angle(deg)
c             rp   = msl dist from source(km)
c             r    = msl dist to recvr (km)
c             z    = ray arrival hieght above msl accross a vert sfc at
c                    the recvr (km)
c             ths  = launch angle last + step in elevation angle(W17 DINP)
   3    zp = f4o - f1o

        dum1 = f4o - f2o
        thr = f10o
        rp = f3o
        r = rmax
c If the ray has just reflected from the bottom or surface then correct the
c angle to incident vice reflected by changing the sign:
        if(abs(zp).le.0.00009.or.abs(dum1).le.0.00009)then
         thr = -thr
        end if
        z = zp + (r - rp) * tand(thr)
c        write(20,100) ths, z
c 100    format(2f9.4)
c       Correct for ray travel time:
c         Define:
c             ds   = path length past vertical receiver surface
c             tp   = total phase travel time to horz recvr surface
c             dt   = travel time for path beyond vert recvr surfc
c             t    =  corrected total ray travel time to vert recvr surf
c             cave1=  ave sound speed for 0-150m array depth = 1.460km/s
c             cave2=  ave sound speed for 150-320m array depth=1.446km/s
c
        cave1 = 1.460
```

```
      cave2 = 1.446
      tp = f7o
      ds = sqrt((z - zp)**2 + (r - rp)**2)
      dt = ds/cave2
      t = tp - dt
c      write(30,200) z,  t
c 200   format(2f9.4)
c
c
c
c   Calculate TL due to spreading (Ching-Sang Chiu, NPS, 1991):
c      Define:
c          ths  = launch angle
c          ths2 = previous ray launch angle
cc          dths = difference btn one ray launch angle and the previous one
c          z    = arrival depth
c          z2   = previous ray arrival depth
c          rmax = vertical reciever range
c          rmax2= rmax (previous vert recvr range)
c          thr  = arrival angle
c          thr2 = previous ray arrival angle
c          h    = xsec distance btn launch ray and previous ray, perp to
c                 launch ray at rmax
c          tlsp = trans loss due to spreading (dB)
c
      if(i.eq.1)go to 5
c
      if(abs(thr).le.0.00009)then
       h = abs(z-z2)
       go to 6
      endif
c
      if(thr.gt.0.00009)then
       phi = -( 90. - thr)
      endif
c
      if(thr.lt.-0.00009)then
       phi = 90. + thr
      endif
c
      a11 = 1.
      a12 = -tand(thr2)
      a21 = 1.
      a22 = -tand(phi)
      b1 = z2 - rmax*tand(thr2)
      b2 = z - rmax*tand(phi)
      w = a11*a22 - a21 * a12
      zi = (b1*a22 - b2 * a12)/w
      ri = (a11 * b2 - b1 * a21)/w
      h = sqrt((z - zi)**2 + (rmax - ri)**2)
c
c Check for Caustic by looking for h near zero.  If so assign the spreading
c loss calc from the last ray (tlspo) equal to this calc (tlspn):
      if(abs(h).le.0.00009)then
         tlspn = tlspo
         go to 5
```

```
      end if
    6 tlspn = 10*log10((rmax*h*1000**2)/(cosd(ths)*dths*3.14159/180.))
c
    5 z2 = z
      thr2 = thr
      ths2 = ths
c     rmax2 = rmax
c      write(40,300) ths, tlspn
c 300  format(2f9.4)
c
c
c     Compute total trans loss (tlt) for each ray as sum of bottom loss
c (tlbot), surface loss (sloss), and spreading loss (tlsp).  Trans loss
c due to absorption will be neglected since its on order 0.3dB for 224 Hz
c over 50 km distance:
      tlt = tlbot + sloss + tlspn
c    Compute relative amplitude (ramp) by subtacting the source level (183 dB)
c from the total transmission loss (tlt):
      ramp = 183 - tlt

      write(50,400)  ths, thr, z, t, tlt, tlbot, sloss, tlspn
  400 format(8f9.4)
c
      tpcnt = tpcnt - (srfcnt + botcnt + 1)
      if(tpcnt.lt.0.00009)then
         tpcnt = 0
      end if
      write(60,500)  ths, thr, z, tpcnt, srfcnt, botcnt, ramp, t
  500 format(8f9.4)

      i = i + 1
      ths = ths + dths
      tlbot = 0
      sloss = 0
      tlspo = tlspn
      tpcnt = 0
      srfcnt = 0
      botcnt = 0
c
c Repeat the process for the next launch ray data set
c
      go to 1
      close(10)
c     close(20)
c     close(30)
c     close(40)
      close(50)
      close(60)
      end
```

```
*                               tgridin.f
*****************************************************************************
*                                                                           *
* Written By: John M. Emblidge Lt/USN, NPS, May 1991                        *
*                                                                           *
* Purpose   : To write the manually gridded topography of the Barents       *
*             Sea Acoustic Tomography Transmission Test study area to       *
*             to an output file (GRIDBATHY.DAT) for use by tgridder.f       *
*                                                                           *
* Modified by: John M. Elliott, LCDR/USN, 28DEC91, to change location of    *
*              bathymetry area closer to Bear Is in support of the          *
*              Barents Sea Polar Front experiment to be conducted Aug 92    *
*                                                                           *
*              J.M. Elliott, LCDR/USN, 16Jan92, to correct the bathy        *
*              grid to a true N-S coord sys.                                *
*****************************************************************************

      IMPLICIT DOUBLE PRECISION (A-H,O-Z)

      INTEGER I,J
      LOGICAL EX

      PARAMETER (MX=13, MY=13)

      REAL*8 BLAT,TLAT,DELLAT,DELLON,LLON,RLON

      DIMENSION BOTGRID(MX,MY)
      DIMENSION XCOORD(MX),YCOORD(MY)
      DIMENSION IN1(MY),IN2(MY),IN3(MY),IN4(MY),IN5(MY),IN6(MY),
     !          IN7(MY),IN8(MY),IN9(MY),IN10(MY),IN11(MY),IN12(MY),
     !          IN13(MY)
C               IN14(MY),IN15(MY),IN16(MY),IN17(MY),IN18(MY),
C               IN19(MY),IN20(MY),IN21(MY)

*****************************************************************************

C DEFINE BATHYMETRY DAT.  TOP ROW IS EASTERN BOUNDARY, RIGHT HAND
C VERTICAL ROW IS NORTHERN BOUNDARY:

      DATA IN1   /279,220,175,137,119,116,113,112,110,107,110,110,100/
      DATA IN2   /310,245,201,159,130,118,117,121,120,121,123,122,108/
      DATA IN3   /340,270,226,190,156,139,130,132,128,127,131,127,119/
      DATA IN4   /359,295,250,222,192,169,152,145,137,136,137,137,127/
      DATA IN5   /369,316,275,249,220,194,173,160,150,144,145,143,135/
      DATA IN6   /386,340,302,272,241,210,197,184,166,156,153,147,140/
      DATA IN7   /406,360,323,296,260,224,210,203,182,167,156,153,149/
      DATA IN8   /420,382,345,312,279,243,220,207,192,178,167,162,158/
      DATA IN9   /428,401,366,330,298,268,240,217,207,193,181,175,170/
      DATA IN10  /438,411,375,338,312,290,265,238,223,212,202,192,185/
      DATA IN11  /442,419,384,342,322,306,288,266,246,229,223,212,196/
      DATA IN12  /440,422,393,358,331,316,303,284,262,239,229,215,203/
      DATA IN13  /433,421,400,370,340,325,313,302,277,250,233,219,212/

*****************************************************************************
C DEFINE THE GEOGRAPHICAL LIMITS OF BATHYMETRY BOX:
```

```
      DATA BLAT,TLAT,LLON,RLON / 74.22d0,74.97d0,22.72d0,25.52d0 /

*************************************************************************

C CHECKING TO SEE IF THE OUTPUT FILE ALREADY EXISTS, AND IF SO DELETING
C IT AND CREATING A NEW ONE TO WRITE THIS RUNS DATA TO.

      INQUIRE (FILE='GRIDBATHY.DAT',EXIST=EX)

      IF (EX) THEN
        OPEN(35,FILE='GRIDBATHY.DAT',STATUS='OLD',FORM='UNFORMATTED')
        OPEN(35,FILE='GRIDBATHY.DAT',STATUS='DELETE',FORM='UNFORMATTED')
      ENDIF

      OPEN(35,FILE='GRIDBATHY.DAT',STATUS='NEW',FORM='UNFORMATTED')

      REWIND 35

*************************************************************************

C CALCULATING THE DEGEE SPACINGS BETWEEN LAT AND LONG GRID LINES.

*************************************************************************

      DELLAT = (TLAT - BLAT)/(MY-1)
      DELLON = (RLON - LLON)/(MX-1)

C FILLING THE X & Y COORDINATE ARRAYS

      DO I=0,(MX-1)
        XCOORD(I+1)=LLON + DELLON*dfloat(I)
      ENDDO

      DO J=0,(MY-1)
        YCOORD(J+1) = BLAT + DELLAT*dfloat(J)
      ENDDO

*************************************************************************

C FORMING THE BOTGRID MATRIX TO BE WRITTEN TO THE OUTPUT FILE.

      DO I=1,MX
        DO J=1,MY
          IF(I .EQ. 1)  BOTGRID(I,J) =  -IN1(J)
          IF(I .EQ. 2)  BOTGRID(I,J) =  -IN2(J)
          IF(I .EQ. 3)  BOTGRID(I,J) =  -IN3(J)
          IF(I .EQ. 4)  BOTGRID(I,J) =  -IN4(J)
          IF(I .EQ. 5)  BOTGRID(I,J) =  -IN5(J)
          IF(I .EQ. 6)  BOTGRID(I,J) =  -IN6(J)
          IF(I .EQ. 7)  BOTGRID(I,J) =  -IN7(J)
          IF(I .EQ. 8)  BOTGRID(I,J) =  -IN8(J)
          IF(I .EQ. 9)  BOTGRID(I,J) =  -IN9(J)
          IF(I .EQ. 10) BOTGRID(I,J) =  -IN10(J)
          IF(I .EQ. 11) BOTGRID(I,J) =  -IN11(J)
          IF(I .EQ. 12) BOTGRID(I,J) =  -IN12(J)
```

```
          IF(I .EQ. 13) BOTGRID(I,J) =  -IN13(J)
        ENDDO
       ENDDO
*******************************************************************************
C WRITTING XCOORD, YCOORD, & BOTGRID TO THE OUTPUT FILE GRIDBATHY.DAT

      WRITE(35) XCOORD
      WRITE(35) YCOORD
      write(6,*) xcoord
      write(6,*) ycoord
      DO I = 1,MX
        DO J = 1,MY
          WRITE(35) BOTGRID(I,J)
C          write(6,*) BOTGRID(I,J)
        ENDDO
      ENDDO
*******************************************************************************
      CLOSE(35)
      STOP
      END
```

```
c                              gridin.f

c*********************************************************************
C                                                                     *
C  Written by: John M. Emblidge, LT/USN, NPS, May 91                  *
C                                                                     *
C  For       : Barents Sea Acoustic Tomography Experiment.            *
C                                                                     *
C  Purpose   : To create the input file (GRIDSVP.DAT) for the HARPO    *
C              subroutine gridder.f.  This file must include the      *
C              spacings in the 3 othonormal planes, and the SSP at    *
C              each point.                                            *
C              The file is written so that gridder.f reads the data as*
C              follows:                                               *
C                  LINE1: XCOORD(MX)                                  *
C                  LINE2: YCOORD(MY)                                  *
C                  LINE3: ZG(MZ)                                      *
C                  LINE4: SVP(MX,MY,MZ)                               *
C                                                                     *
C  Structure :  The most important thing to remember about using this *
C              routine is that the values of MX,MY,MZ must be the same*
C              as they are in GRIDDER, otherwise the data will not be *
C              read by GRIDDER as you intended it to be.              *
C                                                                     *
C  Modified by: J. Mark ELLIOTT, LCDR/USN, NPS                        *
C                     16 JAN 92: TO CORRECT FOR NEW BATHY in support  *
C               of the Barents Sea Polar Front exp - 50km box         *
C               centered at 74.6N 24.12E.                             *
C                     20 Jan 92: to correct for new SSP field         *
C               orientation to along diagonals vice horizontals       *
C                                                                     *
c*********************************************************************
C                                                                     *
C  DATA DICTIONARY  :  Definitions of each variable used              *
C                                                                     *
C         CHARACTERS:                                                 *
C         INTEGERS  :                                                 *
C         REAL      : BLAT = LATITUDE OF BOTTOM OF BOX (SOUTH EDGE)   *
C                     DELLAT = NUMBER OF DEGREES BETWEEN GRID SPACINGS*
C                     DELLON = NUMBER OF DEGREES BETWEEN GRID SPACINGS*
C                     LLON = LONGITUDE OF LEFT SIDE OF BOX            *
C                     RLON = LONGITUDE OF RIGHT SIDE OF BOX           *
C                     TLAT = LATITUDE OF TOP OF BOX (NORTHERN  EDGE)  *
C                                                                     *
C         ARRAYS    : C1 = SVP IN FIRST REGION OF BOX                 *
C                     C2 = SVP IN SECOND REGION OF BOX                *
C                     C3 = SVP IN THIRD REGION OF BOX                 *
C                     CSPD = OUTPUT FOR GRIDDER                       *
C                                                                     *
C         PARAMETERS: MX = # OF GRID SPACINGS || THE EQUATER          *
C                     MY = # OF GRID SPACINGS || THE PRIME MERIDEN    *
C                     MZ = # OF VERTICAL POINTS                       *
C                                                                     *
c*********************************************************************

      IMPLICIT DOUBLE PRECISION (A-H,O-Z)
```

```
      INTEGER I,J,K,IX,IY,IZ
      LOGICAL EX


      PARAMETER (MX = 13, MY = 13, MZ = 151)

      REAL*8 BLAT,DELLAT,DELLON,LLON,RLON,TLAT

      DIMENSION C1(MZ),C2(MZ),C3(MZ)
      DIMENSION AVE1(MZ),AVE2(MZ),AVE3(MZ),AVE4(MZ),AVE5(MZ)
      DIMENSION AVE6(MZ),AVE7(MZ),AVE8(MZ),AVE9(MZ),AVE10(MZ),AVE11(MZ)
      DIMENSION XCOORD(MX),YCOORD(MY),ZG(MZ)
      DIMENSION CSPD(MX,MY,MZ)

      DATA LLON,RLON,TLAT,BLAT / 22.72d0,25.52d0,74.97d0,74.22d0 /

*************************************************************************

      INQUIRE (FILE='GRIDSVP.DAT',EXIST=EX)

      IF (EX) THEN
        OPEN(74,FILE='GRIDSVP.DAT',STATUS='OLD',FORM='UNFORMATTED')
        OPEN(74,FILE='GRIDSVP.DAT',STATUS='DELETE',FORM='UNFORMATTED')
      ENDIF

      OPEN(74,FILE='GRIDSVP.DAT',STATUS='NEW',FORM='UNFORMATTED')

      REWIND 74

*************************************************************************

C OPENING THE FILES THAT HOLD THE SSP'S CREATED IN MATLAB

*************************************************************************

      OPEN(41,FILE='ssp1f.dat',STATUS='OLD',FORM='FORMATTED')
      OPEN(42,FILE='ssp2f.dat',STATUS='OLD',FORM='FORMATTED')
      OPEN(43,FILE='ssp3f.dat',STATUS='OLD',FORM='FORMATTED')
      OPEN(44,FILE='zg.dat',   STATUS='OLD',FORM='FORMATTED')

      REWIND 41
      REWIND 42
      REWIND 43
      REWIND 44

*************************************************************************

C READING IN THE THREE BASIC SOUND SPEED PROFILES, AND DEPTH ARRAY

*************************************************************************

      READ(41,*) (C1(I), I=1,MZ)
      READ(42,*) (C2(I), I=1,MZ)
      READ(43,*) (C3(I), I=1,MZ)
```

```
      READ(44,*) (ZG(I), I=1,MZ)

*************************************************************************

C CALCULATING THE DEGEE SPACINGS BETWEEN LAT AND LONG GRID LINES.

*************************************************************************

      DELLAT = (TLAT - BLAT)/(MY-1)
      DELLON = (RLON - LLON)/(MX-1)

*************************************************************************

C   CALCULATING THE AVERAGED PROFILES TO FILE SMOOTH THE OVERALL C FIELD
C WITH THE FRONT

*************************************************************************

      DO I = 1,MZ
        AVE2(I) = (C1(I) + C2(I))/2
        AVE1(I) = (C1(I) + AVE2(I))/2
        AVE4(I) = (C2(I) + C3(I))/2
        AVE3(I) = (C2(I) + AVE4(I))/2
        AVE5(I) = (C3(I) + AVE4(I))/2
      ENDDO

*************************************************************************

C CREATING A NEW SET OF AVERAGES FOR THE FIELD WITHOUT THE FRONT

*************************************************************************

      DO I = 1,MZ
        AVE6(I) = (C1(I) + C3(I))/2
        AVE7(I) = (C1(I) + AVE6(I))/2
        AVE8(I) = (C1(I) + AVE7(I))/2
        AVE9(I) = (AVE6(I) + C3(I))/2
        AVE10(I) = (AVE9(I) + C3(I))/2
        AVE11(I) = (AVE10(I) + C3(I))/2
      ENDDO

*************************************************************************

C FILLING THE CSPD ARRAY WITH VALUES
C ALSO FILLING THE XCOORD, AND YCOORD ARRAYS

*************************************************************************

C       DO IX = 1,MX
C         DO IY = 1,MY
C           DO IZ = 1,MZ
C             IF(IX .LT. 4)                    CSPD(IX,IY,IZ) = C1(IZ)
C              IF(IX. GT. 3 .AND. IX. LT. 6) CSPD(IX,IY,IZ) = AVE8(IZ)
C              IF(IX. GT.5 .AND. IX. LT. 7) CSPD(IX,IY,IZ) = AVE7(IZ)
C              IF(IX. GT.6 .AND. IX. LT. 8) CSPD(IX,IY,IZ) = AVE6(IZ)
C              IF(IX. GT.7 .AND. IX. LT. 9) CSPD(IX,IY,IZ) = AVE9(IZ)
```

```
C             IF(IX. GT.8 .AND. IX. LT. 11) CSPD(IX,IY,IZ) = AVE10(IZ)
C             IF(IX. GT.10 .AND. IX. LT. 12) CSPD(IX,IY,IZ) = AVE11(IZ)
C             IF(IX .GT. 11)                 CSPD(IX,IY,IZ) = C3(IZ)
C             write(6,*) CSPD(IX,IY,IZ)
C           ENDDO
C         ENDDO
C       ENDDO

      DO I=0,(MX-1)
        XCOORD(I+1)=LLON + DELLON*dfloat(I)
C         write(6,*) XCOORD(I)
      ENDDO

      DO J = 0,(MY-1)
        YCOORD(J+1) = BLAT + DELLAT*dfloat(J)
C         write(6,*) YCOORD(J)
      ENDDO


*************************************************************************
C ASSIGN SSP'S TO DIAGONALS OF BATHYMETRY COORDINATES - ORIENTATION IS
C ALONG BOTTOM LEFT TO TOP RIGHT DIAGONALS:
*************************************************************************
      COUNTERY = 2
      DO IX = 1, MX-2
         DO IY = 1, MY-COUNTERY
            DO IZ = 1, MZ
                CSPD(IX,IY,IZ) = C3(IZ)
            ENDDO
         ENDDO
         COUNTERY = COUNTERY + 1
      ENDDO

      DO IZ = 1, MZ
         CSPD(12,1,IZ) = AVE5(IZ)
         CSPD(11,2,IZ) = AVE5(IZ)
         CSPD(10,3,IZ) = AVE5(IZ)
         CSPD(9,4,IZ) = AVE5(IZ)
         CSPD(8,5,IZ) = AVE5(IZ)
         CSPD(7,6,IZ) = AVE5(IZ)
         CSPD(6,7,IZ) = AVE5(IZ)
         CSPD(5,8,IZ) = AVE5(IZ)
         CSPD(4,9,IZ) = AVE5(IZ)
         CSPD(3,10,IZ) = AVE5(IZ)
         CSPD(2,11,IZ) = AVE5(IZ)
         CSPD(1,12,IZ) = AVE5(IZ)
         CSPD(13,1,IZ) = AVE4(IZ)
         CSPD(12,2,IZ) = AVE4(IZ)
         CSPD(11,3,IZ) = AVE4(IZ)
         CSPD(10,4,IZ) = AVE4(IZ)
         CSPD(9,5,IZ) = AVE4(IZ)
         CSPD(8,6,IZ) = AVE4(IZ)
         CSPD(7,7,IZ) = AVE4(IZ)
         CSPD(6,8,IZ) = AVE4(IZ)
         CSPD(5,9,IZ) = AVE4(IZ)
         CSPD(4,10,IZ) = AVE4(IZ)
```

```
      CSPD(3,11,IZ) = AVE4(IZ)
      CSPD(2,12,IZ) = AVE4(IZ)
      CSPD(1,13,IZ) = AVE4(IZ)
      CSPD(13,2,IZ) = AVE3(IZ)
      CSPD(12,3,IZ) = AVE3(IZ)
      CSPD(11,4,IZ) = AVE3(IZ)
      CSPD(10,5,IZ) = AVE3(IZ)
      CSPD(9,6,IZ) = AVE3(IZ)
      CSPD(8,7,IZ) = AVE3(IZ)
      CSPD(7,8,IZ) = AVE3(IZ)
      CSPD(6,9,IZ) = AVE3(IZ)
      CSPD(5,10,IZ) = AVE3(IZ)
      CSPD(4,11,IZ) = AVE3(IZ)
      CSPD(3,12,IZ) = AVE3(IZ)
      CSPD(2,13,IZ) = AVE3(IZ)
      CSPD(13,3,IZ) = C2(IZ)
      CSPD(12,4,IZ) = C2(IZ)
      CSPD(11,5,IZ) = C2(IZ)
      CSPD(10,6,IZ) = C2(IZ)
      CSPD(9,7,IZ) = C2(IZ)
      CSPD(8,8,IZ) = C2(IZ)
      CSPD(7,9,IZ) = C2(IZ)
      CSPD(6,10,IZ) = C2(IZ)
      CSPD(5,11,IZ) = C2(IZ)
      CSPD(4,12,IZ) = C2(IZ)
      CSPD(3,13,IZ) = C2(IZ)
      CSPD(13,4,IZ) = C2(IZ)
      CSPD(12,5,IZ) = C2(IZ)
      CSPD(11,6,IZ) = C2(IZ)
      CSPD(10,7,IZ) = C2(IZ)
      CSPD(9,8,IZ) = C2(IZ)
      CSPD(8,9,IZ) = C2(IZ)
      CSPD(7,10,IZ) = C2(IZ)
      CSPD(6,11,IZ) = C2(IZ)
      CSPD(5,12,IZ) = C2(IZ)
      CSPD(4,13,IZ) = C2(IZ)
      CSPD(13,5,IZ) = C2(IZ)
      CSPD(12,6,IZ) = C2(IZ)
      CSPD(11,7,IZ) = C2(IZ)
      CSPD(10,8,IZ) = C2(IZ)
      CSPD(9,9,IZ) = C2(IZ)
      CSPD(8,10,IZ) = C2(IZ)
      CSPD(7,11,IZ) = C2(IZ)
      CSPD(6,12,IZ) = C2(IZ)
      CSPD(5,13,IZ) = C2(IZ)
      CSPD(13,6,IZ) = AVE2(IZ)
      CSPD(12,7,IZ) = AVE2(IZ)
      CSPD(11,8,IZ) = AVE2(IZ)
      CSPD(10,9,IZ) = AVE2(IZ)
      CSPD(9,10,IZ) = AVE2(IZ)
      CSPD(8,11,IZ) = AVE2(IZ)
      CSPD(7,12,IZ) = AVE2(IZ)
      CSPD(6,13,IZ) = AVE2(IZ)
      CSPD(13,7,IZ) = AVE1(IZ)
      CSPD(12,8,IZ) = AVE1(IZ)
      CSPD(11,9,IZ) = AVE1(IZ)
```

```
         CSPD(10,10,IZ) = AVE1(IZ)
         CSPD(9,11,IZ) = AVE1(IZ)
         CSPD(8,12,IZ) = AVE1(IZ)
         CSPD(7,13,IZ) = AVE1(IZ)
         CSPD(13,8,IZ) = C1(IZ)
         CSPD(12,9,IZ) = C1(IZ)
         CSPD(11,10,IZ) = C1(IZ)
         CSPD(10,11,IZ) = C1(IZ)
         CSPD(9,12,IZ) = C1(IZ)
         CSPD(8,13,IZ) = C1(IZ)
         CSPD(13,9,IZ) = C1(IZ)
         CSPD(12,10,IZ) = C1(IZ)
         CSPD(11,11,IZ) = C1(IZ)
         CSPD(10,12,IZ) = C1(IZ)
         CSPD(9,13,IZ) = C1(IZ)
         CSPD(13,10,IZ) = C1(IZ)
         CSPD(12,11,IZ) = C1(IZ)
         CSPD(11,12,IZ) = C1(IZ)
         CSPD(10,13,IZ) = C1(IZ)
         CSPD(13,11,IZ) = C1(IZ)
         CSPD(12,12,IZ) = C1(IZ)
         CSPD(11,13,IZ) = C1(IZ)
         CSPD(13,12,IZ) = C1(IZ)
         CSPD(12,13,IZ) = C1(IZ)
         CSPD(13,13,IZ) = C1(IZ)
      ENDDO

*******************************************************************************

C WRITTING TO THE INPUT FILE FOR GRIDDER. (GRIDSVP.DAT)

*******************************************************************************

      WRITE(74) (XCOORD(I), I=1,MX)
      WRITE(74) (YCOORD(J), J=1,MY)
      WRITE(74) (ZG(K), K=1,MZ)
      DO I = 1,MX
        DO J = 1,MY
          WRITE(74) (CSPD(I,J,K), K=1,MZ)
C           write(6,*) CSPD(I,J,K)
        ENDDO
      ENDDO

*******************************************************************************

      CLOSE(41)
      CLOSE(42)
      CLOSE(43)
      CLOSE(44)
      CLOSE(74)

      STOP
      END
```

```
%                                hyd8beam.m

%                          Hydrophone #8 Arrival  Plot
%*************************************************************************
% Written by:  J.M. Elliott, LCDR/USN, NPS, 1992
%
% Purpose:
%     This Matlab program plots HARPO ray arrival structure at a particular
% receiver hydrophone array location. Plotting time vs relative amplitude for
% the eigenrays arriving within one wavelength of the hyd depth and from
% a specified arrival angle.  Rays that follow essentially the same path are
% taken as one (this is indicated by rays with the same # of turning points,
% surface bounces, and bottom bounces).
%     Two different plots are produced:
% 1) representing received pulses as unit impulse and
% 2) representing receiced pulses as gaussian distributed in time with
% a pulse width equal to 1/(band width).
%     Input is data in f3res.dat which is output from the Fortran program
% cordat.f which is corrected HARPO vertical recvr surfaces  data.
%
load f3res.m                                % f3res.m = f3res.dat
% f3res.m = ths, thr, z, tpcnt, srfcnt, botcnt, ramp, t


%   Find the eigenrays arriving within the desired window around the hydrophone.
% Compute the relative amplitude and total TL computed by cordat.f and plot the
% data:
%   Define:
%     z = arrival depth of eigenrays in km above mean sea level (msl) (a neg #)
%     b = index vector corresponding to all rays arriving w/i 1/2 wavelength
%         of the hydrophone
%     c = index vector corresponding to the rays arriving w/i 1/2 wavelength
%         of the hydrophone and coming in from above (neg grazing angle -
%         <-0.00009) or below (pos grazing angle - >0.00009) the horizontal.
%     t = eigenray arrival time in sec
%     D = pulse width (sec) = 1/band width(hz)
      D = 1/16;
%     tlt = total trans loss in dB (absorption is neglected)
%     sls = signal level 1m from the source in dB
      sls = 183;
%     slr = signal level at receiver in dB
%     amp = amplitude of eigenrays at receiver in Pascal
%     s  = amplitude of received signal simulated as gaussian pulses
%     z  = hydrophone depth above msl in km (a negative number)
      z = -0.220;
%     lambda = acoustic wavelength in km = (c(average)/f)*1e-03
      lambda = (1445/224)*1e-03;
%     uz = upper limit of window
      uz = z + lambda/2;
%     lz = lower limit of window
      lz = z - lambda/2;

z = f3res(:,3);
b = find(z<=uz & z>=lz);
%c = find(f3res(b(:,1),2)>0.00009);
[n,m] = size(b);
```

```
%    Define a new matrix "resd(n,7)" for ease in displaying the output data
% for hydrophone.
   resd = ones(n,7);
   resd(:,1) = f3res(b(:,1),1)*resd(1,1);        % launch angle (deg)
   resd(:,2) = f3res(b(:,1),2)*resd(1,2);        % arrival angle (deg)
   resd(:,3) = f3res(b(:,1),4)*resd(1,3);        % no of turning points
   resd(:,4) = f3res(b(:,1),5)*resd(1,4);        % no of surface bounces
   resd(:,5) = f3res(b(:,1),6)*resd(1,5);        % no of bottom bounces
   resd(:,6) = f3res(b(:,1),7)*resd(1,6);      % relative amplitude  (dB)
   resd(:,7) = f3res(b(:,1),8)*resd(1,7);        % arrival time (sec)


%  Now sort the rays in order of increasing arrival time:
[Y,I] = sort(resd(:,7));

%   EIGENRAY DETERMINATION:
%  Eliminate duplicate launch rays and rays that are essentially the same
% due to identical number of turning points, surface bounces and bottom
% bounces.   First define a new matrix resn with the data in order of
% arrival time:
    resn = ones(n,7);
    resn(:,1)=resd(I,1)*resn(1,1);
    resn(:,2)=resd(I,2)*resn(1,2);
    resn(:,3)=resd(I,3)*resn(1,3);
    resn(:,4)=resd(I,4)*resn(1,4);
    resn(:,5)=resd(I,5)*resn(1,5);
    resn(:,6)=resd(I,6)*resn(1,6);
    resn(:,7)=resd(I,7)*resn(1,7);
    for i = 1:n;
      for k = 1:n;
         if i == k;
            else;
                difa = abs(resn(i,1) - resn(k,1));
                diftp = abs(resn(i,3) - resn(k,3));
                difs = abs(resn(i,4) - resn(k,4));
                difb = abs(resn(i,5) - resn(k,5));
                if ((difa == 0.0000) | ((diftp==0) & (difs==0) & (difb==0)));
                    ; resn(i,:)=[0 0 0 0 0 0 0]; break; end;

             end;
          end;
    end;
% Now eliminate the unwanted ray zero data lines and call new data
% matrix resf:
    k = 1;
    for i = 1:n;
        if resn(i,1)~=0;
           resf(k,:)=resn(i,:);
           k = k + 1;
        end;
    end;

%  Now plot the eigenray arrival time vs relative amplitude:
[n,m] = size(resf);
t = ones(n,1);
```

```
tlt = ones(n,1);
slr = ones(n,1);
amp = ones(n,1);
for i = 1:n;
      t(i,1) = (resf(i,7)*t(i,1));
%      tlt(i,1) = (f3res(b(c(i,1),1),5))*tlt(i,1);
%      slr(i,1) = (sls - tlt(i,1))*slr(i,1);
      amp(i,1) = ((1e-06)*10^(resf(i,6)/20))*amp(i,1);
%      if slr(i,1)>=100;
%        slr(i,1) = 0;
%      end;
end;
%axis([34.62 36.0 0 0.01]);
subplot(211),plot(t,amp,'.')
title('HYD #8 EIGENRAY ARRIVALS')
text(34.65,.011,'R17')
text(35.03,0.007,'R18')
text(35.32,0.0085,'R19')
text(35.80,0.003,'R20')
xlabel('Arrival Time (sec)')
ylabel('Relative Amplitude (Pa)')
%text(36.5,2,'Hydrophone Depth = 220m')
%text(36.5,-2,'Arriving w/i 1/2 Lambda')
%axis([1 2 3 4]);axis;
%pause;
subplot(212),plot(t,resf(:,6),'.')
text(34.65,82,'R17')
text(35.03,78,'R18')
text(35.32,80,'R19')
text(35.80,70,'R20')
xlabel('Arrival Time (sec)')
ylabel('Relative Amplitude (dB)')


%  Simulate received eigenrays as gaussian pulses:
%  Define:
%     ta = time axis
%     gisa = gaussian intermediate signal amplitude
%     gsa = gaussian signal amplitude
%ta = 34.500:.002:37.5000;
%[o,p]=size(ta);
%gisa = ones(n,p);
%gsa = ones(1,p);
%ti = [34.7140  35.0917 35.3814 35.8676]';
%ampl = [1e-06*10^(79.5235/20)  1e-06*10^(75.6184/20)...
%       1e-06*10^(77.3569/20) 1e-06*10^(66.5519/20)]';
%for j = 1:p;
% for i = 1:n;
%  if i==1;
%     gisa(i,j)=amp(i,1)*exp(-2*((ta(1,j)-t(i,1))^2)/(D^2))*gisa(i,j);
%    end;
%    if i>1;
%     gisa(i,j)=amp(i,1)*exp(-2*((ta(1,j)-t(i,1))^2)/(D^2))*gisa(i,j)...
%                        + gisa(i-1,j);
%    end;
%  end;
```

```
%end;
%gsa = sum(gisa)
%axis([34.5 37.5 0 0.04]);
%subplot(212),plot(ta,gsa)
%title('SIMULATED PULSE ARRIVALS')
%xlabel('Arrival Time (sec)')
%ylabel('Relative Amplitde (Pa)')
%text(36.3,1e+04,'Pulse Width = 62.5 msec')
%axis([1 2 3 4]);axis;
%text(36,-68,'Launch Angles 0-25 Deg')
%text(36,-71,'Launch Step = 0.01 deg')
%text(36,-74,'Broad Front (40km)')
%text(36,-77,'Hyd Depth = 150m')
```

```
%                                beampat.m

%                        Barents Array Beam Pattern
%*************************************************************************
%   Written by:  J.M. Elliott, LCDR/USN, NPS, 1992
%   Purpose:
%      This Matlab program plots an array plane wave beam pattern based on
% a method for a linear array of point hydrophones by Ziomek (1985).
%
%*************************************************************************

N = 16;                                 % N = # of hydrophones
d = 10;                                 % d = hydrophones interelement spacing (m)
f = 224;                                % f = frequency of interest (Hz)
c = 1450;                               % c = sound velocity (m/s)
for steer =  20  ;                      % steer = angle in deg main lobe is to be
                                                %steered off broadside of array
psip = 90 + steer;                      % psip = steered angle ref to broadside
fxp = f*cos(psip*pi/180)/c;             % fxp = steered angle in 'u' space
n = -(N-1)/2:1:(N-1)/2;                 % n = hyd # index
ac = cos((cos((pi*((2*n-1)/2)/N))));        % ac = cosine amplitude window
theta = (-2*pi*fxp*((2*n-1)/2)*d);          % theta = phase weight
cn = ac'.*exp(j*theta');                    % cn = complex wieghting
SN = (fft(cn,512))/sum(ac);                 % SN = normalized directivity
                                                % function
m = 0:1:511;                            % m = FFT bin #
psi = (acos((c.*m')/(f*512*d)))*(180/pi);   % psi = conversion fm 'u' to deg
%   u = (c.*m')/(f*224*d);
end;
plot(psi,abs(SN))
title('PLANE WAVE BEAM PATTERN')
xlabel('Degrees From Axial (90=broadside, 0=endfire)')
ylabel('Normalized Amplitude')
text(75,0.9,'16 Element Vertical Linear Array')
text(75,0.85,'10m Interelement Spacing')
text(75,0.8,'f = 400 Hz')
text(75,0.75,'Cosine Amplitude Window')
%text(73,0.5,'Steered to 20 deg off Broadside')
text(75,0.7,'Beam Width = 1 deg')
text(80,0.3,'Grating Lobe 21 deg away')
%end
```

```
%                                   resanl.m

%                   Resovability Analysis Table Generator
%*************************************************************************
%
%  Written by:  J.M. Elliott, LCDR/USN, NPS, 1992
%
%  Purpose:
%     This Matlab program uses the output data file <f3res.dat> from the
% fortran program <cordat.f> and provides an output data table of tomograph-
% ically resolvable rays for the whole array as a plane wave beamformer.
%     To compute the data table of tomographically resolvable rays for each
% hydrophone as an omnidirectional receiver, the program should be modified
% as indicated in the comment lines in the body of the program.
%     The data is presented in the fol format columns: launch angle, arrival
% angle, no of turning pts, no srf, bounces, no bot bounces, rel amp and
% arrival time.
%     The data is displayed in order of increasing arrival time and only for
% rays arriving w/i 1/2 wavelength (of the freq of interest) from each
% hydrophone.
%     Rays following essentially the same paths, as indicated by similar
% number of turning points, surface bounces, and bottom bounces, are taken as
% one ray (the first ray of the group arriving in time).
%     Each ray is tomographically resolved in time using a specified pulse
% width.
%
%*************************************************************************
%   Define:
%     z  = hydrophone depth above msl in km (a negative number)
%     lambda = 1/2 acoustic wavelength in km = 0.5 * (c(average)/f)*1e-03
      lambda = 0.5*(1445/224)*1e-03;
%     uz = upper limit of depth window
%      uz = z + lambda;
%     lz = lower limit of depth window
%      lz = z - lambda;
%      dS =   Arrival angle (grazing) sector.  Used for plane wave beam-
%             formed array table only. One of 15 defined as follows:
%             (Three degree beam widths used based on 224 Hz plane wave beam
%              pattern analysis)
%         = d1   (-22.5 to -19.5)
%         = d2   (-19.5 to -16.5)
%         = d3   (-16.5 to -13.5)
%         = d4   (-13.5 to -10.5)
%         = d5   (-10.5 to -7.5)
%         = d6   (-7.5 to -4.5)
%         = d7   (-4.5 to -1.5)
%         = d8   (-1.5 to +1.5)
%         = d9   (+1.5 to +4.5)
%         = d10  (+4.5 to +7.5)
%         = d11  (+7.5 to +10.5)
%         = d12  (+10.5 to +13.5)
%         = d13  (+13.5 to +16.5)
%         = d14  (+16.5 to + 19.5)
%         = d15  (+19.5 to + 22.5)

load f3res.m                          % f3res.m = f3res.dat
```

```
% f3res.m = ths, thr, z, tpcnt, srfcnt, botcnt, ramp, t
% Let z = the third column arrival depths:
z = f3res(:,3);
%
%    Determine all eigenrays or all rays arriving w/i 1/2 wavelength of the
% frequency of interest in depth of the 16 hydrophones:
% First define hydrophone depths in km above mean sea level:
z1 = -.150;
z2 = -.160;
z3 = -.170;
z4 = -.180;
z5 = -.190;
z6 = -.200;
z7 = -.210;
z8 = -.220;
z9 = -.230;
z10 = -.240;
z11 = -.250;
z12 = -.260;
z13 = -.270;
z14 = -.280;
z15 = -.290;
z16 = -.300;

% Next define lambda depth window around each hydrophone:
uz1 = z1 + lambda;
lz1 = z1 - lambda;
uz2 = z2 + lambda;
lz2 = z2 - lambda;
uz3 = z3 + lambda;
lz3 = z3 - lambda;
uz4 = z4 + lambda;
lz4 = z4 - lambda;
uz5 = z5 + lambda;
lz5 = z5 - lambda;
uz6 = z6 + lambda;
lz6 = z6 - lambda;
uz7 = z7 + lambda;
lz7 = z7 - lambda;
uz8 = z8 + lambda;
lz8 = z8 - lambda;
uz9 = z9 + lambda;
lz9 = z9 - lambda;
uz10 = z10 + lambda;
lz10 = z10 - lambda;
uz11 = z11 + lambda;
lz11 = z11 - lambda;
uz12 = z12 + lambda;
lz12 = z12 - lambda;
uz13 = z13 + lambda;
lz13 = z13 - lambda;
uz14 = z14 + lambda;
lz14 = z14 - lambda;
uz15 = z15 + lambda;
lz15 = z15 - lambda;
uz16 = z16 + lambda;
```

```
lz16 = z16 - lambda;

%   Now find the matrix index number associated with the eigenrays arriving
% w/i the depth windows around each hydrophone.  For individual hydrophone
% table generation all but the hydrophone of interest must be commented out
% and the program run individually for each hyd, exiting and reentering
% Matlab each time.
b1 = find(z<uz1 & z>lz1);
b2 = find(z<uz2 & z>lz2);
b3 = find(z<uz3 & z>lz3);
b4 = find(z<uz4 & z>lz4);
b5 = find(z<uz5 & z>lz5);
b6 = find(z<uz6 & z>lz6);
b7 = find(z<uz7 & z>lz7);
b8 = find(z<uz8 & z>lz8);
b9 = find(z<uz9 & z>lz9);
b10 = find(z<uz10 & z>lz10);
b11 = find(z<uz11 & z>lz11);
b12 = find(z<uz12 & z>lz12);
b13 = find(z<uz13 & z>lz13);
b14 = find(z<uz14 & z>lz14);
b15 = find(z<uz15 & z>lz15);
b16 = find(z<uz16 & z>lz16);

%  Let matrix c = all rays arriving w/i 1/2 wavelength of all 16 hyd's. Comment
% out this step when computing individual hyd resolvability table.
c = [b1; b2; b3; b4; b5; b6; b7; b8; b9; b10; b11; b12; b13; b14; ...
     b15; b16];

%    Now determine the rays arriving in which of the 15 beam sectors of
% three degree beam widths each.  The program must be run individually
% for each sector and Matlab must be exited and reentered each time.
% Comment out this step when computing individual hyd resolvability table.
d1 = find(f3res(c(:,1),2)>=-22.5000 & f3res(c(:,1),2)<-19.5000);
%d2 = find(f3res(c(:,1),2)>=-19.5000 & f3res(c(:,1),2)<-16.5000);
%d3 = find(f3res(c(:,1),2)>=-16.5000 & f3res(c(:,1),2)<-13.5000);
%d4 = find(f3res(c(:,1),2)>=-13.5000 & f3res(c(:,1),2)<-10.5000);
%d5 = find(f3res(c(:,1),2)>=-10.5000 & f3res(c(:,1),2)<-7.5000);
%d6 = find(f3res(c(:,1),2)>=-7.5000 & f3res(c(:,1),2)<-4.5000);
%d7 = find(f3res(c(:,1),2)>=-4.5000 & f3res(c(:,1),2)<-1.5000);
%d8 = find(f3res(c(:,1),2)>=-1.5000 & f3res(c(:,1),2)<+1.5000);
%d9 = find(f3res(c(:,1),2)>=+1.5000 & f3res(c(:,1),2)<+4.5000);
%d10 = find(f3res(c(:,1),2)>=+4.5000 & f3res(c(:,1),2)<+7.5000);
%d11 = find(f3res(c(:,1),2)>=+7.5000 & f3res(c(:,1),2)<+10.5000);
%d12 = find(f3res(c(:,1),2)>=+10.5000 & f3res(c(:,1),2)<+13.5000);
%d13 = find(f3res(c(:,1),2)>=+13.5000 & f3res(c(:,1),2)<+16.5000);
%d14 = find(f3res(c(:,1),2)>=+16.5000 & f3res(c(:,1),2)<+19.5000);
%d15 = find(f3res(c(:,1),2)>=+19.5000 & f3res(c(:,1),2)<+22.5000);


%    Define a new matrix "resd(n,7)" for ease in displaying the output data
% for sector dS.  Sector dS must be changed for each program run.
% When computing individual hyd resolvability sector dS should be
% set equal to the hydrophone of interest, bX, vice sector, dX.
   dS = d1;
   [n,m] = size(d1);
```

```
   resd = ones(n,7);
   resd(:,1) = f3res(c(dS(:,1),1),1)*resd(1,1);        % launch angle (deg)
% for hydrophone resolvability table generation use the fol format:
%  resd(:,X) = f3res(dS(:,1),Y)*resd(1,X);
   resd(:,2) = f3res(c(dS(:,1),1),2)*resd(1,2);        % arrival angle (deg)
   resd(:,3) = f3res(c(dS(:,1),1),4)*resd(1,3);        % no of turning points
   resd(:,4) = f3res(c(dS(:,1),1),5)*resd(1,4);        % no of surface bounces
   resd(:,5) = f3res(c(dS(:,1),1),6)*resd(1,5);        % no of bottom bounces
   resd(:,6) = f3res(c(dS(:,1),1),7)*resd(1,6);      % relative amplitude  (dB)
   resd(:,7) = f3res(c(dS(:,1),1),8)*resd(1,7);        % arrival time (sec)


%  Now sort the rays in order of increasing arrival time:
[Y,I] = sort(resd(:,7));

%  Eliminate duplicate launch rays and rays that are essentially the same
% due to identical number of turning points, surface bounces and bottom
% bounces.  First define a new matrix resn with the data in order of
% arrival time:
    resn = ones(n,7);
    resn(:,1)=resd(I,1)*resn(1,1);
    resn(:,2)=resd(I,2)*resn(1,2);
    resn(:,3)=resd(I,3)*resn(1,3);
    resn(:,4)=resd(I,4)*resn(1,4);
    resn(:,5)=resd(I,5)*resn(1,5);
    resn(:,6)=resd(I,6)*resn(1,6);
    resn(:,7)=resd(I,7)*resn(1,7);
    for i = 1:n;
      for k = 1:n;
         if i == k;
            else;
                difa = abs(resn(i,1) - resn(k,1));
                diftp = abs(resn(i,3) - resn(k,3));
                difs = abs(resn(i,4) - resn(k,4));
                difb = abs(resn(i,5) - resn(k,5));
                if ((difa <= 0.0000) | ((diftp<=0) & (difs<=0) & (difb<=0)));
                    ; resn(i,:)=[0 0 0 0 0 0 0]; break; end;

             end;
          end;
       end;
% Now eliminate the unwanted ray data lines:
    k = 1;
    for i = 1:n;
        if resn(i,1)~=0;
           resf(k,:)=resn(i,:);
           k = k + 1;
        end;
    end;

%    Now determine tomographic temporal resolvability by comparing each
% ray arrival time to its neighbor for a distance of the pulse width of
% interest.  If the distance is >= the pulse width then the ray is
% resolvable (R), if not the ray is not resolvable (U).
%         224 Hz source - Pulse width = 1/(band width) = 1/16Hz = 0.0625s
%         400 Hz source - Pulse width = 1/(band width) = 1/100Hz = 0.010s
```

```
% The new [n,1] matrix resg contains the 'U' for unresolved or 'R' for resolved
% info corresponding to the n rows of the resf matrix.
[n,m] = size(resf);
for i = 1:n;
   for k = 1:n;
       if i ==k;
       else;
         dift = abs( resf(i,7)-resf(k,7));
         if dift <= 0.01; resg(i,1)='U'; break; end;
         if dift > 0.01;  resg(i,1)='R'; end;
       end;
   end;
end;

% To get a print out of the plane wave beamformed array resolvability data
% table for the sector of interest (or of the individual hydrophone data
% table for the hydrophone of interest) sorted by time type:  resf.
% To get a print out of corresponding row 'U' or 'R' info type resg.
```

APPENDIX B: INDIVIDUAL HYDROPHONE RESOLVABILITY ANALYSIS TABLE

The following table was generated by treating each hydrophone of the 16 element vertical array (B) as an independent omnidirectional receiver. The table was compiled using the MATLAB computer program 'resanl.m'. A copy of 'resanl.m' can be found in Appendix A. Definitions of RAMP, R, and hydrophone depths can be found at the end of the Appendix.

LAUNCH ANGLE (deg)	ARRIVAL ANGLE (deg)	NUMBER TURNING POINTS	NUMBER SURFACE BOUNCES	NUMBER BOTTOM BOUNCES	RAMP (dB)	ARRIVAL TIME (sec) (R-resolvable).	
			HYDROPHONE 1				
6.9401	-5.9018	24.0000	0	8.0000	81.4618	34.5208	
6.8401	-5.8326	25.0000	0	8.0000	75.6515	34.5254	
6.1600	-5.3830	30.0000	0	8.0000	90.4353	34.5479	
6.1500	-5.4052	33.0000	0	8.0000	79.7049	34.5485	
10.3300	-8.0038	20.0000	5.0000	13.0000	85.4431	34.5504	
7.3601	5.7628	20.0000	0	10.0000	71.2161	34.5647	
5.2700	-3.8777	35.0000	0	12.0000	81.9594	34.5991	
3.7400	-2.0106	36.0000	0	13.0000	84.5104	34.6058	
5.0600	3.1395	126.0000	0	17.0000	79.1791	34.6080	
3.5200	1.2458	29.0000	0	13.0000	84.8566	34.6099	
3.5100	1.7845	28.0000	0	13.0000	81.2695	34.6103	
3.0300	-1.2609	37.0000	0	14.0000	92.8483	34.6109	
3.0700	-1.1903	35.0000	0	14.0000	89.7523	34.6109	
3.0200	-1.5934	36.0000	0	14.0000	90.8481	34.6110	
3.4100	1.2439	31.0000	0	13.0000	86.5363	34.6119	
5.7300	4.6825	42.0000	0	12.0000	76.8802	34.6120	
3.1100	0.1968	33.0000	0	14.0000	90.0005	34.6140	
3.1200	0.6364	31.0000	0	14.0000	90.6720	34.6144	
3.1400	1.4714	32.0000	0	14.0000	87.5234	34.6145	
11.4900	-10.7803	0	19.0000	18.0000	82.0474	34.8858	R
12.7401	10.6750	0	21.0000	21.0000	74.9298	34.9759	R
14.8301	13.4689	0	26.0000	26.0000	72.2280	35.3221	R
17.4301	16.2122	0	32.0000	32.0000	65.2272	35.8038	R
15.4500	15.8085	0	31.0000	31.0000	53.9500	36.0368	
15.5900	-16.5311	0	32.0000	31.0000	62.4927	36.0685	
23.6001	19.8335	0	42.0000	42.0000	32.7316	36.2926	R
22.4401	-20.2319	0	42.0000	41.0000	36.1665	36.5017	R
20.8700	19.5090	0	41.0000	41.0000	37.7131	36.7950	R
19.1901	-19.8838	0	41.0000	40.0000	43.1272	37.0915	R
24.9101	19.7459	0	51.0000	51.0000	6.8913	38.0673	R
			HYDROPHONE 2				
9.8801	-8.3137	23.0000	4.0000	13.0000	74.4526	34.5899	
9.4201	-8.5717	14.0000	9.0000	11.0000	72.9454	34.5945	
5.2600	-4.3751	35.0000	0	12.0000	82.0625	34.5991	
5.4100	4.4178	33.0000	0	12.0000	79.1505	34.6044	
3.7800	-3.1832	33.0000	0	13.0000	84.1878	34.6061	
5.0800	3.9473	28.0000	0	13.0000	82.0240	34.6071	
5.7400	4.9827	42.0000	0	12.0000	82.7198	34.6116	
2.9600	-1.8640	35.0000	0	14.0000	92.9719	34.6118	
2.9100	-2.2746	34.0000	0	14.0000	98.6870	34.6125	
2.9000	-2.2732	32.0000	0	14.0000	100.6569	34.6126	
2.8800	-2.2719	36.0000	0	14.0000	94.1395	34.6128	
2.8700	-2.2722	37.0000	0	14.0000	99.6810	34.6129	

2.2200	-1.1305	33.0000	0	16.0000	83.7539	34.6130	
2.2300	-0.9361	34.0000	0	16.0000	85.1150	34.6130	
2.4300	-1.0742	36.0000	0	15.0000	81.8107	34.6136	
2.4400	0.5384	32.0000	0	15.0000	96.0621	34.6136	
3.1500	2.1998	33.0000	0	14.0000	82.6676	34.6139	
2.4600	1.4276	30.0000	0	15.0000	85.1451	34.6142	
9.5801	-8.2656	23.0000	5.0000	13.0000	72.0275	34.6288	
9.1001	-8.2583	22.0000	4.0000	12.0000	71.2785	34.6429	
8.9601	-8.3064	24.0000	3.0000	12.0000	75.8058	34.6443	
8.7901	7.9245	27.0000	0	14.0000	91.1208	34.6955	
8.6901	7.9230	28.0000	0	14.0000	90.3469	34.7043	
11.5100	-11.0427	0	19.0000	18.0000	80.6225	34.8846	R
12.6501	10.8853	0	21.0000	21.0000	82.0131	34.9881	R
15.4200	-14.1318	0	27.0000	26.0000	63.3988	35.2736	
14.7901	13.7349	0	26.0000	26.0000	74.8372	35.3268	
18.2501	-16.7096	0	33.0000	32.0000	50.9109	35.7055	R
17.3601	16.2069	0	32.0000	32.0000	65.3260	35.8151	R
15.6200	-16.5354	0	32.0000	31.0000	62.7209	36.0650	R
23.5801	19.8342	0	42.0000	42.0000	32.5233	36.2953	R
22.4701	-20.2322	0	42.0000	41.0000	35.1117	36.4973	R
20.8400	19.5091	0	41.0000	41.0000	37.5658	36.7996	R
19.2301	-19.8860	0	41.0000	40.0000	40.9149	37.0848	R
24.8501	19.7428	0	51.0000	51.0000	5.7596	38.0863	R

HYDROPHONE 3

10.3500	-8.4015	21.0000	5.0000	13.0000	71.7701	34.5481	
7.2601	6.5014	20.0000	0	10.0000	77.7699	34.5722	
9.3801	-8.7232	18.0000	8.0000	11.0000	77.7173	34.5971	
5.2500	-4.6341	34.0000	0	12.0000	79.9894	34.5997	
3.8100	-3.5709	33.0000	0	13.0000	85.8399	34.6056	
3.8000	-3.4509	36.0000	0	13.0000	85.6257	34.6058	
4.4600	3.8682	32.0000	0	13.0000	77.9114	34.6080	
5.7600	5.2035	42.0000	0	12.0000	87.7719	34.6099	
2.7500	-2.3802	33.0000	0	14.0000	85.7410	34.6113	
2.7600	-2.3957	31.0000	0	14.0000	90.9100	34.6115	
2.7700	-2.3947	34.0000	0	14.0000	91.0000	34.6116	
2.7800	-2.2828	35.0000	0	14.0000	92.1615	34.6118	
2.2500	1.7588	31.0000	0	16.0000	82.6124	34.6132	
7.7801	8.0024	25.0000	0	13.0000	70.2431	34.7172	R
11.5200	-11.1197	0	19.0000	18.0000	76.0964	34.8853	R
12.4901	10.8812	0	21.0000	21.0000	65.2457	35.0101	R
14.7401	13.7346	0	26.0000	26.0000	76.0389	35.3332	R
17.3001	16.3933	0	32.0000	32.0000	64.8308	35.8241	R
15.6500	-16.5400	0	32.0000	31.0000	62.8901	36.0616	R
23.5601	19.9735	0	42.0000	42.0000	33.1293	36.2980	R
22.4901	-20.2327	0	42.0000	41.0000	35.7968	36.4942	R
20.6700	19.6342	0	41.0000	41.0000	38.6594	36.8374	R
19.2801	-19.8890	0	41.0000	40.0000	41.0320	37.0763	R

HYDROPHONE 4

6.1800	-6.1954	32.0000	0	8.0000	82.1694	34.5488	
9.5501	-8.8282	17.0000	8.0000	11.0000	75.4934	34.5817	
3.9800	-3.7623	35.0000	0	13.0000	82.7061	34.6051	
3.8200	-3.6757	37.0000	0	13.0000	83.5789	34.6055	
3.3800	-3.3398	33.0000	0	13.0000	77.2005	34.6061	
5.7800	5.4669	42.0000	0	12.0000	84.5104	34.6088	
4.0700	3.7742	31.0000	0	13.0000	76.6507	34.6102	
3.4900	3.2803	31.0000	0	14.0000	81.1359	34.6109	
2.7200	-2.7050	35.0000	0	14.0000	86.5136	34.6115	
2.7100	-2.7899	38.0000	0	14.0000	84.2842	34.6117	
2.4100	-2.4460	37.0000	0	15.0000	77.0555	34.6124	
3.1800	2.9932	34.0000	0	14.0000	85.8173	34.6129	
2.2000	-2.3048	36.0000	0	16.0000	79.9480	34.6134	
9.7601	8.3682	17.0000	9.0000	13.0000	82.1069	34.6187	
8.6201	8.2148	27.0000	0	14.0000	85.9763	34.7075	R
11.5300	-11.2162	0	19.0000	18.0000	78.5257	34.8852	R
15.4100	-14.2058	0	27.0000	26.0000	55.6390	35.2809	
14.6701	13.8941	0	26.0000	26.0000	75.5284	35.3425	
13.0801	-14.1102	0	26.0000	25.0000	62.4179	35.5348	R
17.2501	16.3905	0	32.0000	32.0000	63.8601	35.8317	R
15.6800	-16.5439	0	32.0000	31.0000	63.3112	36.0581	R
23.5401	19.9739	0	42.0000	42.0000	33.7756	36.3009	R
22.5201	-20.2345	0	42.0000	41.0000	35.8130	36.4895	R
20.6300	19.6329	0	41.0000	41.0000	38.8646	36.8441	R
19.3301	-19.8921	0	41.0000	40.0000	41.3073	37.0677	R

HYDROPHONE 5

7.0001	-6.9413	19.0000	0	8.0000	75.1270	34.5251	
9.6801	8.4837	22.0000	9.0000	11.0000	75.2540	34.5453	
6.1900	-6.2254	31.0000	0	8.0000	87.4095	34.5485	
6.0400	-6.1733	34.0000	0	8.0000	77.2233	34.5552	
5.2400	-4.9855	34.0000	0	12.0000	78.8796	34.6012	
3.8300	-3.7923	37.0000	0	13.0000	82.6098	34.6046	
3.9700	-3.9770	35.0000	0	13.0000	80.2141	34.6052	
5.8000	5.5693	42.0000	0	12.0000	88.8643	34.6076	
3.4800	3.4689	31.0000	0	14.0000	82.6301	34.6109	
2.7000	-2.9579	34.0000	0	14.0000	83.4417	34.6113	
2.1900	-2.6832	37.0000	0	16.0000	82.2108	34.6134	
2.4700	2.6265	34.0000	0	15.0000	76.2350	34.6135	
9.7501	8.5460	16.0000	9.0000	13.0000	81.8588	34.6225	
8.9001	-8.6710	19.0000	5.0000	11.0000	71.1665	34.6302	
7.6601	-8.2771	26.0000	0	12.0000	76.2699	34.6927	
8.6001	8.3284	27.0000	0	14.0000	86.8713	34.7084	
13.0401	-11.2369	0	22.0000	21.0000	64.0827	34.9991	R
14.6001	13.9993	0	26.0000	26.0000	77.0836	35.3518	R
17.2001	16.5075	0	32.0000	32.0000	64.4111	35.8386	R
15.7200	-16.6072	0	32.0000	31.0000	64.6623	36.0534	R
23.5201	19.9736	0	42.0000	42.0000	34.4221	36.3040	R
22.5501	-20.2361	0	42.0000	41.0000	35.2348	36.4850	R
20.5900	19.7508	0	41.0000	41.0000	39.1042	36.8501	R
19.3801	-19.8953	0	41.0000	40.0000	41.2806	37.0590	R

24.7101	19.9566		0	51.0000	51.0000	-12.5946	38.1403 R

HYDROPHONE 6

6.7301	-6.5062	24.0000	0	8.0000	85.3887	34.5334	
7.2301	-7.0787	21.0000	0	9.0000	73.2176	34.5509	
7.2801	6.8478	19.0000	0	10.0000	81.6423	34.5681	
9.9401	-8.6005	23.0000	4.0000	13.0000	69.7785	34.5846	
5.9400	-6.0241	40.0000	0	11.0000	75.7661	34.5938	
9.3401	-8.9350	16.0000	8.0000	11.0000	73.6931	34.6049	
3.8400	-4.0737	34.0000	0	13.0000	80.4553	34.6053	
5.8400	5.7742	42.0000	0	12.0000	86.7325	34.6054	
4.4500	4.2558	35.0000	0	13.0000	79.1857	34.6063	
4.0800	4.0282	30.0000	0	13.0000	78.6523	34.6089	
2.6700	-3.1992	32.0000	0	14.0000	83.5623	34.6114	
3.4600	3.7739	32.0000	0	13.0000	94.1943	34.6115	
3.4200	3.7723	31.0000	0	13.0000	74.7798	34.6118	
3.4500	3.7727	33.0000	0	13.0000	85.6882	34.6118	
2.1700	-2.8317	36.0000	0	17.0000	84.3708	34.6125	
1.7600	2.6718	37.0000	0	17.0000	93.5275	34.6150	
1.7500	2.6720	34.0000	0	18.0000	87.3795	34.6151	
9.7401	8.6945	16.0000	9.0000	13.0000	81.2176	34.6236	
7.6701	-8.3682	26.0000	0	12.0000	80.8483	34.6935	
8.5201	8.4104	27.0000	0	14.0000	80.9017	34.7146	
11.5400	-11.3108	0	19.0000	18.0000	75.0689	34.8864 R	
14.5301	13.9967	0	26.0000	26.0000	76.7759	35.3615 R	
13.0901	-14.1976	0	26.0000	25.0000	65.9933	35.5365 R	
17.1500	16.5044	0	32.0000	32.0000	64.8475	35.8461 R	
15.7600	-16.6109	0	32.0000	31.0000	63.8014	36.0479 R	
24.3901	-20.5048	0	43.0000	42.0000	21.7995	36.1714 R	
23.4701	20.0874	0	42.0000	42.0000	36.4253	36.3138 R	
22.5701	-20.2370	0	42.0000	41.0000	35.4650	36.4821 R	
20.5300	19.7469	0	41.0000	41.0000	39.4538	36.8622 R	
19.4301	-19.8984	0	41.0000	40.0000	41.1807	37.0503 R	

HYDROPHONE 7

6.7801	-6.5106	24.0000	0	8.0000	73.4603	34.5311
6.7201	-6.5591	23.0000	0	8.0000	73.1443	34.5342
10.1500	-8.6558	23.0000	4.0000	13.0000	79.3014	34.5631
5.2300	-5.3129	34.0000	0	12.0000	78.1413	34.6036
3.3700	-3.8271	31.0000	0	13.0000	80.0934	34.6062
2.2700	2.8957	32.0000	0	16.0000	75.4940	34.6122
3.4300	3.9422	32.0000	0	13.0000	81.2258	34.6122
3.2000	3.6690	33.0000	0	14.0000	77.8934	34.6135
1.6800	2.7534	35.0000	0	17.0000	82.2989	34.6144
1.6900	2.7440	33.0000	0	17.0000	85.5639	34.6146
1.7900	2.8275	33.0000	0	18.0000	84.7492	34.6148
9.7101	8.7181	17.0000	9.0000	13.0000	69.0059	34.6250
8.9501	-8.6845	23.0000	3.0000	12.0000	72.5930	34.6607
10.3900	8.6793	11.0000	11.0000	15.0000	97.7079	34.6670
8.5101	8.4818	27.0000	0	14.0000	82.9342	34.7140

11.5500	-11.3583	0	19.0000	18.0000	76.8271	34.8868	R
14.4501	14.0910	0	26.0000	26.0000	76.9178	35.3719	R
13.1001	-14.2447	0	26.0000	25.0000	66.9958	35.5378	R
17.0900	16.5006	0	32.0000	32.0000	64.6563	35.8554	R
15.7900	-16.6456	0	32.0000	31.0000	63.2850	36.0448	R
24.4001	-20.5035	0	43.0000	42.0000	27.6772	36.1719	
24.5401	20.2243	0	43.0000	43.0000	24.7608	36.1896	
23.4301	20.0846	0	42.0000	42.0000	35.2288	36.3214	R
22.5901	-20.2841	0	42.0000	41.0000	34.9470	36.4795	R
20.4900	19.7453	0	41.0000	41.0000	38.7093	36.8691	R
18.2701	19.5355	0	39.0000	39.0000	43.1664	37.0239	
19.4801	-19.9481	0	41.0000	40.0000	41.0658	37.0429	
18.3901	19.5358	0	40.0000	40.0000	28.6644	37.1677	R

HYDROPHONE 8

6.4901	-6.6551	20.0000	0	9.0000	76.0663	34.5420	
10.1000	-8.7826	17.0000	8.0000	12.0000	83.6994	34.5555	
7.3301	6.9987	20.0000	0	10.0000	76.7346	34.5612	
7.3001	7.0077	21.0000	0	10.0000	78.6764	34.5639	
4.4400	4.5260	33.0000	0	13.0000	80.7661	34.6053	
3.8600	-4.2683	37.0000	0	13.0000	81.0829	34.6072	
3.9300	-4.2713	36.0000	0	13.0000	84.1145	34.6072	
2.1500	-3.0453	34.0000	0	16.0000	77.1946	34.6123	
1.6000	2.8218	31.0000	0	18.0000	84.3046	34.6140	
1.6100	2.8238	33.0000	0	18.0000	88.4607	34.6141	
1.6200	2.8262	34.0000	0	18.0000	87.6881	34.6141	
2.4900	3.2786	34.0000	0	15.0000	79.7407	34.6142	
1.8300	2.9084	36.0000	0	18.0000	88.3969	34.6145	
1.8500	2.9443	37.0000	0	17.0000	88.4486	34.6145	
1.8600	2.9475	38.0000	0	17.0000	89.9119	34.6145	
1.8700	2.9506	36.0000	0	17.0000	88.1069	34.6146	
8.5001	8.4845	27.0000	0	14.0000	79.5235	34.7140	R
12.9801	-12.5758	0	22.0000	21.0000	63.5496	35.0235	R
11.6300	-11.3509	0	21.0000	20.0000	75.6184	35.0917	R
14.3801	14.0919	0	26.0000	26.0000	77.3569	35.3814	R
17.0100	16.5614	0	32.0000	32.0000	66.5519	35.8676	R
15.8300	-16.6487	0	32.0000	31.0000	62.7803	36.0398	R
24.4101	-20.5030	0	43.0000	42.0000	27.3978	36.1725	R
23.4001	20.1411	0	42.0000	42.0000	35.2906	36.3267	R
22.6301	-20.2826	0	42.0000	41.0000	35.1916	36.4719	R
20.4400	19.8024	0	41.0000	41.0000	39.3015	36.8767	R
19.5301	-19.9510	0	41.0000	40.0000	41.0332	37.0341	R

HYDROPHONE 9

6.2100	-6.4777	32.0000	0	8.0000	78.2679	34.5499
10.0500	-8.6481	23.0000	4.0000	13.0000	68.8195	34.5764
4.4300	4.5161	30.0000	0	13.0000	82.3544	34.6034
3.8900	-4.2507	35.0000	0	13.0000	93.0906	34.6071
3.8800	-4.2505	37.0000	0	13.0000	82.3202	34.6073
3.8700	-4.2505	38.0000	0	13.0000	82.3202	34.6075

4.1000	4.3296	31.0000	0	13.0000	92.7447	34.6075	
0.0100	2.4910	29.0000	0	17.0000	88.4711	34.6086	
4.0900	4.4045	32.0000	0	14.0000	76.9184	34.6086	
2.2800	3.0795	34.0000	0	16.0000	77.1096	34.6127	
1.5500	2.8262	35.0000	0	18.0000	83.7825	34.6136	
1.5600	2.8473	37.0000	0	18.0000	83.5262	34.6138	
2.5000	3.2975	35.0000	0	15.0000	82.7834	34.6141	
1.8900	2.9768	36.0000	0	17.0000	85.8600	34.6144	
1.9100	2.9664	37.0000	0	17.0000	86.3548	34.6144	
2.5100	3.2835	34.0000	0	15.0000	83.8681	34.6144	
1.9000	2.9786	35.0000	0	17.0000	87.1345	34.6145	
9.1701	-8.8374	17.0000	7.0000	11.0000	69.9883	34.6214	
7.6801	-8.3897	26.0000	0	12.0000	78.1157	34.6960	R
11.5600	-11.3548	0	19.0000	18.0000	74.7405	34.8880	R
11.6100	-11.3504	0	21.0000	20.0000	73.5302	35.0963	R
14.2901	14.1118	0	26.0000	26.0000	78.1330	35.3934	R
16.9200	16.5555	0	32.0000	32.0000	67.5459	35.8819	R
15.8500	-16.6289	0	32.0000	31.0000	62.4436	36.0383	R
24.3701	-20.4659	0	43.0000	42.0000	23.3981	36.1865	
24.5301	20.2846	0	43.0000	43.0000	25.2338	36.1880	
23.3701	20.1396	0	42.0000	42.0000	35.3201	36.3322	R
22.6501	-20.2531	0	42.0000	41.0000	35.1780	36.4693	R
20.4100	19.8015	0	41.0000	41.0000	38.4805	36.8818	R
19.5701	-19.9216	0	41.0000	40.0000	40.9449	37.0281	R

HYDROPHONE 10

6.3801	6.3986	23.0000	0	9.0000	76.0695	34.5558	
6.0300	6.3075	31.0000	0	9.0000	71.9876	34.5649	
10.0600	-8.6973	23.0000	4.0000	13.0000	82.9998	34.5839	
4.4200	4.4950	30.0000	0	13.0000	80.2070	34.6034	
5.8700	5.9170	41.0000	0	12.0000	81.5520	34.6038	
3.3400	-3.8104	33.0000	0	14.0000	92.5496	34.6081	
3.3300	-3.8091	34.0000	0	14.0000	79.2503	34.6083	
0.0600	2.4245	27.0000	0	17.0000	86.9606	34.6086	
2.6400	-3.3145	36.0000	0	14.0000	82.0412	34.6117	
3.2200	3.7438	30.0000	0	14.0000	80.3134	34.6124	
2.1400	-2.9798	34.0000	0	16.0000	76.7822	34.6128	
1.5300	2.7562	37.0000	0	18.0000	80.9366	34.6133	
1.9400	2.8891	35.0000	0	17.0000	84.2725	34.6142	
9.6401	8.6890	17.0000	9.0000	13.0000	68.3170	34.6314	
8.4401	-8.5524	27.0000	0	14.0000	75.1737	34.6947	
7.7001	-8.3529	26.0000	0	12.0000	83.0101	34.6959	
12.0000	-11.3221	0	21.0000	20.0000	83.9062	35.0291	
11.8800	11.2156	0	21.0000	21.0000	74.8763	35.0802	
14.1801	14.1081	0	26.0000	26.0000	79.2232	35.4087	R
13.1301	-14.2383	0	26.0000	25.0000	73.2166	35.5376	R
16.8300	16.5507	0	32.0000	32.0000	66.6980	35.8963	R
15.8800	-16.6314	0	32.0000	31.0000	63.0770	36.0346	R
24.3801	-20.4657	0	43.0000	42.0000	27.7887	36.1867	R
23.3401	20.1384	0	42.0000	42.0000	34.8557	36.3373	R
22.6801	-20.2545	0	42.0000	41.0000	35.3448	36.4649	R
20.3600	19.8000	0	41.0000	41.0000	39.2907	36.8903	R
19.6201	-19.9235	0	41.0000	40.0000	40.6985	37.0193	R

HYDROPHONE 11

10.2900	-8.5201	22.0000	4.0000	13.0000	74.5918	34.5544	
7.2901	6.9111	19.0000	0	10.0000	76.3183	34.5597	
9.9701	-8.5225	24.0000	4.0000	13.0000	74.1964	34.5874	
4.1100	4.2339	32.0000	0	13.0000	78.7570	34.6069	
0.1200	2.2687	28.0000	0	17.0000	87.5601	34.6085	
9.4101	8.6182	15.0000	8.0000	12.0000	74.1037	34.6112	
2.6100	-3.1218	33.0000	0	14.0000	81.5199	34.6118	
2.2900	2.8892	36.0000	0	16.0000	77.2450	34.6125	
1.5100	2.6044	32.0000	0	19.0000	84.6509	34.6129	
1.9700	2.8663	31.0000	0	17.0000	88.7595	34.6145	
1.9800	2.8316	32.0000	0	17.0000	86.3594	34.6145	
9.2601	8.6170	16.0000	8.0000	12.0000	71.0924	34.6289	
12.5001	11.1888	0	21.0000	21.0000	65.6602	34.9902	
11.8600	-11.3191	0	21.0000	20.0000	77.5419	35.0498	
14.0601	14.0723	0	26.0000	26.0000	78.8534	35.4251	R
13.1501	-14.1958	0	26.0000	25.0000	72.7723	35.5364	R
16.7200	16.5431	0	32.0000	32.0000	66.8359	35.9145	R
15.9200	-16.5941	0	32.0000	31.0000	63.4517	36.0304	R
24.6901	20.3055	0	44.0000	44.0000	14.0856	36.3099	
23.3001	20.1363	0	42.0000	42.0000	35.7012	36.3446	
22.7001	-20.2556	0	42.0000	41.0000	35.6383	36.4617	R
20.3200	19.7987	0	41.0000	41.0000	39.5796	36.8971	R
19.6601	-19.9250	0	41.0000	40.0000	40.5354	37.0123	R

HYDROPHONE 12

6.4301	6.2827	24.0000	0	9.0000	89.6127	34.5511	
5.8800	5.8484	41.0000	0	12.0000	79.4809	34.6035	
4.4000	4.3367	32.0000	0	13.0000	81.1690	34.6044	
5.1800	-5.0945	34.0000	0	12.0000	77.9052	34.6076	
0.1500	2.2201	27.0000	0	17.0000	88.5332	34.6085	
0.1600	2.1676	28.0000	0	17.0000	86.2914	34.6085	
0.1700	2.1561	29.0000	0	17.0000	87.1690	34.6085	
3.3200	-3.6215	34.0000	0	13.0000	80.8535	34.6087	
3.2400	3.5394	32.0000	0	14.0000	79.4335	34.6113	
2.6000	-2.9887	36.0000	0	14.0000	79.7294	34.6118	
1.4800	2.5083	31.0000	0	18.0000	86.1824	34.6128	
2.1300	-2.7349	34.0000	0	16.0000	81.7180	34.6134	
2.0000	2.7577	34.0000	0	17.0000	83.0568	34.6147	
7.7101	-8.3325	26.0000	0	12.0000	79.3245	34.6980	R
11.9700	-11.2825	0	21.0000	20.0000	78.9192	35.0374	
11.8300	11.1377	0	21.0000	21.0000	70.3082	35.0798	
13.9401	14.0684	0	26.0000	26.0000	78.8688	35.4415	R
13.1801	-14.1533	0	26.0000	25.0000	72.5735	35.5344	R
16.6500	16.5382	0	32.0000	32.0000	66.1088	35.9256	R
15.9700	-16.5976	0	32.0000	31.0000	65.5213	36.0232	R
24.5101	20.2899	0	43.0000	43.0000	26.8543	36.1844	R
23.2701	20.1347	0	42.0000	42.0000	35.6155	36.3501	R
22.7301	-20.2143	0	42.0000	41.0000	35.7554	36.4572	R
20.2800	19.7971	0	41.0000	41.0000	39.4713	36.9041	R

19.7501	-19.8870		0	41.0000	40.0000	41.1746	36.9950 R

HYDROPHONE 13

7.3201	6.8537	20.0000	0	10.0000	75.4929	34.5577	
9.8301	8.5903	16.0000	9.0000	13.0000	72.4467	34.6068	
4.1200	4.1334	33.0000	0	13.0000	79.4189	34.6073	
4.1300	4.1085	31.0000	0	13.0000	84.1847	34.6076	
0.2100	2.0172	27.0000	0	17.0000	87.7163	34.6083	
0.9000	-2.1376	32.0000	0	16.0000	92.4143	34.6090	
0.9800	-2.1914	30.0000	0	16.0000	93.9919	34.6091	
1.0100	-2.2061	28.0000	0	17.0000	96.1761	34.6093	
1.0200	-2.2120	29.0000	0	17.0000	93.2634	34.6093	
1.0400	-2.2169	31.0000	0	16.0000	95.1576	34.6093	
1.0500	-2.2217	30.0000	0	17.0000	92.2944	34.6093	
3.3000	-3.5531	32.0000	0	13.0000	83.7259	34.6093	
1.0700	-2.1951	27.0000	0	16.0000	90.1986	34.6094	
1.0800	-2.1601	29.0000	0	16.0000	88.1058	34.6095	
2.3000	2.6582	34.0000	0	16.0000	77.3741	34.6121	
1.4500	2.3618	31.0000	0	18.0000	78.9123	34.6125	
2.1200	-2.6580	36.0000	0	16.0000	81.8799	34.6132	
2.0100	2.6206	34.0000	0	17.0000	80.8960	34.6145	
9.2101	-8.4851	22.0000	3.0000	12.0000	85.5376	34.6262	
7.7201	-8.3059	26.0000	0	12.0000	83.3586	34.6982 R	
12.0100	-11.2540	0	21.0000	20.0000	70.3709	35.0335	
12.0300	11.1396	0	21.0000	21.0000	73.0061	35.0511	
13.8301	14.0650	0	26.0000	26.0000	78.6391	35.4564 R	
13.1901	-14.1535	0	26.0000	25.0000	70.6539	35.5337 R	
16.5700	16.5326	0	32.0000	32.0000	66.5419	35.9380 R	
16.0200	-16.5719	0	32.0000	31.0000	64.9706	36.0168 R	
24.5001	20.2913	0	43.0000	43.0000	26.1304	36.1849 R	
23.2401	20.1331	0	42.0000	42.0000	35.8631	36.3555 R	
22.7601	-20.2160	0	42.0000	41.0000	35.5000	36.4525 R	
20.2400	19.7955	0	41.0000	41.0000	39.8323	36.9108 R	
19.8001	-19.8891	0	41.0000	40.0000	41.0684	36.9859 R	

HYDROPHONE 14

6.4801	6.2757	22.0000	0	9.0000	91.8753	34.5508
6.2200	-6.1502	31.0000	0	8.0000	77.4682	34.5516
6.4701	6.2828	46.0000	0	18.0000	81.7271	34.5520
7.5701	-7.1387	22.0000	0	10.0000	70.7041	34.5776
9.5101	8.5461	16.0000	8.0000	12.0000	70.1657	34.5985
4.3800	4.2230	29.0000	0	13.0000	82.4682	34.6042
4.1400	4.0386	32.0000	0	13.0000	82.6945	34.6073
0.2600	1.9263	29.0000	0	17.0000	88.4186	34.6085
0.8100	-1.9300	31.0000	0	16.0000	89.4463	34.6091
0.8400	-2.0107	31.0000	0	17.0000	88.0979	34.6091
1.1200	-2.0974	28.0000	0	16.0000	86.5873	34.6099
1.1300	-2.0715	30.0000	0	16.0000	87.3547	34.6100
1.4400	2.1630	30.0000	0	17.0000	83.6084	34.6120
2.5300	2.8084	33.0000	0	15.0000	80.2181	34.6126

2.5900	-2.9437	35.0000	0	14.0000	79.2481	34.6130	
2.1100	-2.5425	36.0000	0	16.0000	82.0088	34.6132	
2.0200	2.4829	35.0000	0	17.0000	79.2159	34.6141	
9.0901	8.5378	17.0000	7.0000	12.0000	70.7126	34.6421	
13.0201	-12.2672	0	22.0000	21.0000	73.3231	35.0269	
11.8000	-11.2504	0	21.0000	20.0000	85.7548	35.0636	
11.7100	11.1330	0	21.0000	21.0000	67.3867	35.1003	
13.7301	14.0620	0	26.0000	26.0000	78.6462	35.4699	
13.2301	-14.1189	0	26.0000	25.0000	73.9508	35.5303	
16.4900	16.5270	0	32.0000	32.0000	66.4554	35.9507	
16.0700	-16.5756	0	32.0000	31.0000	65.0836	36.0097	
24.4901	20.2933	0	43.0000	43.0000	22.8931	36.1839	R
23.2001	20.1314	0	42.0000	42.0000	35.7261	36.3628	R
22.8001	-20.1862	0	42.0000	41.0000	36.7023	36.4444	R
20.1900	19.7930	0	41.0000	41.0000	40.0015	36.9198	
19.8501	-19.8572	0	41.0000	40.0000	40.8983	36.9780	

HYDROPHONE 15

6.7501	-6.5497	21.0000	0	7.0000	71.7002	34.5146	
6.6401	6.4043	21.0000	0	8.0000	72.2484	34.5252	
5.9200	-5.8120	39.0000	0	12.0000	79.6993	34.6001	
5.1700	-4.9075	34.0000	0	12.0000	78.6904	34.6083	
0.3300	1.6933	33.0000	0	17.0000	85.0701	34.6084	
0.3400	1.6879	34.0000	0	17.0000	88.9573	34.6084	
0.7700	-1.8513	32.0000	0	16.0000	87.4888	34.6090	
0.7500	-1.8026	30.0000	0	16.0000	88.0382	34.6092	
0.7600	-1.8297	30.0000	0	17.0000	86.8456	34.6092	
9.7801	8.5481	17.0000	8.0000	13.0000	71.7066	34.6093	
5.1500	4.8549	32.0000	0	13.0000	74.4812	34.6105	
1.1700	-2.0037	29.0000	0	16.0000	83.4189	34.6107	
1.4000	1.9883	35.0000	0	17.0000	88.8305	34.6118	
1.4200	2.0785	32.0000	0	17.0000	83.5690	34.6118	
5.1300	4.9142	31.0000	0	13.0000	73.2620	34.6125	
2.0900	-2.3930	38.0000	0	16.0000	80.6079	34.6129	
9.3101	8.5401	17.0000	8.0000	12.0000	67.6847	34.6208	
7.7401	-8.2335	26.0000	0	12.0000	80.9442	34.6987	R
12.1000	-11.2190	0	21.0000	20.0000	72.4460	35.0256	R
13.6401	14.0595	0	26.0000	26.0000	77.7124	35.4819	
13.3101	-14.1211	0	26.0000	25.0000	73.4777	35.5202	
16.4100	16.5214	0	32.0000	32.0000	66.3702	35.9634	
16.1200	-16.5455	0	32.0000	31.0000	64.5200	36.0033	
23.0101	20.1107	0	42.0000	42.0000	35.7648	36.4081	
22.8301	-20.1874	0	42.0000	41.0000	35.8690	36.4395	
20.1500	19.7910	0	41.0000	41.0000	40.1053	36.9270	
19.9001	-19.8594	0	41.0000	40.0000	40.9451	36.9690	
18.3501	-19.7114	0	40.0000	39.0000	33.7800	37.1354	R

HYDROPHONE 16

6.3701	6.1595	25.0000	0	9.0000	89.8872	34.5509
10.3100	8.5578	15.0000	8.0000	13.0000	69.2232	34.5540
4.3500	4.0109	30.0000	0	13.0000	83.0594	34.6031

4.3100	3.9939	29.0000	0	13.0000	84.4584	34.6041	
4.2500	-4.0319	30.0000	0	12.0000	97.4540	34.6053	
4.1900	3.9263	31.0000	0	13.0000	84.1616	34.6054	
4.2400	-4.0558	28.0000	0	12.0000	83.1009	34.6064	
0.4000	1.5370	29.0000	0	17.0000	90.6496	34.6084	
0.4200	1.5062	30.0000	0	17.0000	88.9022	34.6085	
0.7100	-1.7032	31.0000	0	16.0000	87.1150	34.6093	
0.7000	-1.6706	32.0000	0	16.0000	87.8697	34.6094	
3.2700	3.1659	36.0000	0	14.0000	81.2573	34.6104	
1.2100	-1.9175	28.0000	0	16.0000	89.4330	34.6110	
1.2200	-1.9175	27.0000	0	16.0000	90.4993	34.6110	
1.2400	-1.8862	29.0000	0	16.0000	87.8468	34.6110	
1.3700	1.9304	33.0000	0	17.0000	86.8783	34.6119	
2.3200	2.3465	33.0000	0	16.0000	77.0698	34.6119	
1.3500	1.8848	31.0000	0	17.0000	85.9762	34.6120	
1.3600	1.9280	32.0000	0	17.0000	85.5294	34.6120	
2.5500	2.5488	30.0000	0	15.0000	78.9044	34.6122	
2.0800	-2.3105	37.0000	0	16.0000	80.5857	34.6131	
8.9801	-9.0491	17.0000	6.0000	10.0000	69.7367	34.6161	
9.2801	-9.0787	15.0000	8.0000	11.0000	69.5766	34.6247	
8.4501	-8.3734	28.0000	0	13.0000	74.1797	34.7021	R
13.5501	14.0571	0	26.0000	26.0000	77.6399	35.4936	
13.3401	-14.0889	0	26.0000	25.0000	74.2337	35.5176	
16.3500	16.5172	0	32.0000	32.0000	65.0820	35.9726	
16.1600	-16.5484	0	32.0000	31.0000	64.9918	35.9978	
24.4701	-20.1854	0	43.0000	43.0000	23.2387	36.1764	R
22.8701	-19.9860	0	42.0000	42.0000	35.0064	36.4325	R
19.9601	-19.6598	0	41.0000	41.0000	40.3247	36.9591	
19.9501	-19.8615	0	41.0000	40.0000	40.9984	36.9601	
18.3601	-19.7090	0	40.0000	39.0000	36.1161	37.1353	R

RAMP - relative amplitude in dB (RAMP=SL-TL, Sea State 3, 0.5 dB/bottom bounce)

R - ray is temporally resolvable using a 62.5msec pulse separation.

Hydrophone depths in km above mean sea level:

Hydrophone #	Depth
1	-.150;
2	-.160;
3	-.170;
4	-.180;
5	-.190;
6	-.200;
7	-.210;
8	-.220;
9	-.230;
10	-.240;
11	-.250;
12	-.260;
13	-.270;
14	-.280;
15	-.290;
16	-.300;

Note that the ocean bottom at the hydrophone array location is modeled at 318m or -.318km above mean sea level.

APPENDIX C: LINE ARRAY RESOLVABILITY ANALYSIS TABLE

The following table was generated by treating the 16 hydrophones of the vertical linear array at position (B) in Figure 2 as a plane wave beamformer. The compilation was accomplished using the MATLAB computer program 'resanl.m'. A copy of 'resanl.m' can be found in Appendix A. Definitions of RAMP, R, and sector angles can be found at the end of the Appendix.

LAUNCH ANGLE (deg)	ARRIVAL ANGLE (deg)	NUMBER TURNING POINTS	NUMBER SURFACE BOUNCES	NUMBER BOTTOM BOUNCES	RAMP (dB)	ARRIVAL TIME (sec) (R-resovable)
			SECTOR 1			
24.4701	-20.1854	0	43.0000	43.0000	23.2387	36.1764
24.3801	-20.4657	0	43.0000	42.0000	27.7887	36.1867
22.8701	-19.9860	0	42.0000	42.0000	35.0064	36.4325 R
22.4401	-20.2319	0	42.0000	41.0000	36.1665	36.5017 R
19.9601	-19.6598	0	41.0000	41.0000	40.3247	36.9591 R
19.1901	-19.8838	0	41.0000	40.0000	43.1272	37.0915
18.3501	-19.7114	0	40.0000	39.0000	33.7800	37.1354
			SECTOR 2			
18.2501	-16.7096	0	33.0000	32.0000	50.9109	35.7055 R
15.5900	-16.5311	0	32.0000	31.0000	62.4927	36.0685 R
			SECTOR 3			
15.4100	-14.2058	0	27.0000	26.0000	55.6390	35.2809 R
13:1001	-14.2447	0	26.0000	25.0000	66.9958	35.5378 R
			SECTOR 4			
11.5600	-11.3548	0	19.0000	18.0000	74.7405	34.8880 R
13.0201	-12.2672	0	22.0000	21.0000	73.3231	35.0269 R
11.6100	-11.3504	0	21.0000	20.0000	73.5302	35.0963 R
			SECTOR 5			
10.3500	-8.4015	21.0000	5.0000	13.0000	71.7701	34.5481
10.3300	-8.0038	20.0000	5.0000	13.0000	85.4431	34.5504
10.2900	-8.5201	22.0000	4.0000	13.0000	74.5918	34.5544
10.1000	-8.7826	17.0000	8.0000	12.0000	83.6994	34.5555
9.5501	-8.8282	17.0000	8.0000	11.0000	75.4934	34.5817
9.9701	-8.5225	24.0000	4.0000	13.0000	74.1964	34.5874
9.8801	-8.3137	23.0000	4.0000	13.0000	74.4526	34.5899
9.4201	-8.5717	14.0000	9.0000	11.0000	72.9454	34.5945
9.3801	-8.7232	18.0000	8.0000	11.0000	77.7173	34.5971
9.3401	-8.9350	16.0000	8.0000	11.0000	73.6931	34.6049
8.9801	-9.0491	17.0000	6.0000	10.0000	69.7367	34.6161
9.1701	-8.8374	17.0000	7.0000	11.0000	69.9883	34.6214
9.2801	-9.0787	15.0000	8.0000	11.0000	69.5766	34.6247
9.2101	-8.4851	22.0000	3.0000	12.0000	85.5376	34.6262
9.5801	-8.2656	23.0000	5.0000	13.0000	72.0275	34.6288
8.9001	-8.6710	19.0000	5.0000	11.0000	71.1665	34.6302
9.1001	-8.2583	22.0000	4.0000	12.0000	71.2785	34.6429
8.9601	-8.3064	24.0000	3.0000	12.0000	75.8058	34.6443
8.9501	-8.6845	23.0000	3.0000	12.0000	72.5930	34.6607

8.4401	-8.5524	27.0000	0	14.0000	75.1737	34.6947
7.7401	-8.2335	26.0000	0	12.0000	80.9442	34.6987
8.4501	-8.3734	28.0000	0	13.0000	74.1797	34.7021

SECTOR 6

6.7501	-6.5497	21.0000	0	7.0000	71.7002	34.5146
7.0001	-6.9413	19.0000	0	8.0000	75.1270	34.5251
6.8401	-5.8326	25.0000	0	8.0000	75.6515	34.5254
6.7301	-6.5062	24.0000	0	8.0000	85.3887	34.5334
6.7201	-6.5591	23.0000	0	8.0000	73.1443	34.5342
6.4901	-6.6551	20.0000	0	9.0000	76.0663	34.5420
6.1600	-5.3830	30.0000	0	8.0000	90.4353	34.5479
6.1500	-5.4052	33.0000	0	8.0000	79.7049	34.5485
6.2100	-6.4777	32.0000	0	8.0000	78.2679	34.5499
7.2301	-7.0787	21.0000	0	9.0000	73.2176	34.5509
6.2200	-6.1502	31.0000	0	8.0000	77.4682	34.5516
6.0400	-6.1733	34.0000	0	8.0000	77.2233	34.5552
7.5701	-7.1387	22.0000	0	10.0000	70.7041	34.5776
5.9400	-6.0241	40.0000	0	11.0000	75.7661	34.5938
5.9200	-5.8120	39.0000	0	12.0000	79.6993	34.6001
5.1700	-4.9075	34.0000	0	12.0000	78.6904	34.6083

SECTOR 7

5.2600	-4.3751	35.0000	0	12.0000	82.0625	34.5991
4.2500	-4.0319	30.0000	0	12.0000	97.4540	34.6053
3.3800	-3.3398	33.0000	0	13.0000	77.2005	34 6061
3.3700	-3.8271	31.0000	0	13.0000	80.0934	34.6062
4.2400	-4.0558	28.0000	0	12.0000	83.1009	34.6064
3.8900	-4.2507	35.0000	0	13.0000	93.0906	34.6071
3.9300	-4.2713	36.0000	0	13.0000	84.1145	34.6072
3.8800	-4.2505	37.0000	0	13.0000	82.3202	34.6073
3.8700	-4.2505	38.0000	0	13.0000	82.3202	34.6075
3.3200	-3.6215	34.0000	0	13.0000	80.8535	34.6087
0.8400	-2.0107	31.0000	0	17.0000	88.0979	34.6091
1.0100	-2.2061	28.0000	0	17.0000	96.1761	34.6093
1.0200	-2.2120	29.0000	0	17.0000	93.2634	34.6093
1.0500	-2.2217	30.0000	0	17.0000	92.2944	34.6093
3.3000	-3.5531	32.0000	0	13.0000	83.7259	34.6093
0.7100	-1.7032	31.0000	0	16.0000	87.1150	34.6093
0.7000	-1.6706	32.0000	0	16.0000	87.8697	34.6094
1.1300	-2.0715	30.0000	0	16.0000	87.3547	34.6100
1.2100	-1.9175	28.0000	0	16.0000	89.4330	34.6110
1.2200	-1.9175	27.0000	0	16.0000	90.4993	34.6110
1.2400	-1.8862	29.0000	0	16.0000	87.8468	34.6110
2.7600	-2.3957	31.0000	0	14.0000	90.9100	34.6115
2.7100	-2.7899	38.0000	0	14.0000	84.2842	34.6117
2.4100	-2.4460	37.0000	0	15.0000	77.0555	34.6124
2.9100	-2.2746	34.0000	0	14.0000	98.6870	34.6125
2.1700	-2.8317	36.0000	0	17.0000	84.3708	34.6125
2.9000	-2.2732	32.0000	0	14.0000	100.6569	34.6126
2.8900	-2.2730	33.0000	0	14.0000	94.1395	34.6127
2.8800	-2.2719	36.0000	0	14.0000	94.1395	34.6128

2.8700	-2.2722	37.0000	0	14.0000	99.6810	34.6129
2.1800	-2.7653	37.0000	0	17.0000	84.5048	34.6129
2.0900	-2.3930	38.0000	0	16.0000	80.6079	34.6129
2.5900	-2.9437	35.0000	0	14.0000	79.2481	34.6130
2.2000	-2.3048	36.0000	0	16.0000	79.9480	34.6134
2.1900	-2.6832	37.0000	0	16.0000	82.2108	34.6134
2.1300	-2.7349	34.0000	0	16.0000	81.7180	34.6134

SECTOR 8

3.5200	1.2458	29.0000	0	13.0000	84.8566	34.6099
3.0300	-1.2609	37.0000	0	14.0000	92.8483	34.6109
3.0700	-1.1903	35.0000	0	14.0000	89.7523	34.6109
3.4100	1.2439	31.0000	0	13.0000	86.5363	34.6119
2.2200	-1.1305	33.0000	0	16.0000	83.7539	34.6130
2.2300	-0.9361	34.0000	0	16.0000	85.1150	34.6130
2.4300	-1.0742	36.0000	0	15.0000	81.8107	34.6136
2.4400	0.5384	32.0000	0	15.0000	96.0621	34.6136
3.1100	0.1968	33.0000	0	14.0000	90.0005	34.6140
2.4600	1.4276	30.0000	0	15.0000	85.1451	34.6142
3.1200	0.6364	31.0000	0	14.0000	90.6720	34.6144
3.1400	1.4714	32.0000	0	14.0000	87.5234	34.6145

SECTOR 9

5.4100	4.4178	33.0000	0	12.0000	79.1505	34.6044
4.4500	4.2558	35.0000	0	13.0000	79.1857	34.6063
5.0600	3.1395	126.0000	0	17.0000	79.1791	34.6080
5.0700	3.3391	29.0000	0	13.0000	86.2085	34.6085
0.1600	2.1676	28.0000	0	17.0000	86.2914	34.6085
0.0100	2.4910	29.0000	0	17.0000	88.4711	34.6086
0.0600	2.4245	27.0000	0	17.0000	86.9606	34.6086
4.0800	4.0282	30.0000	0	13.0000	78.6523	34.6089
3.5100	1.7845	28.0000	0	13.0000	81.2695	34.6103
3.2700	3.1659	36.0000	0	14.0000	81.2573	34.6104
3.4800	3.4689	31.0000	0	14.0000	82.6301	34.6109
3.2400	3.5394	32.0000	0	14.0000	79.4335	34.6113
3.4200	3.7723	31.0000	0	13.0000	74.7798	34.6118
3.4500	3.7727	33.0000	0	13.0000	85.6882	34.6118
2.3200	2.3465	33.0000	0	16.0000	77.0698	34.6119
1.4400	2.1630	30.0000	0	17.0000	83.6084	34.6120
2.2700	2.8957	32.0000	0	16.0000	75.4940	34.6122
3.4300	3.9422	32.0000	0	13.0000	81.2258	34.6122
2.5500	2.5488	30.0000	0	15.0000	78.9044	34.6122
3.2200	3.7438	30.0000	0	14.0000	80.3134	34.6124
2.2900	2.8892	36.0000	0	16.0000	77.2450	34.6125
2.5300	2.8084	33.0000	0	15.0000	80.2181	34.6126
2.2800	3.0795	34.0000	0	16.0000	77.1096	34.6127
3.1800	2.9932	34.0000	0	14.0000	85.8173	34.6129
1.5100	2.6044	32.0000	0	19.0000	84.6509	34.6129
2.2500	1.7588	31.0000	0	16.0000	82.6124	34.6132
1.5500	2.8262	35.0000	0	18.0000	83.7825	34.6136
1.5600	2.8473	37.0000	0	18.0000	83.5262	34.6138
3.1500	2.1998	33.0000	0	14.0000	82.6676	34.6139

1.6000	2.8218	31.0000	0	18.0000	84.3046	34.6140
2.5000	3.2975	35.0000	0	15.0000	82.7834	34.6141
2.5100	3.2835	34.0000	0	15.0000	83.8681	34.6144
1.8300	2.9084	36.0000	0	18.0000	88.3969	34.6145
1.8600	2.9475	38.0000	0	17.0000	89.9119	34.6145
1.9000	2.9786	35.0000	0	17.0000	87.1345	34.6145
1.9700	2.8663	31.0000	0	17.0000	88.7595	34.6145
1.9800	2.8316	32.0000	0	17.0000	86.3594	34.6145
1.6900	2.7440	33.0000	0	17.0000	85.5639	34.6146
1.8700	2.9506	36.0000	0	17.0000	88.1069	34.6146
2.0000	2.7577	34.0000	0	17.0000	83.0568	34.6147
1.7900	2.8275	33.0000	0	18.0000	84.7492	34.6148
1.7600	2.6718	37.0000	0	17.0000	93.5275	34.6150
1.7500	2.6720	34.0000	0	18.0000	87.3795	34.6151

SECTOR 10

6.6401	6.4043	21.0000	0	8.0000	72.2484	34.5252
6.4801	6.2757	22.0000	0	9.0000	91.8753	34.5508
6.3701	6.1595	25.0000	0	9.0000	89.8872	34.5509
6.4301	6.2827	24.0000	0	9.0000	89.6127	34.5511
6.4701	6.2828	46.0000	0	18.0000	81.7271	34.5520
6.3801	6.3986	23.0000	0	9.0000	76.0695	34.5558
7.3001	7.0077	21.0000	0	10.0000	78.6764	34.5639
6.0300	6.3075	31.0000	0	9.0000	71.9876	34.5649
7.2801	6.8478	19.0000	0	10.0000	81.6423	34.5681
7.2601	6.5014	20.0000	0	10.0000	77.7699	34.5722
4.4300	4.5161	30.0000	0	13.0000	82.3544	34.6034
5.8700	5.9170	41.0000	0	12.0000	81.5520	34.6038
4.4400	4.5260	33.0000	0	13.0000	80.7661	34.6053
5.1500	4.8549	32.0000	0	13.0000	74.4812	34.6105
5.7300	4.6825	42.0000	0	12.0000	76.8802	34.6120
5.1300	4.9142	31.0000	0	13.0000	73.2620	34.6125

SECTOR 11

9.6801	8.4837	22.0000	9.0000	11.0000	75.2540	34.5453
10.3100	8.5578	15.0000	8.0000	13.0000	69.2232	34.5540
9.7801	8.5481	17.0000	8.0000	13.0000	71.7066	34.6093
9.4101	8.6182	15.0000	8.0000	12.0000	74.1037	34.6112
9.3101	8.5401	17.0000	8.0000	12.0000	67.6847	34.6208
9.7401	8.6945	16.0000	9.0000	13.0000	81.2176	34.6236
9.2601	8.6170	16.0000	8.0000	12.0000	71.0924	34.6289
9.6401	8.6890	17.0000	9.0000	13.0000	68.3170	34.6314
9.0901	8.5378	17.0000	7.0000	12.0000	70.7126	34.6421
10.3900	8.6793	11.0000	11.0000	15.0000	97.7079	34.6670
8.6901	7.9230	28.0000	0	14.0000	90.3469	34.7043
8.5201	8.4104	27.0000	0	14.0000	80.9017	34.7146
7.7801	8.0024	25.0000	0	13.0000	70.2431	34.7172

SECTOR 12

11.7100	11.1330	0	21.0000	21.0000	67.3867	35.1003 R

14.8301	13.4689	0	26.0000	26.0000	72.2280	35.3221 R

SECTOR 13

13.5501	14.0571	0	26.0000	26.0000	77.6399	35.4936 R
17.2101	16.3884	0	32.0000	32.0000	64.2685	35.8375 R
15.4500	15.8085	0	31.0000	31.0000	53.9500	36.0368 R

SECTOR 14

16.3500	16.5172	0	32.0000	32.0000	65.0820	35.9726 R

SECTOR 15

24.5401	20.2243	0	43.0000	43.0000	24.7608	36.1896 R
24.6901	20.3055	0	44.0000	44.0000	14.0856	36.3099 R
22.9801	20.1094	0	42.0000	42.0000	35.6819	36.4136 R
20.1000	19.7883	0	41.0000	41.0000	40.1243	36.9360 R
18.2701	19.5355	0	39.0000	39.0000	43.1664	37.0239 R
18.3901	19.5358	0	40.0000	40.0000	28.6644	37.1677 R
24.7101	19.9566	0	51.0000	51.0000	-12.5946	38.1403 R

RAMP - relative amplitude in dB (RAMP=SL-TL, Sea State 3, 0.5 dB/bottom bounce)

R - ray is temporally resolvable using a 62.5msec pulse separation

SECTOR 1 - Grazing angles from -22.4 to -19.5 degrees
SECTOR 2 - Grazing angles from -19.5 to -16.5 degrees
SECTOR 3 - Grazing angles from -16.5 to -13.5 degrees
SECTOR 4 - Grazing angles from -13.5 to -10.5 degrees
SECTOR 5 - Grazing angles from -10.5 to -7.5 degrees
SECTOR 6 - Grazing angles from -7.5 to -4.5 degrees
SECTOR 7 - Grazing angles from -4.5 to -1.5 degrees
SECTOR 8 - Grazing angles from -1.5 to +1.5 degrees
SECTOR 9 - Grazing angles from +1.5 to +4.5 degrees
SECTOR 10 - Grazing angles from +4.5 to +7.5 degrees
SECTOR 11 - Grazing angles from +7.5 to +10.5 degrees
SECTOR 12 - Grazing angles from +10.5 to +13.5 degrees
SECTOR 13 - Grazing angles from +13.5 to +16.5 degrees
SECTOR 14 - Grazing angles from +16.5 to +19.5 degrees
SECTOR 15 - Grazing angles from +19.5 to +22.5 degrees

INITIAL DISTRIBUTION LIST

		No.Copies
1.	Defense Technical Information Center Cameron Station Arlington, VA 22304-6145	2
2.	Library, Code 52 Naval Postgraduate School Monterey, CA 93943-5000	2
3.	Chairman (Code OC/Co) Department of Oceanography Naval Postgraduate School Monterey, CA 93943-5000	1
4.	Library Scripps Institution of Oceanography P.O. Box 2367 La Jolla, CA 92037	1
5.	Professor Ching-Sang Chiu (Code OC/Ci) Department of Oceanography Naval Postgraduate School Monterey, CA 93943-5000	1
6.	Professor James H. Miller (Code EC/Mr) Department of Electrical and Computer Engineering Naval Postgraduate School Monterey, CA 93943-5000	1
7.	Professor Anthony A. Atchley (Code PH/Ay) Department of Physics Naval Postgraduate School Monterey, CA 93943-5000	1
8.	Director Naval Oceanography Division Naval Observatory 34th and Massachusetts Avenue NW Washington, DC 20390	1

9. Commander 1
Naval Oceanographic Command
Stennis Space Center
Bay St Louis, MS 39529-5000

10. Commanding Officer 1
Naval Oceanographic and Atmospheric
Research Laboratory
Stennis Space Center
Bay St Louis, MS 39529-5004

11. Dr. Thomas Curtin 1
Office of Naval Research
800 North Quincy Street
Arlington, VA 22217-5000

12. LCDR John M. Elliott, USN 1
USS Mariano G. Vallejo (SSBN 658) Blue
FPO Miami 34093-2087

13. Professor James F. Lynch 1
Department of Applied Ocean Physics and
Engineering
Woods Hole Oceanographic Institution
Woods Hole, MA 02543